PERCEPTION AND USE OF MAGNETIC FIELD INFORMATION IN NAVIGATION BEHAVIORS IN ELASMOBRANCH FISHES

A DISSERTATION SUBMITTED TO THE GRADUATE DIVISION OF THE UNIVERSITY OF HAWAIʻI AT MĀNOA IN PARTIAL FULFILLMENT OF THE REQUIREMENTS FOR THE DEGREE OF DOCTOR OF PHILOSOPHY

IN

ZOOLOGY, SPECIALIZING IN MARINE BIOLOGY

JULY 2018

By

James Murray Anderson

Dissertation Committee:
Kim Holland, Chairperson
Timothy C. Tricas
Kathleen Cole
Masato Yoshizawa
Patricia Couvillon

Keywords: Magnetoreception, Navigation, Shark, Behavior, Magnetite, Raman Spectroscopy

Dedication & Acknowledgements

I dedicate this dissertation and the body of work it represents to the memory of my mother, Irene, who always believed in me, with unwavering love and support.

I would like to thank my wife, Catherine and my children, Sonny, Zane, Loki and Kai (a.k.a. the four horsemen), for their own unwavering love and support, for putting up with me, and providing me with a counterbalance to the stresses and demands of graduate school.

There are a host of people whom I need to thank; my advisors through my graduate career, Kim Holland and Tim Tricas, for taking me on, having faith in me, and for their help and guidance through a tricky and complicated research topic. I owe a debt of thanks to several amazing people who took an active interest in my research, gave their time and effort to help me, and ultimately provided critical input to the success of the study – so thank you Kristen Ewell and Miyoko Bellinger (U.H. Histology Core), Tina Weatherby Carvalho (B.E.M.F), Fukun Hoffman (CMB), Alexandra Gurary (Molecular and Cellular Immunology Core), Kara Yopak (UNCW). I also owe a debt of thanks to Tamrynn Clegg for her dedication and hard work in assisting with much of the study.

I also extend my thanks to Shaun Collin, Gary Cowin, Marilyn Dunlap, Carl Meyer, Kelly Williams, Kelsey Maloney, Christine Ambrosino, Luisa Queiroz, Mark Royer, Danny Coffey, Melanie Hutchinson, Kevin Izumi, Kaylee Rossing, Jeff Muir, Mariana Azevedo and the many interns in the lab for their help in data collection and husbandry. I thank the members of my dissertation committee, Drs. K. Cole, M. Yoshizawa, P. Couvillon, K. Holland, and T. Tricas, for help with experimental methodology and constructive manuscript editing. Finally, I would like to thank all my friends and family for their support and help throughout my time as a graduate student.

Abstract

Three principal hypotheses prevail regarding the sensory means by which animals, including elasmobranchs, perceive and use magnetic field information. Of these three hypotheses, the iron (magnetite) based magnetoreceptor hypothesis is regarded as being the most basal, and is proposed to be conserved across taxa, from invertebrates through to high vertebrates. Magnetoreception via magnetic-electric induction and the radical pairs mechanism is considered more derived. Modern elasmobranch and teleost fish share a common ancestry. Although they evolved independently, the apparent evolutionary conservation of functional magnetite containing structures (as in teleosts and birds) might suggest such structures are also present in the elasmobranchs.

Elasmobranch fishes have been both hypothesized and empirically shown to respond to changes in magnetic fields. However, empirical evidence to support orientation and navigation via magnetic field information in elasmobranch fishes is scant; sensory acuity to magnetic stimuli is undescribed, and the physical mechanisms and sensory pathways by which sharks may perceive and use magnetic information continue to be the subject of debate.

The investigations detailed in the following chapters aim to examine the ability of sharks to perceive and use magnetic field information in navigation behaviors. Using conditioned behavior experiments as a proxy, these experiments confirm sharks' ability to perceive magnetic stimuli, quantify sensory acuity, determine ability to discriminate contrasting magnetic stimuli, and provide insight into the possible mechanisms used. Morphological and physiological analyses aimed to identify critical structures required for an elasmobranch homologue to the iron/magnetite based olfactory magnetoreceptor described in teleost fish.

Sharks were able to perceive magnetic field changes as low as 0.03 microtesla (μT), and could repeatedly and reliably discriminate between contrasting but similar magnetic landmarks. This demonstrates sharks could not only perceive ecologically relevant magnetic stimuli, but could learn, internalize and organize that information – a key

component in the formation of a cognitive map, required in navigation. Sensory deprivation/impairment techniques incorporated suggested the likely use of at least two sensory mechanisms (magnetic-electric induction & a putative magnetite based magnetoreceptor). Finally, morphological and physiological investigations suggest sharks possess the critical structures required in a magnetite-based olfactory housed magnetoreceptor.

Table of Contents

List of Tables

List of Charts/Figures

List of Abbreviations

cm	Centimetre	n	Number
CR	conditioned response	nT	nano-Tesla
*d*b	change in magnetic field	nV	nano-Volt(s)
DC	direct current	R	resistance (in Ohms)
*d*t	change in time	r_1	distance from magnetic coil centre
e^x	raised to the power of	s	second(s)
emf	electromotive force	s^{-1}	per second
Hz	Hertz	S+	stimulus (active)
I	current (in amperes)	S-	non-stimulus
k	1000	µT	micro-Tesla
m	metre(s)	V	voltage/Volts
mV	milli-volts	Ω	ohms
m+	magnetic cell population	m-	non- magnetic cell population
ALLn	anterior lateral line nerve	CNVII	cranial nerve seven
CNV	cranial nerve five	SOA	superficial ophthalmic nerve

Chapter 1 – *An Introduction To Orientation & Navigation In Animals Sharks & Other Animals*

1.1 *General Introduction*

The elasmobranch fishes (sharks, skates and rays) are considered a prehistoric group of fishes, whose chondrichthyan ancestors evolved over 400 million years ago (Grogan et al. 2012). Chondrichthyans, characterized by the absence of typical bony fish characteristics (osseous bone, swimbladder, teeth/tooth plates not fused to the jaw, multiple gill openings), are thought to have diverged from bony vertebrates (Osteichthyes) between 415 million years ago (Mya) (Giles et al. 2015) and 450–475 Mya (Heinicke et al. 2009). Both Osteichthyans and Chondrichthyans emerged as distinct assemblages in a group of four distinct assemblages (the other two being Acanthodians and Placoderms) descended from gnathostomes (jawed vertebrates) (Brazeau & Friedman, 2015). Osteichthyes, whose extant members represent the largest class of vertebrates (around 96% of all fishes), can be split further into two groups (Actinopterygii and Sarcopterygii), distinguished by their paired fins. Actinopterygian fins are formed by dermal fin rays, where the endoskeleton and muscles control the fins internally. Sarcopterygian (lobe-finned fish) fins are 'fleshy', with externally projecting skeleton-muscular structures. Actinopterygii divide into three infraclasses; the Chondrosteans, the Holosteans, and the Teleosts. Sarcopterygii are comprised of three orders; Rhipidistia, Actinistia, and Dipnoi, and are generally considered closely related to the ancestral tetrapods.

The class Chondrichthyes includes all of the cartilaginous fishes (chimaeras, sharks, skates, and rays), whose extant members number at least 1,207 species (Cotton and Grubbs, 2015). Chondrichthyans are further divided into two subclasses; Holocephali (chimaeras) and Elasmobranchii (sharks, skates, and rays). Despite many decades of study, the exact relationships of chondrichthyans to other groups of fishes, including other chondrichthyans, remain the subject of debate (*inter alia* Naylor et al. 2005). However, it is generally accepted that after Schaeffer and Williams (1977), the extant elasmobranchs (Neoselachii) are a monophyletic group comprising all species of sharks, skates and rays (Naylor et al. 2005).

The class Elasmobranchii is divided into 12 orders, comprising 61 families (Van Der Laan et al. 2014), and over 500 species (Eschmeyer & Fong 2018). Elasmobranch fishes can be found across marine environments, from shallow coastal systems, to bathyal shelves, although they seem largely absent from abyssal habitats (below 3000m) (Priede et al. 2006; Musick & Cotton 2015). Despite being present in such a variety of marine environments, it is estimated that sharks are confined to approximately 30% of the ocean, with populations outside of continental shelves often centered around oceanographic features such as seamounts, islands and ocean ridges (Priede et al. 2006).

Life history of elasmobranchs is similarly variable, and this variation is often reflected in their core habitat and home range sizes. A home range can be described as "the relatively circumscribed area over which an organism travels to acquire the resources it needs for survival and reproduction" (Dingle 1996). It must also be kept in mind, that much of an animal's home range is in 3-dimensional space. So not only the surface and the floor of the sea/ocean, but potentially the entire water column in between. The degree to which elasmobranchs utilize this 3D space in both the horizontal and vertical plane is again, highly variable. Many species can be considered comparatively sedentary making fewer, or smaller scale movements or journeys on a daily basis, while some may be considered migratory, or highly migratory (~ 19% and <5% respectively) (Fowler 2014). Regardless of these variations, for an animal to establish a home range, regardless of scale, it requires the ability to infer where it is. To do this, it must make use of available cues and information from it's environment, and orient itself based on the information gained from such external, environmental cues. In a zoological context, orientation can be defined as a change in an organism's position in response to an external (environmental) stimulus. For some lower organisms (e.g. Paramecium), movement is mostly undirected and random. Undirected orientation such as this is termed kinesis. Conversely, movement in response to a stimulus (toward or away from) is termed taxis. Animal orientation is thus a complex behavior, requiring the animal to correlate information received from the external environment across multiple channels.

Orientation can be described as the ability of an animal to determine its position in space and among individuals of the same or other species. Animal orientation is a complex

process that involves integrating and correlating received information about the external environment through various channels of communication, and forming a (motor) response. The nature of that motor response will be governed by the integration of sensory cues, correlated with the context under which they were received. Thus, depending on the situation, one or another receptor system plays a predominant role. Such an integrated system ensures the reliability (freedom from interference) and flexibility of orientation.
Navigation is a more complex form of spatial awareness. To navigate, an animal must have a sense of it's environment, and a means/mechanism by which to orientate itself within those surroundings. Thus, animals navigate through orienting to cues generated by their own movements (self-movement cues or idiothetic cues that give the animal a contextual frame of reference with respect to it's change in position/location as it moves through it's environment), as well as the cues they encounter in their environment (distal cues or allothetic cues – cues that help frame the environment itself).
Navigation behaviors may involve one of three forms of orientation:
1) Pilotage; which can be considered a non-compass form of orientation, involves an animal recognizing and following familiar landmarks (allothetic cues) in order to reach a goal or location.
2) Path integration; is the name given to animal equivalent of dead reckoning – the process of determining current position through correlation self-movement (idiothetic) cues over time to estimate distance travelled from an arbitrary starting location (i.e. integrating velocity with respect to time, to obtain position/location as a function of time), and allothetic cues to track direction. The correlation of this information facilitates homing.
3) Compass orientation; is the ability of an animal to travel in a constant direction, seemingly without reference to physical-environmental or idiothetic cues. In-fact, a wide body of evidence supports hypotheses that animals can gain directional/compass information from celestial cues such as the position of the sun or stars (Sandberg & Holmquist, 1998 (*intra alia*)), as well as the geomagnetic field (Wiltschko & Wiltschko 2006).
Some animals may also be capable of true navigation – the ability determine their position in an unfamiliar environment relative to a goal/location, without the use of familiar

landmarks, or cues that emanate from that goal/location (Griffin, 1952; Phillips et al., 2006). This concept requires the animal to have some level of knowledge of both the immediate and wider environment in which is positioned. This knowledge may be innate, imprinted, or learned through experience, as has been suggested in fish and turtles (Putman et al., 2014).

The scale over which true navigation movements occur varies by species, and by species' life history, and ranges from tens to hundreds of kilometers (Phillips et al., 2006), in both homing and migratory behaviors. Kramer (1953), proposed the "map and compass" hypothesis, which argues that true navigation requires (1) a map step – by which an animal can gain a sense of position relative to a goal/location, and (2) a compass step – by which having established the direction of it's goal from it's current position, the animal can move along an appropriate vector or compass heading.

The nature of "maps" that animals may use is the subject of debate, and likely do not conform to the human concept of a cartographic map, which is an integrated representation of a given environment. However, it is accepted that there are at least two types of spatial representation (maps) that animals use; a mosaic map, and a gradient map (Akesson et al., 2014). Mosaic maps require the animal to learn the spatial relationships of features within its environment relative to "home" (Walraff, 1974). It is assumed that features comprising a mosaic map are encoded as compass directions, and that the size of the map is governed by the animal's experience of its' environment (Akesson et al., 2014). It would follow, therefore, that mosaic maps would not (solely) form the map step in true navigation. Gradient maps require knowledge of the alignment and the steepness (rate of change) of one or more environmental gradients in and around an animal's home range, which (in concept) allows extrapolation the gradients beyond its area of familiarity (Phillips, 1996). Bi-coordinate gradient maps are comprised of a combination of two gradients, (e.g. geomagnetic inclination and field strength), thus can provide site-specific information regarding position (Akesson et al., 2014), even when specific environmental gradient is variable.

Sharks are among a diverse array of animals shown to occupy well-defined home ranges. Home range size and the scale of movements vary hugely across shark species. Several

species of shark have been shown to swim with straight movement paths, with some species migrating to specific locations many 100's to 1000's of kilometers away (Weng et al. 2007; Meyer et al. 2010; Papastamatiou et al. 2011). How do animals that move across large spatial areas navigate between known locations? It is suggested that such animals, including sharks (particularly highly migratory sharks), likely utilize cognitive maps to locate resources (Montgomery & Walker 2001). This latter point refers to the fact that sensory cues that may assist navigation at any given point in time may often be beyond the reach of a sharks' sensory systems. The mental encoding and commitment to memory of the environmental information that forms these (mosaic and/or gradient) maps constitute a cognitive map. Tolman (1948), defined a cognitive as the "representation of the environment which indicated the routes, paths and environmental relationships that an animal uses in making decisions about where to move". This definition was further developed by O'Keefe & Nadel (1978), who argued that an animal's ability to make novel short-cuts distinguished the movement between two given points from route following/taxon strategies, i.e., the animal's awareness of the spatial relationships of features within it's environment allows it to travel along the most parsimonious vector, which may represent an unknown or untried route.

Whether or not shark and ray species, or any other animal, actually uses a cognitive map in the manner proposed by Tolman (1948), and later O'Keefe and Nadel (1978) is somewhat contentious, as it is argued that although studies have demonstrated animals may form some manner of internal model of their environment (see Gallistel, 1990), this alone does not constitute evidence of the use of a cognitive map as described by the hypothesis (Poucet, 1996; Bennet 1996).

In order to locate (or re-locate) a specific resource, an animal must be able to combine memory of specific features of their environment with sensory cues. Lohman et al. (2008), concluded that long distance migrations in marine animals would require at least the bi-modal use of sensory mechanisms, used sequentially across spatial scales. Schleussel & Bleckmann (2005) concluded that their study using captive stingrays demonstrated they use of a visual cognitive map, combined with egocentric and/or other orientation strategies. They further suggested the exact nature of this combination may be governed by

the complexity of the task at hand. Mobile animals (including sharks and rays) might therefore use a variety of correlated sensory cues to build and encode a mental representation of their environment.

1.2 *Sensory systems in orientation, homing and navigation behaviors in sharks*

1.2.1

The sensory systems of many shark species are well described, and sharks in general are regarded as having sensory organs that are acutely sensitive to weak environmental stimuli. It is through this sensory array that sharks are proposed to derive the necessary information to navigate successfully.

1.2.2

The visual system may have an important role in navigation and homing behaviors. Elasmobranchs not only possess well develop lateral eyes, but also have a median or pineal eye (the *epiphysis cerebri*) (Gruber, 1975;1977), which is equipped with photoreceptors similar to those in the retina, capable of detecting illumination from a full moon (Hofmann, 1990). Thus, sharks, like many other animals, may gain directional or positional information from celestial cues (e.g. a sun compass), as well as from visible physical features in their environment. A significant body of evidence exists to support the use of time-compensated sun compass mechanisms across a broad range of taxa, including a variety of teleost fish species (*intra alia*: Winn et al., 1964; Ogden & Quinn, 1984; Mouritsen et al., 2013). By this mechanism, animals, from insects, to larval fish, to birds and turtles can estimate a vector of orientation or movement by comparing the azimuth of the sun in the sky relative to the time of day, as measured/perceived via circadian rhythms (an internal clock) (reviewed in Akesson et al, 2014). Interestingly, this compass mechanism has been demonstrated to cease to function in some fish and birds at night, or when the sun is blocked/hidden by significant cloud (Winn et al., 1964). The continued ability of some animals to maintain a consistent compass direction in the dark, or when the sun is obscured suggests the use of other celestial cues (e.g. polarized light, star light). While it therefore follows that it is highly possible, and even postulated (e.g. Gruber et al., 1988)

that elasmobranch fishes might also use celestial cues such as a sun compass in orientation and navigation behaviors, there is no published empirical data to support this.

By contrast, there is empirical evidence that demonstrates use of the visual system in recognition and discrimination of physical features of the environment as part of orientation and navigation strategies in different elasmobranch species. Schleussel and Bleckmann (2005), demonstrated that ocellate river stingrays (*Potamotrygon motoro*) were able to develop a visually based cognitive map, used in navigation tasks. Animals in the study were required to navigate a maze to receive a food reward. To do so, test subjects had to find a specific location, or use specific turn strategies, both of which required recognition of specific visual cues. In a later (2012) study, the same authors found that grey bamboo sharks (*Chiloscyllium griseum*) were able to complete spatial learning tasks via visual cues in order to gain a food reward, and that they were able to retain learned information for up to six weeks. Fuss and Schluessel (2015) further demonstrated that the same species was able to successfully able to discriminate between specific visual stimuli and their corresponding optical illusions in order to navigate a maze to receive a food reward, and that this ability was retained for up to 50 weeks without reinforcement. Thus, elasmobranchs could use visual cues in migratory and homing behaviors, and may be able to visually recognize features in their environment up to a year later. Both *P. motoro* and *C. griseum* are adapted to a benthic life history, often found in sandy and muddy substrates of calm, inshore waters (and river systems in the case of *P. motoro*) (Drioli & Chiaramonte 2005; Lisney & Cavanagh 2003). Neither species would be characterized as visual predators, unlike purely oceanic species such as the shortfin mako (*Isurus oxyrinchus*) and the bigeye thresher (Alopias superciliosus), and yet they clearly have the ability to visually discriminate shapes and patterns. This suggests visual cues in elasmobranch orientation behaviors may important over small geographic scales. Such an ability may be key to finding and recognizing specific locations in lotic riverine and estuarine systems, where sediment load in the water column may be high, and visibility levels low.

1.2.3

Large bodied, highly migratory sharks make regular return movements across great distances (Weng et al. 2008; Yannis P Papastamatiou et al. 2013; Werry et al. 2014). A

growing body of evidence indicates that the extent of these movements are governed by environmental factors, particularly temperature, in terms of both seasonal variation, and the physiological constraints of thermal minima and maxima (Lea et al. 2018; Payne et al. 2018). Thus, navigation behaviors across great distances may be influenced by ocean currents, and subsequent temperature gradients to and from home ranges. For smaller bodied elasmobranchs, that do not make such large-scale movements, the importance of temperature gradients as a navigational cue is less clear. Klimley (1993) investigated highly directional movements of scalloped hammerhead sharks (*Sphyrna lewini*) in Baja, California (Mexico), and found that movement patterns were not correlated with sea surface temperature or irradiance. This suggests that where movement distances are smaller (comparatively speaking), temperatures and temperature gradients are not important cues to homing and navigation. However, in a displacement study using New Zealand eagle rays (*Myliobatis tenuicaudatus*), Marcotte (2014), concluded that water temperature within a large embayment was a potential predictor of homing success. Thus, the extent to which temperature gradients are used as cues to orientation and navigation in elasmobranch fishes likely varies by species, and likely reflects life history characteristics.

1.2.4

Olfactory acuity in elasmobranchs has also been well studied (Gilbert et al. 1964; Silver 1979; Theisen et al. 1986; Tricas et al. 2009). Commonly, studies on the role of olfaction in elasmobranch behaviors has focused on klinotaxis to olfactory cues in prey location. However, more recent studies have proposed or argued that olfaction may play an important role in homing behaviors (Edrén & Gruber 2005; Heupel & Simpfendorfer 2005). Olfactory cues may serve in the formation of a mosaic map, as has been (contentiously) suggested in avian species through animals recognizing specific olfactory cues associated with a location, and the associated olfactory cue relationships of other features in the environment to that location (reviewed in Able, 2001). Olfactory cues may also serve in a gradient map, whereby the gradient (difference in strength) of an olfactory cue can serve as an orientation cue, and provide a compass direction for homing behaviors. In teleost fish, olfactory cues have been demonstrated to be key to the return migration of Salmonids to

their natal streams (Cooper et al. 1976; Bett et al. 2016). It follows therefore that sharks and rays might also use olfactory cues in a cognitive map that may help localize specific resources within a home range. Gardiner et al. (2015) and Nosal et al. (2016), separately demonstrated that olfactory-impaired juvenile black tip sharks (*Carcharhinus limbatus*) and leopard sharks (*Triakis semifasciata*) (respectively) were significantly less able to return to the vicinity of their capture site after being geographically displaced, compared with a control/sham group that had not undergone the impairment procedure.
Long and short distance klinotaxis (comparing the strength of the olfactory cues across the paired olfactory receptors to locate the source of the cue) to these cues could be governed by interspecific olfactory eco-physiological morphology. In bathyal species, the olfactory organs, and the olfactory bulbs (the center of processing for olfactory information) are often comparatively larger than their coastal, pelagic and oceanic counterparts, with some oceanic species having notably small olfactory bulbs (Yopak et al. 2015). While this physical adaptation indicates olfactory specialization in a variety of species that likely reflects evolved foraging strategy, it does not preclude the possibility that sharks and rays with smaller olfactory bulbs may orient to olfactory cues emanating from specific locations. Such cues may be transported long distances via estuarine flows, tidal cycles, predominate currents, and even gyres.

1.2.5

The lateral line and auditory and senses of fish (both teleost and cartilaginous) are proposed to be important in conspecific detection, prey detection and predator avoidance. The lateral line system of fishes (posterior lateral line in elasmobranchs) has been demonstrated to function in the detection of movement, vibration and pressure gradients in the surrounding water. In elasmobranch fishes, characterization of posterior lateral line function has been constrained to prey detection and rheotaxis (Gardiner & Atema 2007; Gardiner et al. 2012), specifically via the superficial (rather than canal) neuromasts (Montgomery & Skipworth 1997; Peach 2001), which are sensitive to changes in the direction of flow of water (currents) surrounding the animal. Thus, environmental cues such as tidal flux, estuarine flows and prevailing current lines could aid in orientation,

navigation and homing behaviors. Recent evidence suggests rheotactic capability is influenced and possibly augmented through using the geomagnetic field as a frame of reference (Cresci et al., 2016) The scale at which such cues operate may well vary by species, life history, and geographic context.

Auditory acuity has been characterized in a small range of elasmobranch species (Kritzler & Wood 1961; Nelson 1967; Kelly & Nelson 1975; Casper et al. 2003; Casper & Mann 2006; Casper & Mann 2009). The macula neglecta (which lacks otoconia, unlike the other maculae of the inner ear labyrinth), is contained in a duct that connects the base of the parietal fossa to the saccule, is considered the elasmobranch auditory receptor structure, responding to the particle motion (not pressure) component of sound. Three hypotheses propose explanations of how sharks can orient to distant auditory cues (reviewed by Myrberg, 2000). Essentially, they resolve directionality of the source of the sound, but cannot resolve the actual location of the source.

The first of these (Schuijf, 1974; 1975) suggests the animal can resolve the directionality (but not the location of the source) of a sound by comparing the time of arrival of sound waves at differently oriented hair cells in the macula neglecta. The model suggests that sound reaches the inner ear directly from the source, or indirectly after having reflected off the water surface, with the time delay of the indirect wave being relative to the direct wave. This model solves for 180° ambiguity (resulting from particle motion), but would be constrained depths shallower than 20m.

The second hypothesis (Corwin 1981a; b), suggests sharks attend to sound waves received directly, and that the directionality of the source is resolved by the strength of the response of the sensory maculae. The strength of the response is governed by the direction of sound origin - due to the morphology of the labyrinth and the location of the macula neglecta, sound waves originating from in-front of the animal will produce a stronger response than from behind, with the strongest response being generated by waves originating anteriodorsomedially.

The third hypothesis (Kalmijn, 1988) suggests sharks may orient to the near-field acoustic/acceleration fields produced by prey. As these fields are dipoles, the shark can follow the angular rate of change of the field lines by maintaining a constant angle between

it's body and the sound waves received by the inner ear, thus bringing the animal to the vicinity of the sound source. Other sensory systems can then locate the source.

Generally auditory acuity of elasmobranchs could be described as poor (Casper & Mann 2006) in comparison to their otophysan teleost counterparts, while auditory acuity in those elasmobranch species tested is variable, and likely reflects ecomorphotype (life history) (Corwin 1978). The ability of sharks to orient to sounds has been well documented (*intra* alia; Clark, 1959, Nelson & Gruber, 1963, Nelson, 1967). Of the species tested, those that can be classified as pelagic or coastal-pelagic showed the best sensitivities to low frequency sounds (40-800 Hz) (Myrberg, 2000), although the lowest frequency tested across all published studies is 20 Hz. It is these low frequency sounds that are most likely to serve as long-distance cues to navigation or homing by auditory cues. Infra-sound (sound with frequencies <20 Hz) can propagate over long distances (100s to 1000s of km) without suffering significant attenuation (Sand & Karlsen 2000).

Sources of infrasound that might serve as relevant cues to orientation and navigation in the marine environment are surf (on the shoreline), water currents on under water topography, aurorae, and low seismic activity. Sand & Karlsen (2000) proposed that infrasound propagating from seismic activity on the sea floor, as well as changes in the pattern of waves at the surface of the ocean) associated with changes in water depth), and distance from land may serve as important cues for orientation and navigation in fishes. Moreover, they specifically implicated the use of otolithic structures (rather than the Weberian apparatus of otophysans) in detection of such infrasound stimuli, making such sources applicable and relevant to elasmobranchs. Testing of auditory acuity below 20 Hz is needed to confirm this capability. Whether or not elasmobranchs actually make use of infrasound in orientation and navigation behaviors remains an open question.

1.3 *The sixth and seventh senses – Electroreception and Magnetoreception in Orientation and Navigation.*

1.3.1

Many animals from several taxa are able to perceive and respond to changes in the earth's magnetic field (Wiltschko & Wiltschko 2006). The ability to detect and orient to magnetic fields has been observed in bacteria (Mann et al. 1990; Blakemore 1975), algae (Torres et al. 1986), invertebrates (Brown et al. 1964; Lohmann et al. 1995; Hsu et al. 2007) and vertebrates, including birds (Beason & Nichols 1984; Wiltschko & Wiltschko 1972; Thalau et al. 2006; Wiltschko et al. 2010), rodents (Thalau et al. 2006; Marhold et al. 1997), amphibians (Deutschlander et al. 1999; Deutschlander et al. 2000; Freake & Phillips 2005), quelonians (Lohmann & Lohmann 1994; Light et al. 1993), cetaceans (Kirschvink et al. 1986) and teleost fish (Durif et al. 2013; Mora et al. 2014; Mora et al. 2009; Walker 1984; Diebel et al. 2000; Walker et al. 1997; Walker et al. 2004; Quinn 1980; Quinn & Brannon 1982).

Since the 1970's, it has been recognized that (teleost) fish are able to perceive and respond to experimental manipulation of the background magnetic field (Rommel Jr. & McCleave 1973; Varanelli & McCleave 1974; McCleave & Power 1978). Salmonids in particular have been used as the "model species" for studies investigating magneto-receptive capabilities in teleost fish (Walker et al. 1988; Chew & Brown 1989; Walker et al. 1997; Hellinger & Hoffmann 2009; Lohmann et al. 2008), and have been shown to respond to changes manipulations in background magnetic field intensity (magnitude) and direction. While work in salmonids continues to elucidate the role of the geomagnetic field in fish behaviors (e.g. Putman et al., 2018), recent studies have focused on other teleost species, including Zebra fish (*Danio rerio*), and European and Japanese eels (*Anguilla anguilla, Anguilla japonica*). These studies further extend the phylogenetic pattern of magnetoreception across actinopterygian fish orders, and provide further insight into both the roles and mechanisms of magnetoreception. For example, studies in Zebra fish and both eel species have demonstrated a bi-modal magnetic compass sense (e.g. Durif et al., 2013; Naisbett-Jones et al., 2017; Osipova et al., 2016; Nishi et al., 2018), have demonstrated the presence of magnetite in the lateral line system (Dixson, 2012; Moore & Riley, 2009), as well as

studies in Zebra fish providing evidence that they may utilize both magnetite-based and a cryptochrome-based receptor mechanisms (Mykalatun et al., 2018; Zhou et al., 2018). Recent genetic studies in rainbow trout (*Oncorhynchus mykiss*) have also shown expression of genes associated with oxidative repair, ferritin transport and repair of photoreceptive structures after exposure to strong magnetic field pulses (Fitak et al., 2017; Arniella et al., 2018).

Geo-magnetic field parameters such as field direction, field vector (horizontal & vertical components), inclination, declination & magnitude/intensity could all provide positional information. The characteristics/parameters of the magnetic field that are perceived by organisms have been found to vary across taxa (Table 1.1).

The reasons behind this apparent heterogeneity in magnetic field perception are un-explained. It may be possible that more than one characteristic of the geomagnetic field can be discriminated for the purposes of homing and navigation behaviors. 'True' navigation requires a positional/map component that determines position relative to the goal, and a compass/directional component to fix and maintain the direction to the goal (Griffin 1952; Walker 1998). Thus, an animal can make highly directional movements & return journeys without the use of physical landmarks (Boles & Lohmann 2003), which is exactly what is required in an often seemingly featureless, fluid 3D environment.

The earths' magnetic field can arguably provide three kinds of information (see Fig. 1.2):

(1) Polarity (compass) information from the horizontal component of the geomagnetic vector, allowing an animal to determine north & south (Kalmijn 1982; Hodson 2000).

(2) Intensity and (3) inclination of the magnetic field, which exist as gradients between magnetic poles and the magnetic equator, providing positional (map) information (Wiltschko & Wiltschko 2006).

Table 1.1
Taxa demonstrated to perceive or respond to magnetic field changes. Table provides examples of taxa across different phyla, the magnetic field parameter perceived, as well as the orientational or navigational step associated with the magnetic field parameter perceived.

Systematic Group	Perceived Magnetic Parameter	Reference
Proteobacteria		
Magnetotactic bacteria	Polarity (compass)	(Blakemore 1975; Baumgartner et al. 2013)
Euglenophyta		
Magnetotactic algae	Polarity (compass)	(Torres et al. 1986)
Mollusca		
Snail	Polarity (compass)	(Prato & Kavaliers 1996)
Arthropoda		
Spiny Lobster	Vector (compass)	(Lohmann et al. 1995)
Honey bee	Intensity (map)	(Hsu et al. 2007)
Chordata (Vertebrata)		
Newt	Vector (compass)	(Deutschlander et al. 2000)
Salamander	Inclination (compass)	(Phillips 1986; Phillips et al. 2010)
European Robin	Inclination (compass)	(Wiltschko & Wiltschko 1972)
Homing pigeon	Polarity (compass)	(Mouritsen & Ritz 2005; Mora et al. 2004)
Mole Rat	Polarity (compass)	(Marhold et al. 1997)
Eel	Polarity (compass)	(Durif et al. 2013)
Turtle	Inclination (map)	(Light et al. 1993; Lohmann & Lohmann 1994)
Cetacean	Intensity (map)	(Kirschvink et al. 1986)
Salmon	Inclination (map)	(Quinn 1980; Quinn & Brannon 1982)
Trout	Intensity (map)	(Walker et al. 1997; Diebel et al. 2000)
Tuna	Intensity (map)	(Walker 1984)
Elasmobranch	Polarity (compass)	(Kalmijn 1982)
	Intensity (map)	(Anderson et al. 2017)

1.3.2

Broadly, there are three generally accepted mechanisms by which organisms may perceive and transduce information from the geo-magnetic field. One proposed system is often referred to as the "radical pairs" or "cryptochrome" mechanism, which has been largely attributed to avian species, but also has been suggested in anurans (Deutschlander et al. 2000; Phillips et al. 2010). The mechanism was first proposed by Schulten et al. (1978) who found that orientation to magnetic fields in birds was a light dependent process, and that birds tested responded to changes in magnetic field inclination, rather than polarity (direction). While empirical studies with animals have not been able to verify the proposed photochemical processes involved, they have been able to demonstrate support for a visual/optical based magnetoreceptor mechanism (Wiltschko & Wiltschko 2006). Light-dependent models of magnetoreception are proposed to involve an interaction between the magnetic field and either magnetite particles located within a photoreceptor or excited states of photopigment molecules (Deutschlander et al. 2000). The models require polarized light (those in the blue to green range (490–450 nm & 560–520 nm)) (Johnsen & Lohmann 2005; Liedvogel et al. 2007; Maeda et al. 2008). In short, cryptochromes (flavoproteins sensitive to blue light) within the retina absorb photons of blue light from white light. The absorption of these photons causes a change in spin state of electrons within atoms of these cryptochrome molecules to a singlet state. These molecules form singlet radical pairs (two molecules with an unpaired electron each) (Wiltschko & Wiltschko 2006). The theory suggests that the geomagnetic field (inclination) interacts with these radical pairs, creating a singlet-triplet interconversion between the pair (Ritz et al. 2000). This singlet-triplet interconversion within the cryptochrome molecules of the retina is argued to create an aberration in a birds' vision. Effectively, this aberration allows the bird to "see" the inclination of the geomagnetic field. The radical pairs hypothesis has not been invoked in teleost or elasmobranch fishes to date. However, this does not preclude its occurrence.

1.3.3

Elasmobranch fishes have been both hypothesized (Paulin 1995; Akoev et al. 1976; Brown & Ilyinsky 1978) and empirically shown to respond to changes in magnetic fields (Kalmijn

1981; Meyer et al. 2005; Kalmijn 1982; Andrianov et al. 1974; Anderson et al. 2017; Newton & Kajiura 2017). Certainly, several species make large scale movements that could be assisted by even coarse-scale perception of magnetic fields (Bonfil et al. 2005; Weng et al. 2007; Papastamatiou et al. 2011; Papastamatiou et al. 2013). However, the physical mechanisms and sensory pathways by which sharks may perceive and use magnetic information have been the subject of continuing debate. Kalmijn (1981; 1982; 2000) proposed elasmobranch magnetoreception may be facilitated through the electrosensory system, which transduces magnetic field components into electrosensory stimuli. Later refinement of the electromagnetic induction theory by Paulin (1995) set out a feasible mechanism by which elasmobranchs could perceive the geomagnetic field. Paulin argued that based on the work of Montgomery (1980), electroreceptors do not have the characteristics necessary to make DC measurements, because the rapid desensitization of electroreceptors to a DC field would preclude detection of electromotive fields in the manner suggested by Kalmijn. Alternatively, a directional compass sense may be facilitated by a comparison of inputs from the vestibular and electrosensory systems, making use of directional asymmetry in the voltage drop across electroreceptors during movement of the head (Paulin 1995). That is, as the animal swims, the head moves side to side in a sinusoidal manner, producing phasic/cyclical stimuli to sensory maculae within the vestibular system, as well as a voltage drop across the ampullae of Lorenzini corresponding to the change in head position relative to the external electrical field as the animal moves.

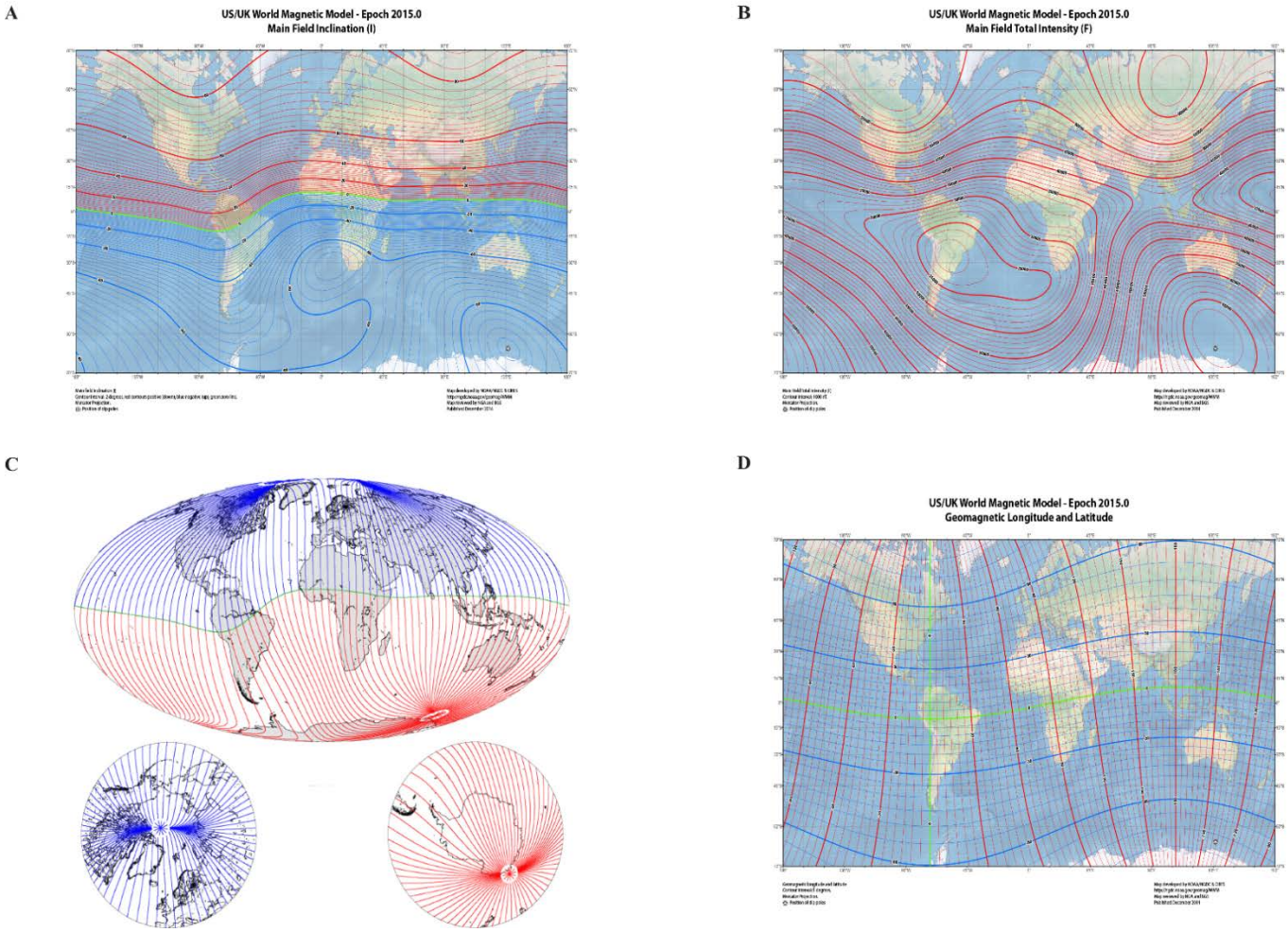

Figure 1.1 *Parameters of the geomagnetic field that may provide organisms with information regarding position, and direction of travel*: **(A)** Main field inclination; **(B)** Main field total intensity; **(C)** Magnetic field polarity (direction); **(D)** Conceptual grid of geomagnetic longitude and latitude (derived from all geomagnetic field parameters). Figures A,B & D reproduced from NOAA/National Geographic Data Center (2015). Figure C reproduced from C.I.R.E.S/Maus (2010).

These common-mode electrosensory stimuli (i.e. they occur across all electrosensory afferents) are suppressed or eliminated by an adaptive filter or common mode suppression mechanism in the dorsal octavolateral nucleus of the shark brain (Montgomery & Bodznick 1993; Montgomery & Bodznick 1999), allowing a high signal to noise ratio. In-fact, it has been demonstrated that even artificial common-mode stimuli are cancelled by the adaptive filter mechanism (Montgomery & Bodznick 1999). Sharks could maintain a constant swimming direction relative to the geomagnetic field by maintaining a constant electrosensory "chord", comprised of different amplitudes at the harmonics of the vestibular frequency (Molteno & Kennedy 2009). Via this electrosensory-vestibular hypothesis, receptor field projection could facilitate discrimination of changes to the polarity (north-south directionality) of geomagnetic fields (relative to the shark) as the animal moves either across or along geomagnetic field lines (assuming movement in a relatively constant horizontal plain). This has yet to be empirically shown.

1.3.4.

The prevailing hypotheses propose that these fish possess an iron (magnetite - Fe_3O_4) based receptor, with a the candidate receptor structure being housed in the epithelium of the nasal organ (olfactory rosette) (Walker et al. 1997; Diebel et al. 2000; Johnsen & Lohmann 2005). Essentially, the hypothesis requires the presence of magnetite in sufficient quantities, and suitably arranged within tissues that the combined magnetic moment (the magnetic moment is a quantity that describes the torque a magnetized crystal/particle will experience in an external magnetic field – e.g. a change or anomaly in the geomagnetic field) is sufficient to transduce changes in the background magnetic field (Johnsen & Lohmann 2005). The torque experienced by the magnetized crystals/particles is argued to be sufficient to induce conformational change in the tissues they are contained in. This conformational change may open stretch-gated ion channels within cells, that could induce an action potential in a proximal nerve (Winklhofer & Kirschvink 2010).

The magnetic properties of magnetite vary with the size (and shape) of the particle/crystal (see Figure 1.2). Small particles (10-20 nm in length) are termed *superparamagnetic* (SP). Ordinarily, their magnetic moment will oscillate/fluctuate under background

(physiological) thermal energy. The net effect of this oscillation under 'normal' circumstances is that the magnetization of the particle(s) will vary in a random manner - they do not remain permanently magnetized (Sung Lee et al. 2015). However, under an external magnetic field, or a change in the background magnetic field, the magnetic axis of SP particles will align (track) the external field (Gould 1984), although individual particles/crystals will not physically rotate (Shcherbakov & Winklhofer 1999).

Under earth strength changes in the background magnetic field, the axial alignment of SP crystals is sufficiently strong enough to attract or repel proximal crystals (Kirschvink & Gould 1981). The magnetic interactions between clusters/groups of SP crystals can therefore result in the conformational change in the cells/tissues they are contained within. SP magnetite has been identified as a candidate magnetoreceptor in pigeons (Winklhofer et al. 2001), but has yet to be identified or characterized as a putative magnetoreceptor in fish.

Single domain (SD) magnetite particles are commonly found in an approximate size range between 30-70 nm, after which the magnetization behavior of the particle is likely to shift to a multidomain state (Butler & Banerjee 1975). SD magnetite has higher coercivity than both superparamagnetic and multidomain magnetite (SP has a coercivity value of zero), meaning it remains permanently magnetized, and it is more difficult to reverse its magnetization (Sung Lee et al. 2015).

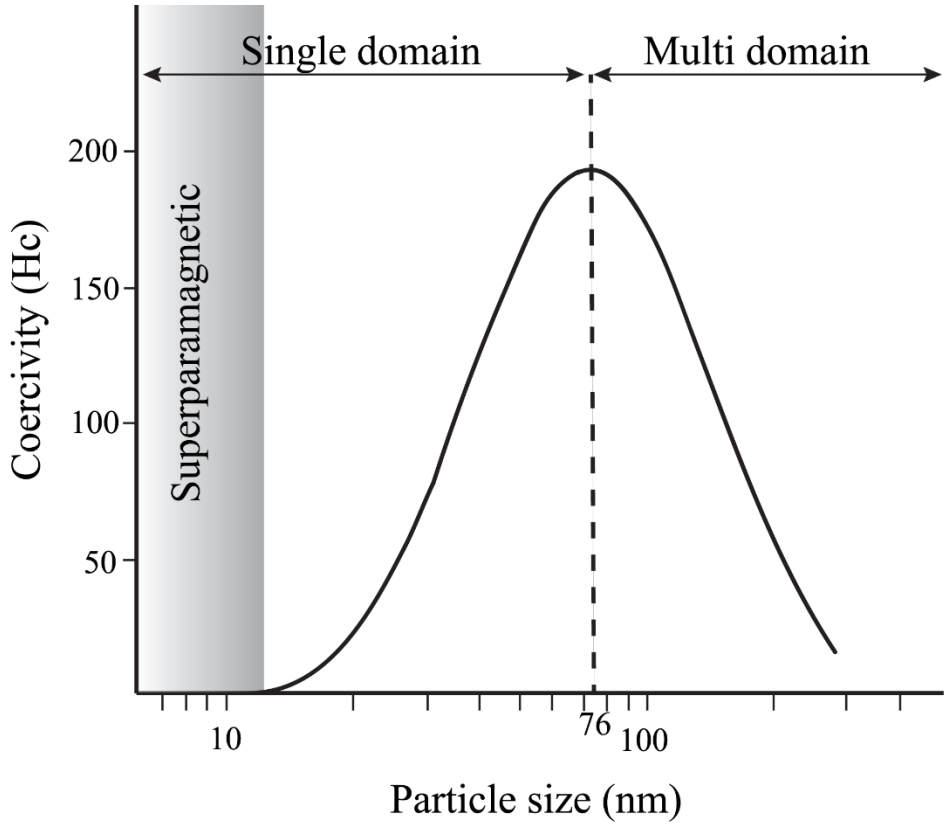

Figure 1.2 *Schematic showing the coercivity (H_c) behavior of a magnetic particle as a function of particle*. Adapted from Li et al. (2017).

The strong magnetic properties of SD particles mean that unlike SP particles, SD particles will physically align with an external magnetic field, rather than their magnetic axes alone. Thus, SD particles/crystals can act individually, or as a cohesive unit when in chains or clusters, to affect a conformational change in cells/structures or tissues they are contained within. Single domain magnetite has been described in variety of structures, in a variety of fish species. These include ethmoid tissues in thunnids and salmonids (Walker et al. 1984; Mann et al. 1988), the lateral line of anguillids and cyprinids (Moore & Riley 2009; Dixson 2012), and the olfactory tissues of salmonids (Diebel et al. 2000), the latter being specifically invoked as a putative magnetoreceptor structure, innervated by the superficial ophthalmic branch of the fifth cranial nerve (trigeminal nerve) (Walker et al. 1997; Diebel et al. 2000; Hellinger & Hoffmann 2009).

Magnetite has been described in regions of the otolithic organs of the shovelnose guitar fish (*Rhinobatos productus*), and was suggested by the authors to function in magnetic field perception (O'Leary et al. 1981; Vilches-Troya et al. 1984). They proposed the crystals they imaged could rotate under an external magnetic field, which could be sensed by proximal hair cells of the vestibular system. However, the authors themselves reported that the crystals they found were far larger than typical SD crystals, and could be visualized with optical microscopy. This could suggest the magnetite crystals found were more likely to be multidomain than single domain, and would therefore be unlikely to function as a magnetoreceptor (Gould 1984; Winklhofer & Kirschvink 2010). Particles with magnetic properties have also been described from statoconia in the otolithic mass of the dogfish (*Squalus acanthias*) (Hanson et al. 1990). In this case however, the authors ruled out the role of such particles in any magnetoreceptive function, suggesting instead that they served to increase the mass of the otolith, and thus improve the sensitivity of the otolith to inertia. Gould (2008), suggested that if animals do indeed possess and use magnetosense, then a magnetite based system is probably ancestral, and that light based/chemical mechanisms (e.g. radical pairs), that are largely attributed to migratory birds (although recent gene expression studies in *Oncorhynchus mykiss* indicate a visually mediated system may also exist in the species (Fitak et al. 2017; Arniella et al. 2018)), are more derived.
Based on the knowledge in which direction the gradients are decreasing and increasing locally, animals may predict how the same gradients will vary across unknown terrain further away from their range of experience.

1.4 *Scope of the study & dissertation organization*

Exactly how elasmobranchs may use magnetic fields in navigation remains an ongoing subject of debate. Certainly, it is highly likely that the electrosensory system might provide compass information as described in 1.3.3 above. An intricate study by Rivera-Vicente et al. (2011) lent further support to the likely use of magnetic electric induction in elasmobranch magnetoreceptive behaviors. The authors proposed that in accordance with the functional sub-unit hypothesis (Tricas, 2001), the directional projections and lengths of specific canal clusters of the ampullae of Lorenzini (namely the Superficial Ophthalmic Cluster in sharks,

and the Hyoid cluster in rays) render them highly suited to detecting the weak induced fields generated via the passive and active modes of electromagnetic induction.

It would seem unlikely, however, given the widespread magnetoreceptive capability across other taxa, by means other than electromagnetic induction, that this is not the only means by which elasmobranchs could perceive and use geomagnetic field information. Magnetite based systems have been proposed or described from bacteria to lobsters (Frankel et al. 1979) in invertebrates, and from teleosts, to birds to cetaceans in vertebrates (Moore & Riley 2009; Fleissner et al. 2007; Zoeger et al. 1981), it follows that elasmobranch species may possess a magnetite based magneto-receptor.

It is apparent from this review that there is a large variety of cues to orientation and navigation available, and that they function at different geographic scales. It would seem very likely that, as suggested, elasmobranch fishes employ bi-modal (Lohmann, Lohmann, et al. 2008) or perhaps more likely, multi-modal strategies in order to gain these cues. Of all the cues available, the geomagnetic field is the only one that pervades throughout the range of any and every shark species and can function on both large (ocean basins) and small (specific places/areas) scales. It is similarly the only environmental cue that can be considered 'stand-alone' in terms of true navigation, as it is possible to derive direction of travel, and latitudinal position from it, providing both the compass and map steps of true navigation.

Much of the evidence supporting sensory involvement in orientation and navigation behaviors has come from empirical studies in both field and laboratory settings, as referenced in the text above. However, empirical evidence to support orientation and navigation via magnetic field information in elasmobranch fishes is scant, and the bases by which it may be achieved could at best be described as uncertain. The following chapters describe empirical behavioral and bench studies designed to elucidate the magnetoreceptive capability, sensory acuity, sensory mechanisms, orientation behaviors and possible magnetoreceptor structures using two shark species; the scalloped hammerhead shark (*Sphyrna lewini*) and the sandbar shark (*Carcharhinus plumbeus*).

Chapter 2 was written for publication in a peer-reviewed journal. The format has been modified to the appropriate format for the requirements of the University of Hawai'i at

Mānoa. Chapter 2 investigates the ability of sandbar sharks to perceive small changes or modifications to the background magnetic field using conditioned behavioral responses as the proxy measurement. Chapter 2 goes on describe sensory impairment experiments that address criticisms of previously published behavioral response experiments, and further attempts to provide evidence for putative receptor systems in use.

Chapter 3 describes behavioral experiments designed to examine the ability of scalloped hammerhead sharks to discriminate differing/contrasting magnetic field cues, as would be required in the map step of true navigation, and the formation of a cognitive map based on geomagnetic cues. It goes on to further examine the sensory means by which the sharks tested perceived the magnetic cues.

Chapter 4 documents extensive methods employed to find physical evidence of an iron/magnetite-based receptor structure, focused on a putative elasmobranch homolog to the olfactory housed magnetoreceptor proposed in salmonids.

Chapter 2 – *Magnetic Field Perception In The Sandbar Shark (Carcharhinus Plumbeus)*

2.1 *Abstract*

Elasmobranch fishes are among a broad range of taxa believed to gain positional information and navigate using the earth's magnetic field, yet in sharks, much remains uncertain regarding the sensory receptors and pathways involved, or the exact nature of perceived stimuli. Captive sandbar sharks, *Carcharhinus plumbeus* were conditioned to respond to presentation of a magnetic stimulus by seeking out a target in anticipation of reward (food). Sharks in the study demonstrated strong responses to magnetic stimuli, making significantly more approaches to the target (p = < 0.01) during stimulus activation (S+) than before or after activation (S-). Sharks exposed to reversible magnetosensory impairment were less capable of discriminating changes to the local magnetic field, with no difference seen in approaches to the target under the S+ and S- conditions (p = 0.375). This study provides quantified detection and discrimination thresholds of magnetic stimuli presented, and quantify associated transient electrical artefacts. The study shows that the likelihood of such artefacts serving as the stimulus for observed behavioural responses was low. These impairment experiments support hypotheses that magnetic field perception in sharks is not solely performed via the electrosensory system, and that putative magnetoreceptor structures may be located in the naso-olfactory capsules of sharks.

2.2 *Introduction*

As referenced in Chapter 1, it is widely regarded that sharks and rays likely use cues gained from the geomagnetic field in orientation and navigation behaviors. Much of the focus of hypotheses to this regard has been centered on the role of the electrosensory system in perceiving electrical fields induced around the body of the animal as it moves through the geomagnetic field. However, there are few empirical studies (none of them physiology based) to provide support to these hypotheses. Further, only one of these published studies (Walker et al. 2006), has attempted to determine the sensory mechanism involved.

Behavioural studies in elasmobranchs that have provided empirical evidence for magnetic field perception have been criticised (Johnsen & Lohmann 2005; Johnsen & Lohmann 2008) for failing to sufficiently control for the possibility that sharks were responding to transient electrical artefacts caused by activation of experimental magnetic stimuli rather than changes in the ambient magnetic field *per se* (Meyer et al. 2005), or that magnetosensory impairment methods used (Walker et al. 2006) may have similarly resulted in induced electrical field stimuli that could possibly impact an induction-based magnetosensory system. The bulk of subsequent studies into the ability of elasmobranch's to perceive magnetic fields have used lanthanide metals ('rare earth' metals with strong magnetic properties) that produce strong electrical fields as a results of galvanic action as potential bycatch deterrents in fisheries (Brill et al. 2009; Robbins et al. 2011; C. P. O'Connell et al. 2011; C. O'Connell et al. 2011; Hutchinson et al. 2012; McCutcheon & Kajiura 2013). On their own, lanthanide metals are paramagnetic, meaning that they have low magnetic permeability (do not retain magnetization). Their magnetic axes will align with an external magnetic field however (Cullity & Graham 2009). Thus, metals from the lanthanide series are combined with other metals to form compounds, giving the compound strong magnetic permeability (Fraden 2010). For example, 'Neodymium' magnets are usually a compound comprised of Neodymium (the lanthanide metal), Iron and Boron. These deterrent/repellent studies have shown that different compound metals derived from the lanthanide series have differing and species–specific efficacies as a repellent, and these impacts are generally minimal, transitory and context-specific. This

latter point refers to the fact that behavioural responses are impacted by hunger motivation and the number of animals involved in the test.

Recently, Newton and Kajiura (Newton & Kajiura 2017) reported that yellow stingrays (*Urobatis jamaicensis)* could be trained to locate and feed over specific neodymium magnets in behavioural choice test experiments, which demonstrates that these metals have no intrinsic repellent properties An exception to this came from a study using adult sandbar sharks (n=3) in individual feeding trials that determined neodymium magnets could be effective as a repellent (Siegenthaler et al. 2016). Animals in the study were not fasted prior to testing.

Thus, it is apparent that the capability, physical mechanisms and sensory acuity of elasmobranch fishes in the perception and use of remains poorly understood. The experiments described herein are designed to address the points raised in the 2005 and 2008 reviews of Lohmann and Johnsen.

Specifically, the objectives of these experiments are as follows:

(1) To replicate the experiments of Meyer et al. (2005), and confirm the nature of any electrical field transient induced within the experimental tank as a function of modification to the background magnetic field.
(2) To examine the sensory acuity of the magnetosense in *C. plumbeus*.
(3) To examine the sensory mechanisms used in magnetic field perception by animals in the study. In particular, the study aims to gather supporting evidence for a non-electrosensory receptor system. Specifically, the experiment is designed to test that sharks possess an olfactory based magnetoreceptor, possibly homologous to that proposed in some teleost fish.

2.3 *Materials & Methods*

We adapted the protocol of Meyer *et al*. (Meyer et al. 2005) to condition sharks to respond to a modification of the local magnetic field. Captive Sandbar sharks were adapted the protocol of Meyer *et al*. (Meyer et al. 2005) to condition sharks to respond to a modification of the local magnetic field. Captive Sandbar sharks were housed in a 7m diameter circular tank, surrounded by 100 turns of 18 AWG copper wire, spaced over a vertical distance of 120 cm. In training and conditioning, a charge ranging from 12 V DC to 1.5 V DC with a 5.6k Ω resistor was applied to the coil, producing a localised magnetic field that varied in total intensity from 2.8 μT to 0.029 μT respectively. In testing trials, a 1.5 V DC charge with a 5.6k Ω resistor was used, to modify the local magnetic field within the experimental arena by 0.029 μT.

2.3.1 *Animal Training and Testing*

Training and test trials were carried out over a six-month period. A maximum of two weeks was allowed for training of new sharks. Up to seven animals were held and trained together during training and testing phases, as social learning in sharks has been demonstrated to be faster and more effective in behavioural studies than training novice animals alone (Guttridge et al. 2013; Guttridge & Brown 2014). To produce the conditioned response, captive sharks were presented with a food reward over an 80 x 80 cm target every time the magnetic field was modified, field modification in training varied pseudo-randomly, ranging between 2.8 μT to 0.029 μT. Animals were fed a ration of food this way every day over the course of the study period except during testing phases. To maximise feeding motivation, sharks were not fed for 24 hours prior to testing. To ensure that observed responses (convergence upon the target) were due to the conditioning protocol used, sharks in the study were not given a food reward during test trials.

Ten test trials were carried out under both unimpaired (normal) and magnetosensory impaired conditions (see *Sensory Impairment* subsection for description of impairment methods). Behavioural trials were carried out pseudo-randomly over the last four months of the six-month experimental period, with continued reinforcement training

between trials. Following the methodology of Meyer et al.(2005), each trial duration lasted 21 minutes, during which time shark behaviours were observed over a time-series comprised of 10 minutes observation under normal background magnetic field (S-), followed by a one minute modification of the local magnetic field (S+), followed by a further 10 minutes observation (S-). *Per* Meyer et al.(2005), counts of the total number of passes by all sharks over the target in each trial were pooled into one-minute time bins, across all trials.

Animals that became too aggressive, or were judged to disrupt normal conditioned behaviours by dominating or outcompeting other sharks were removed from the study once replacement animals had been trained. Under unimpaired conditions, five sharks were used for the first eight trials. Two sharks were subsequently added to the group for training, prior to the removal of two sharks from the existing pool that were judged to outcompete other sharks and disrupt conditioned behaviours. Two trials were completed with seven sharks. The increased number of sharks did not appear to affect the overall number of passes over the target during stimulus presentation (see results and Table 2.1), thus no further trials were run under control conditions.

2.3.2 *Sensory Impairment*

To induce magnetoreceptor impairment in test trials, 1.2 x 0.3 x 0.3 cm neodymium magnets (Apex Magnets, Petersburg, WV, USA) were placed in gelatine filled 2.5 x 2.5 x 1 cm plastic boxes which were temporarily (and reversibly) attached to the heads of the test animals following behavioural conditioning (Fig. 2.1).

Figure 2.1
Placement of magnets designed to impair magnetic stimulus perception. Neodymium magnets were embedded horizontally into gelatin within a sealed container, and aligned with the longitudinal axes of the olfactory organs.

The magnets were embedded horizontally within the gelatine and the boxes sealed. The gelatine serves as a semi-liquid matrix, allowing small movement of the magnets in conjunction with movement of the animal, thus maintaining a small but constant magnetic flux. Sealing the containers prevented any contact between the magnet and sea water, eliminating the possibility of electrical currents forming as a result of galvanic action. Maximal magnetic flux over putative magnetoreceptor structures was achieved through alignment of the longitudinal axes of the magnets magnets and the olfactory organs. Thus, the magnetic flux created generated a constant source of magnetic 'noise'. These boxes were glued to the skin of the shark over the dorsal surface of olfactory capsules. Sharks continued behavioural reinforcement/training under variable strength magnetic field modification, as per the methods used in the control series.
To ensure that sharks that had undergone impairment treatment were capable of producing the conditioned response (CR), five trials were conducted at higher presented magnetic field strengths (8 – 1.2μT). These initial tests followed the same protocol as that used in control/unimpaired testing (trials carried out pseudo-randomly, animals not fed during testing, constant training/reinforcement with food reward between trials).

Five sharks were used in initial training and testing in the magnetic impaired series. However, two sharks were removed from the study prior to commencement of trials at 0.03μT, both of which had grown considerably larger than, and outcompeted the remaining three sharks. Two trials at 0.03μT were initially run with three sharks, before a fourth shark was added to the test group. When this shark had been sufficiently conditioned, a further seven trials were run using four sharks. One further shark was removed (due to the same reasons) for the remaining trial. Sharks in both the unimpaired and impaired groups were trained and tested together, with the exception of the final shark added in the impaired trial series, which was trained but not tested under control conditions.

All experiments were approved by the University of Hawaii Institutional Animal Care Advisory Committee (IACUC), protocol # 13-1749. All methods used were in accordance with the approved protocol, and the IACUC guidelines set out.

2.3.3 *Data Collection and Analysis*

A total of 20 trials were carried out under control/normal (unimpaired, n=10) and experimental (sensory impaired, n=10) conditions. Each trial was recorded remotely from an aerial perspective for subsequent analysis using a high-resolution video camera. Sharks in the study were tested as a group, as count information was not available on an individual level, due to the difficulty in reliably identifying individual sharks in each trial across the series. Thus, counts of total passes over the target by all sharks, in each minute of each trial were pooled into one-minute time bins. The median number of passes and the standard error of the mean for each one-minute time bin across all ten trials under both experimental conditions (unimpaired/impaired) was subsequently calculated.

The number of sharks used in testing was not constant across either series of trials (unimpaired/impaired), thus, to standardize our data we calculated the proportion of passes across the target, averaged per shark, per minute, for every trial, in each series. Our data did not follow a normal distribution, thus, Friedman Rank Sum tests and Wilcoxon Signed Rank post-hoc analysis were used to discriminate any differences in

mean proportion of passes, per shark, between time bins and to identify where differences arose for each trial series (unimpaired/impaired).
Wilcoxon Rank Sum tests were used to compare mean proportion of passes across the target, per shark, in the 11th minute (S+) time-bin under normal and impaired conditions.

2.3.4 *Characterising the Magnetic and Electric Fields*

Modifications to the local magnetic field were measured using a MR3 Milligauss Meter (AlphaLab Inc., Salt Lake City, UT, USA). Measurement of any induced transient electrical artefact in the uniform electrical field associated with supplying power to the coil was measured using a Trifield® Natural EM Meter (AlphaLab Inc., Salt Lake City, UT, USA). Equipment normally used in electrophysiological experiments was also modified to measure transient voltage gradients. Nonpolarizable Ag-AgCl half-cell electrodes (World Precision Instruments Inc, Sarasota, Fl) were fitted to agar-filled capillary tubes that were immersed in the water in different locations throughout the test arena. The output from the two electrodes was differentially amplified (DP-304; Warner Instruments) at 1000x–10,000x, filtered at 60 Hz (Hum Bug, Quest Scientific, Vancouver, British Columbia), digitized on a recording oscilloscope (Tektronix Inc, Beaverton, Or).

2.3.5 *Electric Field Calculation*

The induced electrical field (Volts m) at any point in time, at any point in the tank can be calculated from Faraday's Law of Induction:

$$\varepsilon_{ind} = \oint \vec{E}_{ind} \cdot d\vec{s} = -\frac{d}{dt}(\Phi_B)$$

Whereby the induced electrical field (ε_{ind}) within the coil is equal to the negative time rate of change of the rate of magnetic flux ($-\frac{d}{dt}(\Phi_B)$).

(1)

∴

$$\oint \vec{E} \cdot d\vec{s} = 2\pi r|E|$$

Thus, we can calculate ε_{ind} around the whole circuit, using a line integral, summing the EMF produced at each and every point over the length of the wire (coil).

(2)

While

$$\frac{d}{dt}(\Phi_B) = \frac{d}{dt}\ (B\ A)$$

ε_{ind} is equal to the time rate of change magnetic flux, which is equal to the time rate of change of the product of the perpendicular component of the magnetic field (B) and the area inside the coil (A).

(3)

$$\therefore$$

$$= \frac{d}{dt}(B\ \pi\ r^2)$$

(4)

$$=\ \pi\ r^2\ \mu_\circ \frac{d}{dt}(I(t))$$

Alternatively, ε_{ind} can expressed as formula 5; the area inside the coil multiplied by the time rate of change of the current in the circuit ($\frac{d}{dt}(I(t))$), where ($\mu_\circ$) is the magnetic permeability constant according to Biot-Savart law.

(5)

This can be simplified to formula 6.

$$=\ \pi\ r^2\ \cdot\ \mu_\circ\ b$$

Where (b) is a constant equal to $\frac{d}{dt}(I(t))$.

(6)

Therefore, using Faraday's Law in general form:

$$2\pi r\mathrm{E} = \pi r^2 \cdot \mu_\circ\ b$$

(7)

Thus

$$\mathrm{E} = \frac{(-\pi r^2\ \mu_\circ\ b)}{2\pi r}$$

Where r is the distance (metres) from the axis of the coil (the centre of the tank).

(8)

Change or flux in the magnetic field within the tank occurs during the time taken for the current moving through the circuit (coil) to reach its' maximum value. To determine *d*t, it is first necessary to calculate inductance within the coil. As the length (height) of the coil is not greater than its diameter, it is not appropriate to use standard equations for coil inductance. Instead, it is appropriate to model inductance using Wheelers' formula (11) (Wheeler 1982), which improves upon the equation put forward by Nagaoka (Nagaoka 1909).

$$L_s = .002\pi d N^2 [\ln\left(1 + \frac{\pi d}{2\ell}\right) + \frac{1}{2.3004 + \frac{3.2\ell}{d} + 1.7636\left(\frac{\ell}{d}\right)^2}]$$

where L_S is in μH; d= coil diameter (cm); ℓ =coil height (cm); N=number of turns.

(9)

Having calculated inductance, we then modelled current flow in the circuit using the LTspice IV (Linear Technology, CA, USA) modelling program, to determine *d*t (time taken for current in the circuit to reach its steady-state value). However, we must express ε_{ind} as a function of time (as ε_{ind} is dependent upon magnetic flux, and magnetic flux is dependent upon the time taken to reach steady state value, i.e. the time taken for current in the circuit to reach a steady state) (formula 9).

$$\varepsilon_{ind}(\mathrm{t}) = \frac{r}{2} \,.\, \mu_{\circ}\, b$$

r = distance (metres) from the axis of the coil (the centre of the tank)

(10)

Finally, we can account for the specific physical characteristics of the coil used in our experiments; namely determining the number of turns of the coil per unit height.

$$\varepsilon_{ind}(\mathrm{t}) = \frac{\mu_{\circ}\, \mathrm{r}\, \mathrm{N}\, \mathrm{b}}{2h}$$

Where $\mu_{\circ}$ is the magnetic permeability of the medium, r is the distance (metres) from the axis of the coil (the centre of the tank), N is the number of turns of the coil, b is time rate

of change of the current in the circuit to reach a steady state [$\frac{d}{dt}\big(I(\mathrm{t})\big)$], h is the height of the coil.

(11)

2.4 *Results*

2.4.1 *Responses to magnetic stimuli*

Sharks were successfully conditioned to respond to the presentation of a magnetic stimulus (S+). Unimpaired, conditioned sharks produced a 100% response (all sharks demonstrating a conditioned response) to all applied magnetic field intensities used in training and conditioning, which ranged from 0.03 to 2.89 micro-Tesla (μT). Conditioned sharks reacted by increasing tail beat frequency and swim speed, then converging on the target in anticipation of receiving a food reward. In test trials (food reward not given), the number of passes over the target by all animals combined during the S+ minute ranged between 6 and 19, with a median pass rate of 13.5 ± 3.8 (Fig. 2.2 (A)).

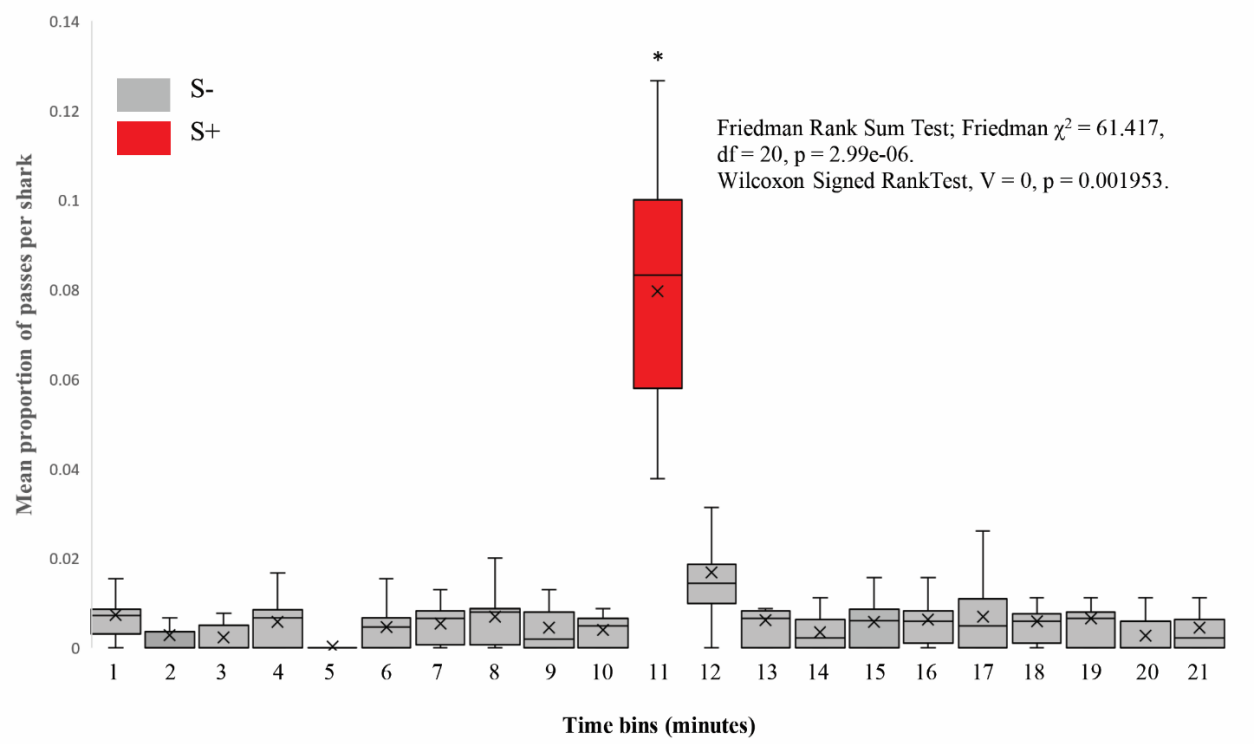

Figure 2.2 *Behavioral responses of unimpaired sharks to presented magnetic stimulus.* Box & Whisker plot showing mean proportion of passes over the target, per shark, across the series of ten unimpaired trials, mean value is denoted by x. S+minute is shaded red, all other 1 minute time bins (S−) are shaded grey. Friedman Rank Sum tests were used to determine any differences in time bins. Wilcoxon Signed Rank Tests were used to compare mean proportion of passes over the target, averaged per shark in the eleventh minute time bin with each other one minute time bin. Averaged per shark, a significantly higher proportion of passes over the target was seen in the S+ (11th) minute. *p <0.01.

By comparison, median number of passes for all S- one-minute bins across all 10 trials ranged from 0-2. The median number of passes for all other one minute time bins combined under 'control' (non-stimulus) conditions was 1 ± 0.89. The number of sharks used across the series of 10 unimpaired trials did not remain constant. 5 animals were used for the first eight trials, 7 animals were used in the final two trials. The number of passes across the target in the S+ minute during the final two trials in this series did not increase as a result of more sharks being present. The 95% confidence intervals for the control group were 0.0589 and 0.100. One data point fell above this interval, from a trial with five sharks. Three data points fell below this range (i.e. proportion of responses, averaged per

shark was low) (Table 2.1). One of these data points came from a trial using five sharks, the other two came from the two trials using seven sharks (Table 2.1).

Proportion of passes over the target, averaged per shark, during the S+ minute were significantly greater than in any other one-minute time bin (Fig. 2.1 (B)), Friedman Rank Sum Test; Friedman $\chi^2 = 61.417$, df = 20, $p = 2.99e^{-06}$, Wilcoxon Signed Rank Test, Test, V = 0, $p = 0.001953$.

Table 2.1 *Proportion of passes over the target, per shark, across the series of ten unimpaired trials*. The number of sharks tested in each trial is shown. 95% confidence intervals were 0.0589 and 0.100. S+ (11th) minute is highlighted in red.

Trial #	**1**	**2**	**3**	**4**	**5**	**6**	**7**	**8**	**9**	**10**
# Sharks	5	5	5	5	5	5	5	5	7	7
Minute										
1	0	0.009	0.008	0.006	0	0.015	0.02	0.008	0.004	0.003
2	0	0	0.004	0	0	0.015	0.007	0	0	0.003
3	0	0	0.004	0	0	0.008	0.007	0	0	0.005
4	0.007	0.009	0	0	0	0.008	0.007	0.017	0	0.011
5	0	0	0	0	0	0	0	0	0	0.003
6	0.007	0	0.004	0	0	0.015	0.007	0	0.009	0.005
7	0.007	0.009	0	0.006	0	0.008	0	0.008	0.013	0.003
8	0.02	0.009	0	0.013	0	0.008	0	0.008	0.009	0.003
9	0	0	0.004	0.013	0	0.008	0	0	0.013	0.008
10	0.007	0.009	0.008	0.006	0	0	0	0	0.004	0.005
11	0.127	0.07	0.063	0.097	0.1	0.046	0.1	0.1	0.056	0.038
12	0.013	0	0.031	0.019	0.044	0.015	0.013	0.017	0.009	0.005
13	0.007	0.009	0.008	0.006	0	0.023	0	0.008	0	0
14	0	0	0	0	0.011	0.008	0.007	0	0.004	0.005
15	0	0.009	0.016	0.013	0	0.008	0	0	0.004	0.008
16	0.007	0.009	0.016	0.006	0	0.015	0	0	0.004	0.005
17	0	0.026	0.012	0	0	0	0.013	0.008	0.004	0.005
18	0	0.017	0.008	0.006	0.011	0	0.007	0	0.004	0.005
19	0	0	0.008	0.006	0.011	0	0.007	0.025	0	0.008
20	0	0	0.008	0	0.011	0	0	0	0	0.008
21	0	0.017	0	0	0.011	0	0.007	0	0.004	0.005

2.4.2 *Responses to magnetic stimuli following sensory impairment*

To induce magnetosensory impairment in sharks, magnets were (reversibly) attached to the dorsal surface of the head (Fig. 2.1). The test animals showed no adverse responses to the manipulations involved with attachment and removal of the sensory impairment devices.

Table 2.2 *Conditioned behavioural responses of sensory-impaired sharks to presentation of stronger magnetic stimuli*. Counts of passes over the target, summed for all sharks (n=5), for each minute of each trial are shown. S+ (11th) minute is highlighted in red.

Trial no.	1	2	3	4	5
***B* field (μT)**	8	8	5.3	1.2	1.4
No. sharks	5	5	5	5	5
Minute	**Passes over target**				
1	1	0	5	1	1
2	3	0	2	1	1
3	0	2	1	2	1
4	0	1	1	1	2
5	1	0	4	0	2
6	0	1	0	1	4
7	0	2	3	2	2
8	1	1	4	2	1
9	1	3	3	2	2
10	2	0	2	3	2
11	9	12	8	5	3
12	4	2	2	0	1
13	2	1	1	3	1
14	2	2	1	1	2
15	0	1	3	1	1
16	0	3	2	1	1
17	1	0	2	0	1
18	1	0	1	3	0
19	1	1	2	0	5
20	2	0	5	2	2
21	0	1	1	2	2

Animals were observed to swim in a normal fashion, and fed readily when presented with the food reward in training/conditioning. Sharks that had undergone impairment treatment successfully produced the CR in as little as thirty minutes following application of the impairment devices. A strong conditioned response continued to be evoked during training and reinforcement across the duration of the impaired trial series. Thus, the physical manipulation of the animals and attachment of the magnets was judged not to impair conditioned feeding responses. In initial impairment testing, sharks again produced the conditioned response (faster swimming, elevated tailbeat frequency, convergence upon the target) upon presentation of these higher magnetic stimuli. Notably, the magnitude of the conditioned response decreased when the magnetic stimulus presented was reduced (Table 2.2).

To compare the conditioned responses of control/normal and impaired sharks, magnetic stimuli of ecologically relevant magnitudes (0.03 μT) were applied to the experimental arena. Four sharks were used in seven of the ten trials, three in the remaining three trials. In all cases the CR evoked from impaired animals when presented with the 0.03 μT stimulus was markedly diminished when compared to sharks without sensory impairment. Increases in tailbeat frequency were visibly smaller and a faster return to 'normal' background behaviour was also observed in impaired animals. However, the magnitude of the conditioned response during impairment testing was variable (range = 0 - 7 passes per trial). In these tests, both the highest and lowest number of passes across the target occurred in trials with four animals. No significant difference was seen in the overall response in the S+ minute across all ten trials in this impaired series (Friedman Rank Sum Test, $\chi^2 = 22.765$, df = 20, p = 0.301). The median pass rate in the S+ minute was 2 ± 2.4, median pass rate for all other time bins was 1 ± 0.98 (Fig. 2.3 (**A**)). No difference was found in the proportion of passes, averaged per shark, over the target between the S+ and S- conditions (Fig. 2.3 (**B**), Friedman Rank Sum Test, $\chi^2 = 21.382$, df = 20, p = 0.375).

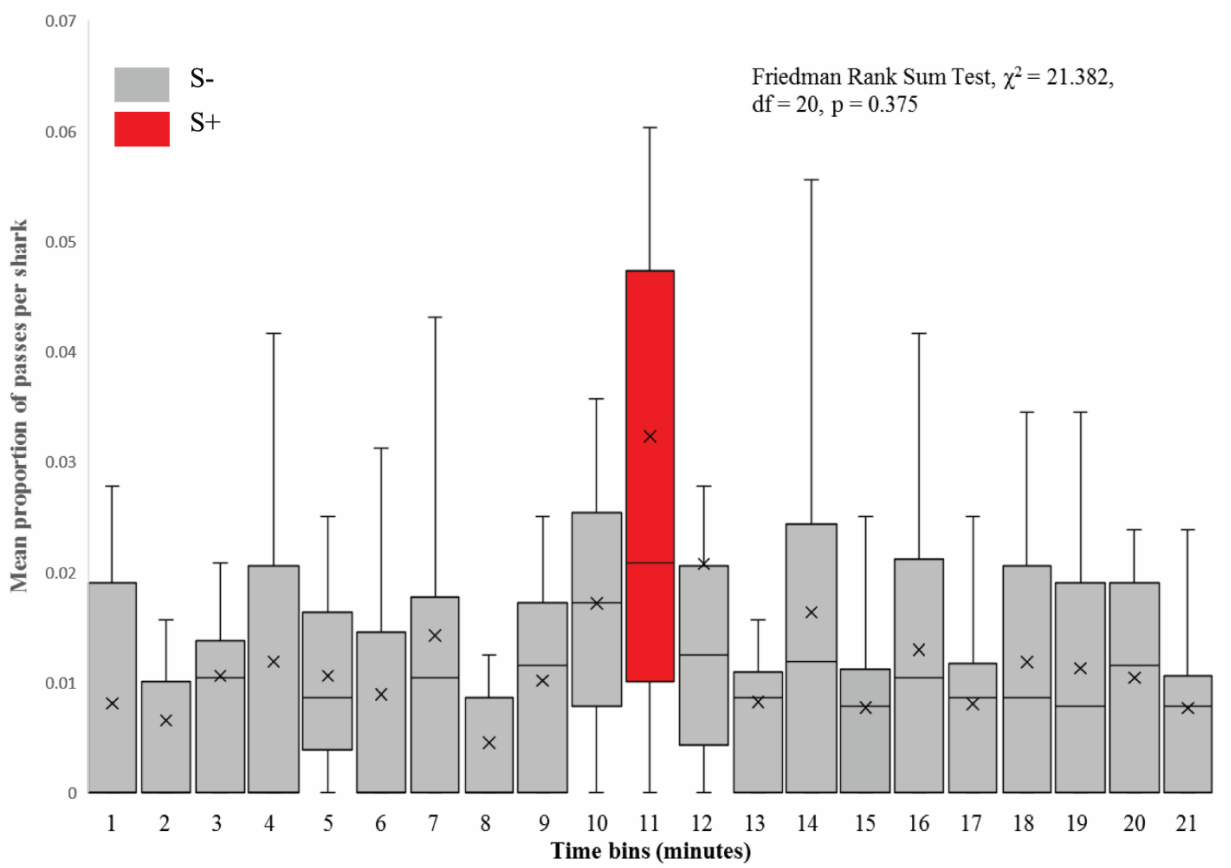

Figure 2.3. *Behavioural responses of sensory impaired sharks to presented magnetic stimulus.* Box & Whisker plot showing mean proportion of passes over the target, per shark, across the series of ten sensory-impaired trials, mean value is denoted by x. S+ minute is shaded red, all other 1 minute time bins (S-) are shaded grey. Friedman Rank Sum tests were used to determine any differences in time bins. No difference was found under S+ or S- conditions when animals had undergone magnetic impairment treatment.
S+ minute is shaded red. Error bars show standard error.

95% confidence intervals were 0.012 and 0.059. Four data points fell below this range, two from trials using three sharks, two from trials using four sharks (Table 2.3). One data point was above this range (four shark trial). The remaining five trials fell within the confidence interval (Table 2.3). The proportion of passes over the target, averaged per shark, in the S+ minute of the unimpaired/normal series of trials was found to be significantly greater than in the S+ minute of the sensory-impaired series (Wilcoxon Ranked Sum Test, W = 85, p = 0.009).

Table 2.3. *Mean proportion of passes over the target, per shark, across the series of ten impaired trials.* The number of sharks tested in each trial is shown. 95% confidence intervals were 0.012 and 0.059. S+ (11th) minute is highlighted in red.

Trial #	**1**	**2**	**3**	**4**	**5**	**6**	**7**	**8**	**9**	**10**
# Sharks	5	5	5	5	5	5	5	5	7	7
Minute										
1	0.000	0.023	0.000	0.000	0.017	0.021	0.000	0.028	0.000	0.000
2	0.000	0.011	0.016	0.009	0.009	0.000	0.000	0.028	0.000	0.000
3	0.012	0.011	0.016	0.009	0.000	0.021	0.010	0.000	0.038	0.000
4	0.024	0.000	0.039	0.009	0.017	0.000	0.042	0.000	0.000	0.000
5	0.012	0.023	0.008	0.009	0.009	0.021	0.010	0.000	0.025	0.000
6	0.012	0.011	0.031	0.026	0.017	0.000	0.000	0.000	0.000	0.000
7	0.012	0.023	0.000	0.043	0.000	0.000	0.010	0.000	0.013	0.056
8	0.012	0.000	0.008	0.009	0.009	0.000	0.000	0.000	0.013	0.000
9	0.012	0.011	0.008	0.017	0.017	0.000	0.021	0.000	0.025	0.000
10	0.036	0.023	0.016	0.017	0.017	0.021	0.031	0.028	0.000	0.000
11	0.036	0.011	0.039	0.009	0.060	0.021	0.000	0.056	0.013	0.111
12	0.024	0.011	0.016	0.009	0.017	0.000	0.000	0.028	0.013	0.111
13	0.036	0.011	0.016	0.009	0.009	0.000	0.010	0.000	0.000	0.000
14	0.012	0.034	0.000	0.009	0.000	0.021	0.021	0.028	0.000	0.056
15	0.012	0.000	0.008	0.000	0.009	0.021	0.010	0.000	0.025	0.000
16	0.000	0.011	0.000	0.009	0.017	0.042	0.010	0.028	0.025	0.000
17	0.012	0.011	0.000	0.009	0.000	0.021	0.010	0.000	0.025	0.000
18	0.024	0.034	0.008	0.009	0.017	0.000	0.010	0.028	0.000	0.000
19	0.000	0.034	0.008	0.017	0.000	0.021	0.031	0.000	0.013	0.000
20	0.024	0.011	0.008	0.017	0.000	0.021	0.021	0.000	0.013	0.000
21	0.024	0.023	0.008	0.009	0.009	0.000	0.000	0.000	0.013	0.000

2.4.3 *Electrical field measurement and calculation*

The magnetic field within the tank varied according to the current applied (Fig. 2.4). Incorporation of a 5.6k ohm (Ω) resistor in the circuit resulted in small and more uniform magnetic field across the diameter of the tank. A 1.5v applied charge combined with the 5.6k Ω resistor resulted in a magnetic field generation of 0.029 μT above the local field (Fig. 2.4).

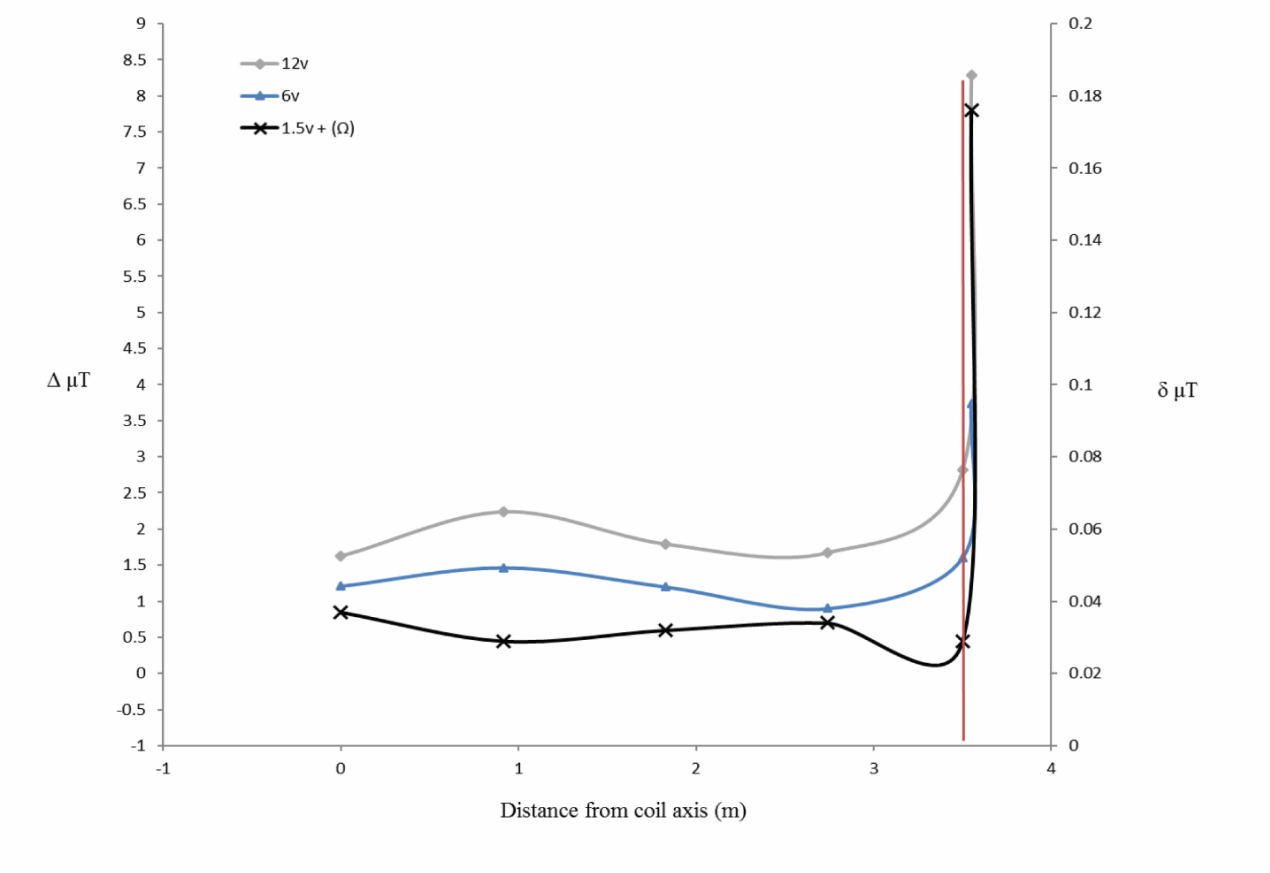

Figure 2.4. *Measured profiles of total magnetic intensity*. Changes in magnetic field intensity (μT) associated with magnetic stimulus presentation were measured across the diameter of the tank at increments of 3 ft (0.9144m), from centre (0m) to periphery (3.5m) (coil axis is the centre of the tank). Y axis values correspond to magnetic field changes (Δ μT) associated with use of 12 volt and 6 volt power sources. Z axis values correspond to magnetic field changes (δ μT) associated with use of 1.5 volt power source, with 5.6k Ω of resistance built into the circuit. Vertical red line indicates tank periphery.

Electric field measurements taken with a Trifield® Natural EM Meter before, during and after circuit activation revealed a variable background electrical field oscillation with a range as high as 51 milliVolts per metre (mV/m^{-1}) occurring over a period 0.5 seconds (Fig. 2.5). Thus, background electrical flux was as high as 1 mV/ cm/s^{-1}. Transient electrical artefacts induced by changing the magnetic field occurred within this range of background noise, and thus were undetectable using the meter. Subsequent efforts to measure transient induced voltage gradients using electrophysiological equipment also proved unsuccessful, due to the complexity of background electrical noise (Fig. 2.5).

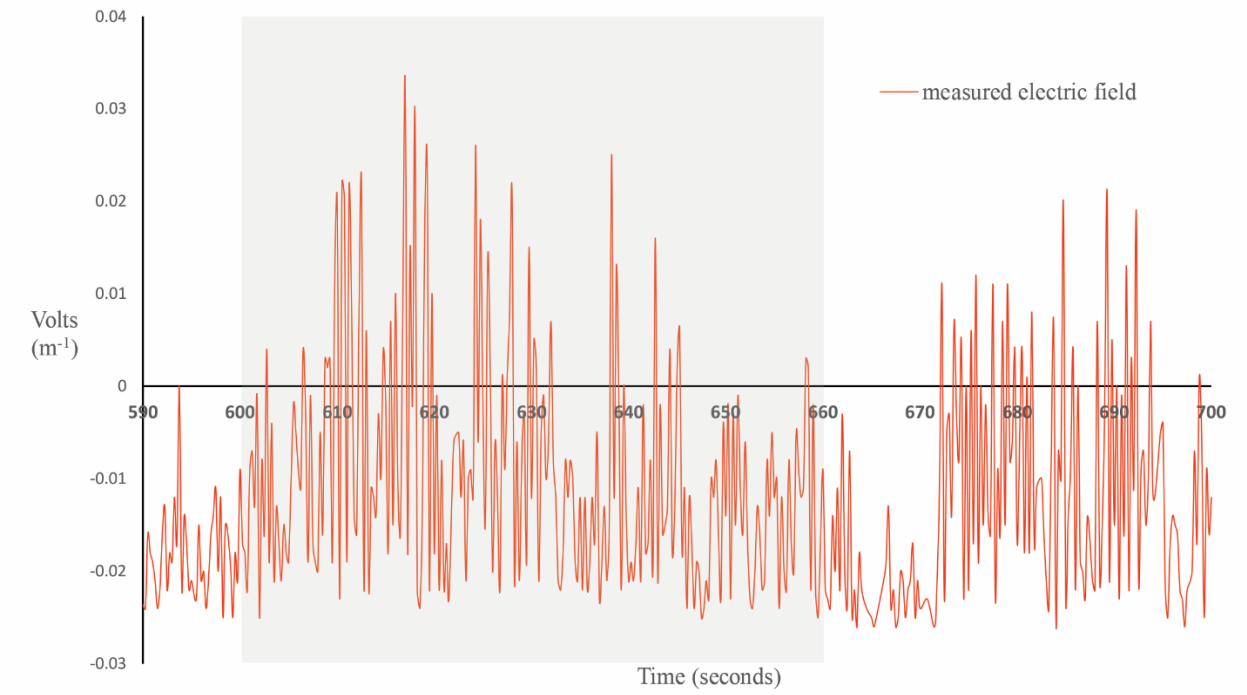

Figure 2.5. *Electrical field measurements associated with background electrical noise*. Electrical field artefacts occurring during presentation of the magnetic stimulus were measured using a Trifield® Natural EM Meter (AlphaLab Inc., Salt Lake City, UT, USA), capable of taking measurements every millisecond. Grey shaded region indicates period of magnetic field activation (S+ minute; 600 - 660 seconds). *N.b*. the constant and random fluctuation of background electrical noise in the environment, both before, during and after magnetic field activation. Maximum range of recorded background electrical field oscillation (noise) during the period of stimulus activation was 51 mV, occurring at rate of 1.02 mV/cm/s-1. Peak voltage (maximum "spike" above zero) was 33 mV, or 3.3e^{7} nV which occurred 17 seconds after stimulus activation.

Thus, we calculated the magnitude of any transient voltage gradient using a combination of Faraday's Laws and Maxwell's equations (see Methods). Calculated transient voltage gradients were highest at the periphery of the tank and weakest (zero) in the centre (Fig. 2.6). Under application of weak magnetic fields (0.029 μT) used in testing, the maximum transient voltage gradient was calculated to be 74.35 nanoVolts (nV) cm/s^{-1} (Fig. 2.6) at the periphery of the tank. This induced electric field decays as a function of the inverse cube of the distance from the coil, but our calculations indicate that it remained above the 30 nV cm^{-1} median sensory threshold across more than half of the experimental arena (Fig. 2.6). The time taken for the current flowing in the circuit to reach a steady state, thus the duration of a transient voltage gradient within the experimental arena, was 2.7 milliseconds. We observed 100% response to presentation of magnetic fields of this magnitude (0.029 μT) in unimpaired sharks.

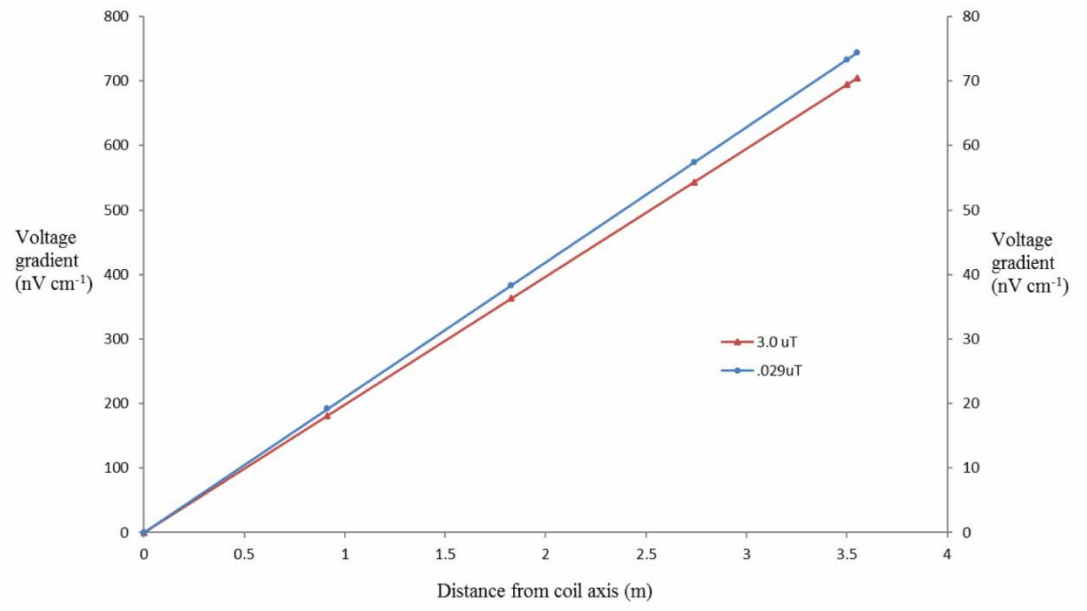

Figure 2.6. *Calculated induced voltage gradient associated with magnetic stimulus*. Modelled gradients correspond to changes in total magnetic field intensity of 3 μT (red line) and 0.029 μT (blue line) respectively. Red line corresponds to Y axis, blue line corresponds to Z (secondary) axis. Voltage gradients induced by modification of the local magnetic field within the tank were calculated from centre (coil axis – 0m) to periphery (3.5m) at increments of 3 ft (0.9144m). Induced voltages increased linearly with distance, peaking at 73.3 nV cm-1 at the tank periphery when a magnetic field modification of 0.029 μT was applied. Calculated time to reach peak induced voltage gradient following onset of magnetic stimulus was 2.7 milliseconds.

2.5 *Discussion*

2.5.1

In their 2005 review, Johnsen and Lohmann suggested that conditioned-behaviour magnetic field experiments such as those of Meyer et al. (2005) could not unequivocally claim that shark responses were to magnetic stimuli *per se* because it was possible that the activation of a Helmholtz coil (or similar magnetic field generation method) would produce a transient electrical field that could be detected by the electrosensory receptors of the test animals. They similarly argued that experiments reported by Walker (2006) may also have been influenced by induced electrical effects that were not accounted for. In the current experiment, the background ambient electric field environment was quantified and transient voltage gradients induced through activation of an altered magnetic environment were calculated. All sharks used in the study (normal and impaired conditions) were fasted for 24 hours before testing, and were not fed during test trials. Thus, motivation to feed would not be expected to be a factor that might alter the response of the animals under presentation of different strengths of magnetic stimuli used in training and in testing.

In the experiments reported here, a single coil with 100 loops was used to introduce an altered magnetic field within the tank. Electrical field tests using both a field probe and an electrophysiological recording set-up, conducted within the tank from the periphery to centre at intervals of three feet (91 cm), were unable to register a transient voltage gradient during activation of the stimulus coil. This was largely due to complex and fluctuating background electrical noise (Fig. 2.5). In the test arena used in the study, electrical noise fluctuated unpredictably, and fell within a range of 0 to 51 mV (Fig. 2.5). Empirical investigation has found the minimum voltage required to elicit any behavioural response in C. *plumbeus* was found to be 0.5 nV cm^{-1}, while the median behavioural response threshold for C. *plumbeus* was found to be 30 nV cm^{-1} (Kajiura & Holland 2002). The median sensitivity to electrical stimuli reported across elasmobranch species is 35 nV cm^{-1} (Bedore & Kajiura 2013).

The magnitude of possible transient electrical field artefacts at different points in the tank were calculated using the different magnetic field strengths applied in both training and

testing. Modelling induced transient electrical fields in this way estimated a maximum voltage gradient of 74.35 nV cm/s^{-1} (Fig. 2.6) at the periphery of the tank, when a magnetic field change of 0.03 μT was presented. Sharks swimming through more than half of the radial area (from periphery to core) of the tank, at the time the charge was applied to the coil, would be exposed to transient electrical voltage gradients that previous experiments indicate were of a magnitude detectable via their electrosensory system (Bedore & Kajiura 2013). Thus, it cannot be definitively ruled out that the shark electrosense is involved in observed conditioned responses. The responses of conditioned animals tested under these circumstances are discussed hereon. For reasons described below, it is unlikely that the transient voltage gradient acts as the stimulus or cue for the conditioned behavioural response.

In trials under control (unimpaired) conditions, the proportion of passes across the target, averaged per shark, was found to be significantly greater in the S+ minute than any other one-minute time bin (Fig. 2.1(**B**)). This finding is unsurprising, as it replicates the findings reported by Meyer et al. (2005), although the applied magnetic field intensities in the Meyer et al. study were considerably higher than those applied in the present study. Nonetheless, response rates were comparable.

2.5.2

Perception thresholds of elasmobranchs to electrical stimuli have been well studied. Elasmobranch primary afferent (sensory neuron) response characteristics indicate adaptations to detection of weak phasic (sinusoidal) electrical fields near 1-2 hertz (Hz) (Tricas & New 1998), such as those generated by ventilatory apparatus movement in prey. For an animal in the study to respond to any transient electrical artefact as a behavioural cue, it would need to distinguish the 'signal' of the induced electrical artefact from background electrical noise, as well as common-mode stimuli such as fields generated from its own ventilatory and osmoregulatory functions (Montgomery & Bodznick 1993). Habituation to electrical noise is possible, as long as it is a common-mode stimulus. Electrical noise in our experimental arena comes from multiple sources from within and

outside of the building. Thus, it does not occur predictably, cyclically, or phasically. It is possible however, that once a source of electric field noise has become active, sharks in the experimental arena could habituate to some of this noise produced.

Key sources of random and unpredictable noise in this study come from electromagnetic interference (EMI), or radio-frequency interference (RFI), much of which is generated from the nearby airbase. These sources of noise are constant, but random and variable in both size and frequency. Thus, there is constant electrical noise in the tank from a variety of sources, with varying amplitude and frequency. It is very unlikely that the adaptive filter mechanism will suppress all this noise. Thus, entraining to the very small induced "spike" or electrical artefact seen when the coil is turned on is highly unlikely. The electrical artefact in the current experiments is small (maximum 74.35 nV/cm/s^{-1}) not phasic, is very brief (2.7 milliseconds), and is presented against a complex electrical background comprised of e-fields several orders of magnitude greater (up to 1 mV/ cm/s^{-1}) than those generated by activation of the coil (Fig. 2.7).

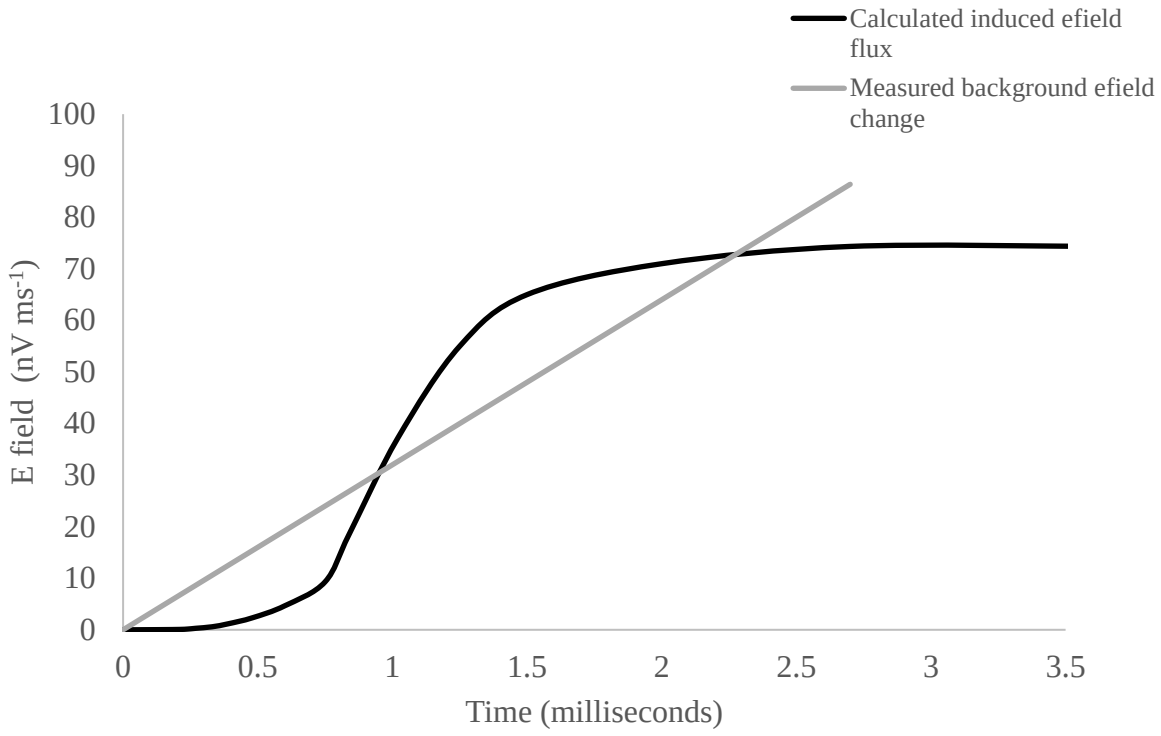

Figure 2.7 *Graph of background efield change against induced efield flux*.

In the example of background field flux shown in Figure 2.5, the change in background electrical field environment measure is 8000 nV (0.008 mV) over a quarter of a second. If one assumes this flux is uniform, then the rate of change of the electric field from the point of coil activation to ¼ of a second later is 32 nV ms^{-1} (Fig. 2.7). The calculated flux (in nV) induced by activation of the coil is variable, but overall is a change of 74.35 nV, occurring over 2.7 ms (Fig. 2.7), thus, the average rate of change of the e-field as a result of coil activation is 27.5 nV ms^{-1}. In this particular example, the measured background electric field continues to increase beyond the 2.7 ms it takes for the current within the coil to achieve a steady state (i.e. zero flux) (Fig. 2.5), thus, the change in the background field seen cannot be attributed to the flux generated by coil activation alone. Certainly, the flux from coil activation would contribute to measured background field change, but if the contribution is smaller than that from other sources, it is likely not distinguishable by the meter, or by the animal. Again, entraining to the transient 'signal' generated by coil activation as a behavioural cue would be very challenging, and would likely still be challenging in a "quieter" environment.

Given the constant noisy electrical background described, it could be expected that if the electrosensory system was solely responsible for detecting magnetic fields, a reduction in behavioural response would occur when presented with such weak magnetic stimuli and associated electrical transients. Such a diminished response with unimpaired animals was not observed. It cannot definitively concluded that the responses observed resulted solely from perception of the magnetic stimulus rather than perception of any transient electrical artefact. However, the hypothesis that the ampullae of Lorenzini and the shark electrosensory system may not be the sole sensory receptor structures used to perceive magnetic field stimuli can still be invoked. The magnitude of magnetic stimuli presented in these experiments is within the range of values that Klimley (1993) hypothesised for navigation via magnetic fields in scalloped hammerhead sharks, *Sphyrna lewini* (Griffith and Smith, 1834), found in association with the Espirito Santo seamount complex in the Gulf of California. Klimley mapped the associated magnetic gradients in this region and

found there to be less than a 50 nT range between magnetic maxima and minima. These data lend support to Klimley's hypothesis that sharks can navigate via geomagnetic topotaxis (see chapter 3), whereby he argued sharks navigate between seamounts through recognition of the magnetic field gradients at specific locations. To achieve this, sharks must be able to perceive weak changes in the background magnetic field. Sharks in the present study were able to perceive and respond to changes as low as 0.03 μT, or 30 nT. This was the lowest field strength we could reliably measure. It is possible then, that sharks could perceive and respond to field changes weaker than those reported here. The modifications to the vertical component of the local magnetic field in the experimental tank affected the intensity or strength of the field within the tank, but did not affect magnetic field polarity (north-south directionality of the magnetic field). According to the principles of the active mode of induction proposed by Kalmijn (1981; 1982), Paulin (1995), and Molteno & Kennedy (2009), it is the horizontal (polarity) component of the earth's magnetic field that induce vertical electric fields that could convey information regarding magnetic field directionality. Rivera-Vicente et al. (2011) proposed that in sandbar sharks, the Superficial Ophthalmic (posterior) cluster of the ampullae of Lorenzini are the most sensitive to changes in the horizontal electric field, that would coincide with the passive mode of induction as the animal experiences changes in the vertical component of the magnetic field. It is therefore possible that animals in the study can perceive the presented magnetic field changes via these pore clusters. However, there is not *a priori* reason for the placement and location of the magnet-containing capsules to interfere with this system. Perhaps, therefore, sharks do not solely rely on the passive mode of magnetic-electric induction for detection of changes to the vertical component, or overall intensity of the geomagnetic field. This can help explain why observed responses in the impairment series were notably reduced, but not removed entirely. The induction based magnetoreceptor system is used to gain a compass heading regarding direction of travel, whereas direct magnetoreceptor mechanisms (e.g. a magnetite-based system) are proposed to facilitate detection of anomalies or changes in magnetic field inclination or intensity, as occurred in this study (intensity). These results therefore lend further support to hypotheses of non-electrosensory mediated magnetoreception.

2.5.3

An alternative hypothesised mechanism is magnetite-based magnetoreception, based on the presence of single-domain biogenic magnetite (Fe_3O_4) within specific tissues. These ferromagnetic crystals are proposed to form chains within cells, and changes in the ambient magnetic field directs the orientation of these chains. Clusters or chains of such crystals are necessary, as opposed to individual crystals, as this prevents oscillation of individual crystals in response to background thermal energy. Such structures have been described in some teleost and avian species (Walker et al. 1997; Diebel et al. 2000; Beason & Nichols 1984; Beason & Semm 1996). The impairment experiments incorporated into this study were based on the hypothesis that elasmobranchs may be able to discriminate magnetic field intensities via a system homologous to that exhibited in some teleosts and birds. Thus, the sensory impairment trials were designed to further elucidate the existence of such structures.

Neodymium magnets embedded into gelatine filled, sealed containers were used to functionally block shark putative magnetoreceptor structures by creating a constant source of magnetic noise in the region of putative magnetoreceptor structures (in this case, putative structures housed within the olfactory organs). Encasing the magnets protects them from any galvanic action or electrochemical reactions arising from contact with the seawater, which may cause irritation to sharks in the form of overwhelming the electrosensory system, or a localized change in pH (Brill et al. 2009; McCutcheon & Kajiura 2013). Sharks that had undergone impairment treatment were observed to swim normally, and feed readily with the magnets in place, without presentation of the magnetic stimulus. Normal behaviors of sharks in the tank were thus judged to not be affected by magnetic impairment treatment.

To ensure any change in response rates was due to the magnetic noise created by the impairment devices, rather than being a function of handling or application of the boxes containing the magnets, impaired sharks were presented with higher intensity magnetic stimulus (8 – 1.2μT) but were not fed or given a food reward, *per* the protocol used in testing. Strong conditioned responses where observed when impaired sharks were

presented with stronger magnetic stimuli (8 – 5.3μT) (Table 2.2), by comparison, weaker conditioned responses were observed when the magnetic stimulus was reduced (1.2 – 1.4μT) (Table 2.2). Impairment treatment was judged to not effect response rates at higher applied magnetic intensities. This indicated magnetic flux and noise created by the neodymium magnets was not sufficient to mask stronger stimuli. Observations during these initial trials indicated that application of the magnet containing boxes to the heads of sharks, and the physical weight of the magnets within boxes had no adverse effect on normal behaviours, or conditioned responses. However, comparative control trials with empty boxes attached were not conducted. Thus, one cannot rule out the possibility (however unlikely) that despite observations and data pointing to the contrary, the presence of the boxes themselves (rather than their contents) may have acted as a chronic irritant that influenced conditioned responses over time.

2.5.4

A series of ten trials was carried out to compare conditioned responses of impaired sharks with the results of trials using unimpaired sharks (magnetic stimulus = (0.03μT). Median response (median number of passes over the target by all sharks combined) during stimulus presentation in sensory impaired trials was 2 (Fig. 2.3 (**A**)), compared with 13.5 in unimpaired trials (Fig. 2.1 (**A**)). Again, to ensure validity of our findings, the proportion of passes across the target, averaged per shark, per one-minute time bin, for each of the ten trials was calculated. Sharks with magnetic impairment showed no significant statistical difference the proportion of passes across the target, averaged per shark, across all 21 of the one-minute time bins over the ten-trial series (Fig. 2.3 (**A**)).

Studies into the repellent properties of permanent magnets have shown a density effect, where a positive relationship was found between the number of sharks and the depredation of baits (Robbins et al. 2011; Brill et al. 2009; C. P. O'Connell et al. 2011). These studies have also demonstrated that sharks quickly habituate to the repellent effect of permanent, that may be caused by irritation (Brill et al. 2009; McCutcheon & Kajiura 2013). The minimum of three sharks was required to elicit this effect (Robbins et al. 2011). In

these impairment trials, the minimum number of sharks used was three (in 3 of 10 trials), four sharks were used in the remaining 7 trials. Reduced responses seen (averaged per shark) are therefore not considered to be related to the presence of fewer sharks compared with the control trials. In-fact, in our unimpaired trials, the maximum responses seen were not in the two trials with 7 sharks. Galvanic action that may cause irritation was prevented in our experiments through encasing the magnets.

The results of the trials with impaired sharks (those with magnets attached) may lend further evidence that the observed conditioned responses were not mediated by the electrosensory system. There is no *a priori* reason to believe that the head-mounted magnets interfered with any voltage transients induced by coil activation, thus the cue for the conditioned behaviours seen in the impairment experiments were likely magnetic field changes *per se* rather than to electrical artefacts. Impaired animals produced a strong conditioned response under a stronger (8μT) magnetic stimulus, and a reduced conditioned response under a reduced (0.03 μT) magnetic stimulus. If irritation were the cause for a reduced response, one might expect it would be seen under the stronger stimulus presentation too, which it was not.

2.5.5

Johnsen and Lohmann (2005) commented that the results of magnetic impairment studies by Walker (2006) did not account for the possibility that the magnets used induced an electrical signal through lag in the movement of the magnets relative to the head. The magnetic noise created by the impairment methods used serves to mask the magnetic signal presented during the S+ condition in testing, decreasing the chance of the conditioned response being produced. Contrary to the concerns raised by Johnsen and Lohmann (2005), it is unlikely that magnetic noise created by the impairment methods interferes with the ability of the shark electrosensory system to determine changes in the background electrical field. The electrosensory adaptive filter mechanism is central to the sensitivity of the shark electrosense to very small voltage gradients. It is not known if such an adaptive filter exists for magnetic field stimuli perceived via any non-electrosensory means. Magnetic noise created by the magnets placed on the head of a shark induces an electrical field in much the same way as the body of the shark does as it swims through the

ambient magnetic field. The placement of the magnets in gelatin can be likened to the function of the shark otoconia within the gelatinous cupula of the vestibular sensory maculae. The magnets are heavier than their surrounding medium, and their movement will lag slightly behind the movement of the head. The induced electric field generated by the attached magnets as the shark swims is characteristically phasic due to the sinusoidal movement of the shark's head, and thus becomes a common mode stimulus that would be effectively negated by the adaptive filter mechanism. When a change to that phasic pattern occurs (i.e. when a transient voltage gradient is generated through presentation of the magnetic field in the S+ minute), the induced electrical signal that change creates is more prominent (signal to noise ratio is higher). Such a signal should be no less discernable than if the magnets were not attached. Thus, when the magnetic stimulus is presented, perception of the resulting induced electrical transient would not be impaired by the magnets placed on the sharks' head.

These data, in combination with the arguments set out, lend support to the existence of a non-electrosensory/induction-based magnetoreceptor structure capable of perceiving changes in magnetic field intensity. The placement of the magnets was designed to test the hypothetical existence of an olfactory based magnetoreceptor in elasmobranch fishes that functions in a homologous manner to that described in some teleost and avian species, as has been proposed previously (Kirschvink et al. 2001; Walker et al. 2004; Mora et al. 2004). Our results cannot definitively support the existence and use of such a magnetoreceptor. They do, however, provide support to hypotheses that the electrosensory system of sharks may not be the sole means by which they are able to detect magnetic stimuli.

2.6 *Conclusions*

It is likely the diminished responses seen under magnetic impaired conditions were as a result of impairment to a non-electrosensory magnetoreceptor structure. This conclusion could, however, be further supported through incorporation of further experimental replicates with sham magnets (inert objects of the same approximate size and weight). Sharks used in the impairment study produced the CR when presented with stronger

magnetic stimuli than used in unimpaired testing, and showed no observable change in 'normal' behaviors. It is very unlikely therefore, that the diminished response seen in testing under weak magnetic stimuli using sensory-impaired sharks was an artefact of the placement of the boxes containing the magnets, or were due to the weight of the magnets, rather than being due to the magnetic fields that stem from the magnets themselves. Thus, there is no *a priori* reason for the attachment of the boxes, or the weight of the contents of the boxes to affect the sharks' reactions to the magnetic stimuli used in testing. However, as this control group was not incorporated into the study, the results must be interpreted with a degree of caution.

While not definitive, these data present a platform for future study to further elucidate which sensory structures are involved, and which are the neural pathways relaying information to the brain. It is unlikely that sharks possess only one modality or mechanism for detection of magnetic fields, as has been suggested (Gould 2008b). Indeed, most vertebrates and invertebrates either hypothesised or demonstrated to respond to magnetic field stimuli do not have an electrosense, and other theories have been proposed as to the means for detection of magnetic stimuli. Whether such mechanisms have arisen through convergent or divergent evolutionary processes also remains the subject of debate. These mechanisms include a light governed chemical reaction based either on the radical pair hypothesis (Schulten & Swenberg 1978; Ritz et al. 2000; Mouritsen & Ritz 2005), or a pineal window/light based magnetoreception hypothesis (Gruber et al. 1975; Semm & Demaine 1986; Phillips et al. 2001; Freake & Phillips 2005).

The magnetite based system has been argued to be the ancestral means by which magnetoreception has arisen across taxa (Kirschvink et al. 2001; Gould 2008b), including the elasmobranch fishes (Kirschvink et al. 2001), thus other proposed or demonstrated systems are argued to be more derived. Migratory birds are postulated to make use of the both a magnetite based receptor system, as well as a light based/radical pairs mechanism in photoreceptors (Wiltschko & Wiltschko 2005). It is equally possible that sharks possess the capability to perceive the different parameters of the geomagnetic field via different physical mechanisms.

Light-dependent models of magnetoreception are proposed to involve an interaction between the magnetic field and either magnetite particles located within a photoreceptor or excited states of photopigment molecules (Deutschlander et al. 2000). The models require polarized light, making this system less likely a source of constant magnetic field information in elasmobranchs. In percomorph teleosts the threshold saturation for detection of polarized light is 60%. At 2 metres below the surface in pelagic waters, polarized light saturation is ~ 40% (Novales Flamarique & Hawryshyn 1997). Thus, unless an animal is swimming within the first two metres of the water column, it would not receive sufficient irradiation required by light-based mechanisms. It should be noted however that crepuscular periods offer optimal polarized light saturation (63%) (Novales Flamarique & Hawryshyn 1997), thus could aid in explaining crepuscular "spike dive" behaviour seen in many pelagic fish species, including sharks.

Further studies into magnetic sensory capabilities in sharks are needed to further elucidate these mechanisms. Of course, the ability to perceive a sensory stimulus does not confer the use of that sensory capability in a functional role. Thus, further studies should seek to qualify and quantify roles and functions of different putative sensory systems/structures and should test the ecological validity of such hypotheses.

Chapter 3 – *Magnetic field discrimination & sensory mechanisms.*

3.1 *Abstract*

To navigate via magnetic field information, animals must be able to not only perceive a magnetic stimulus, but also learn, internalize and organize that information as part of an accessible spatial representation of their environment. In chapter 2, sharks were demonstrated to be able to perceive earth-scale changes to the background magnetic field. However, confirmation of sensory capability does not confer functionality, thus it remains to be seen whether (and how) elasmobranchs use changes in the background magnetic field as cues to navigation. Thus, empirical evidence is needed to demonstrate that elasmobranchs possess just such a capability.

This chapter describes behavioral experiments based on operant conditioning (based on voluntary behavior) designed to (i) examine the functional use of magnetoreceptive capability in scalloped hammerhead sharks, and (ii) further examine the sensory mechanisms by which magnetic information is perceived using sensory deprivation techniques.

Overall, sharks tested demonstrated they possess the functional capability to locate and identify a specific magnetic stimulus, and could discriminate between contrasting magnetic stimuli in doing so. This capability is a key requirement in navigation between specific locations according to their associated geomagnetic gradients, as proposed by Klimley's hypothesis of geomagnetic topotaxis. Further, these data are the first empirical data to demonstrate this functional capability. Sensory deprivation treatments were incorporated into two-target/landmark testing, designed to examine the sensory mechanisms potentially used in magnetic field perception in sharks. Sharks demonstrated continued ability to orient to magnetic landmarks despite sensory deprivation/impairment. These sensory treatments provide support to the likely use of the electrosensory system in orienting to magnetic field stimuli, and lend support to the use of alternative mechanism for magnetic field perception, which could involve putative iron-based mechanisms, or an optically based mechanism, or both. Suggestions are made for the direction of future studies.

3.2 *Introduction*

In the previous chapter, sandbar sharks (*Carcharhinus plumbeus*) were demonstrated to respond to presentation of a magnetic stimulus in order to receive a food reward. Stimuli presented under test conditions were consistent with small changes in geomagnetic field intensity that might be encountered across the course of a homing or migratory movement. Sensory impairment methods incorporated lent support to a hypothesized olfactory housed magnetoreceptor, functioning separately to the shark electrosensory system. However, confirmation of sensory capability does not confer functionality, thus it remains to be seen whether (and how) elasmobranchs use changes in the background magnetic field as cues to navigation.

Klimley and colleagues (Klimley 1993; Klimley et al. 2005) suggested that scalloped hammerhead sharks (*Sphyrna lewini*) and bat rays (*Myliobatis californica*) make highly directional/highly oriented movements through geomagnetic topotaxis. The term was coined by Klimley (1993), who found that movements of *S. lewini* between two oceanographic features (the Espiritu Santu seamount & Las Animas islands, Baja California) were, repeated, highly directional and highly correlated with geomagnetic minima and maxima. In biological systems, topotaxis refers to the movement of a cell, or an organism along some environmental gradient. Klimley's use of the term was that that the prefix "topo" refers to the relationship of the animal's movement to environmental topography, in this case, the geomagnetic topography. Klimley stated that "the intensity of the geomagnetic field over the earth's surface forms topographic features such as alternating ridges and valleys from magnetic reversal lineations and peaks from magnetic dipoles associated with seamounts".

Thus, Klimley suggested that tracked sharks used the gradient of the magnetic field (the difference in minima and maxima) as reference points or cues to navigation, swimming along geomagnetic "valleys". This would imply that the sharks used a mosaic map comprised of information regarding the geomagnetic relief in the area surrounding and leading away from the seamount. By understanding the spatial relationships of the geomagnetic features in the environment, the animals can move through the environment via piloting or path integration. Klimley further stated that geomagnetic topotaxis must be

distinguished from a compass sense. However, it is also possible that the geomagnetic "valleys" he proposed the sharks swam along provide bi-modal compass directions, separate to topotaxis. If Klimley's hypothesis is correct, these animals must be able to discriminate and recognize specific geomagnetic features to use them as cues to navigation. Essentially, they would use a learned cogntive magnetic map.

The concept of a cognitive map in animal navigation was put forward by Tolman (1948), the principle of which is that animals internally organize learned spatial information regarding their environment to form a cognitive representation of that environment (a mental map) (Ellen & Anschel 1981). A cognitive map is therefore formed through a combination of experience and path integration (estimation of current position based on movements from the last known location - and advancing that position based upon known rate of movement over elapsed time and course). Thus, through experience, animals are proposed to be aware of the environment beyond their field of perception (Poucet 1993), and draw on a variety of cues (sensory and physical) in deciding their movement path. A cognitive map therefore facilitates highly directed movements between locations, seen in many species across many taxa, as well as the ability to make seemingly random movement paths, yet return to the same starting point. Whether or not animals can form cognitive maps has been the subject of some debate (e.g. Bennett, 1996), although there are numerous studies that support hypotheses that animals form some measure of cognitive representation of their environment under certain conditions (see Gallistel, 1990). Similarly, many studies have shown that animals are able to use latitudinal information, likely derived from the earth's magnetic field to gain a sense of position with respect to their environment, thus comprising a magnetic map (Lohmann et al. 2007).

Cognitive maps are not limited to animals that are highly migratory or make regular journeys over large spatial scales. The extent to which an animal or population of animals disperses is governed by life history (Bowler & Benton 2005), and reflects the need to exploit heterogeneously distributed resource patches (areas that provide critical resources, including prey, safety from predators and potential mates) (Papastamatiou et al. 2011). Not all classes of movement involve or require the use of a cognitive map. Random walks (movement paths that consists of a succession of random steps, e.g. Brownian motion and

Lévy flights) are used when the locations of resources are unknown, or are beyond the range of sensory perception (Papastamatiou et al. 2011). Such movements are also seen in non-territorial species with well-defined home ranges, and are suggested to involve a two-step working memory strategy, where patch location and the reduced quality of visited patches are remembered (Van Moorter et al. 2009). Thus, these movement patterns facilitate learning, contributing resource specific information to a cognitive map.
Directed movements/walks occur when the location of a resource is known, thus require a cognitive map to allow vector calculation between present location and destination. Straight movement paths do not necessarily confer a directed walk, and are distinguished from random movements, or correlated random movements/walks by the scale over which they occur, producing paths with greater displacement (Nams 2006). Migratory movements comprise seasonal, long-distance movements that are often highly directed (Papastamatiou et al. 2013), and are exhibited by most groups of fishes at some level (Chapman et al. 2012). Many shark species are considered highly migratory, making journeys 100's to 1000's of kilometers (Weng et al. 2007; Meyer et al. 2010; Papastamatiou et al. 2011). Regardless of the scale over which a directed movement occurs, knowledge of the environment both within and beyond the range of sensory perception is required. This in turn requires sufficient cognitive ability to learn and retain spatial information.
While it is not known whether the ability of elasmobranch fishes to perceive and use geomagnetic field information is inherited (e.g. in monarch butterflies (Brower 1996)) or learned. The importance of learning in elasmobranch behaviors has become the focus of attention in recent years (see Guttridge et al. 2009). Learning capabilities of sharks were first described by Clark (1959), who used an operant conditioning regime to train lemon sharks (*Negaprion brevirostris*) to bump a target upon presentation of an auditory stimulus to receive a food reward. Aronson et al. (1967), demonstrated that the rate of learning in nurse sharks (*Ginglymostoma cirratum*) used in conditioned discriminative choice experiments was comparable to other vertebrates. Learned information is a critical component of a cognitive map. The marine environment is subject to high variability and plasticity. Thus, animals with well defined (smaller) home ranges may be required to update organized and stored information regarding their environment throughout their

lives (Odling-Smee & Braithwaite 2003), while animals that are more migratory may need to imprint on specific information regarding a resource, for example a specific olfactory cue as seen in salmonids (Cooper et al. 1976; Bett et al. 2016), or on gemagnetic cues as proposed in both salmonids and marine turtles (Lohmann, Putman, et al. 2008b; Putman & Lohmann 2008). Imprinting is a form of rapid, irreversible learning of a specific visual, auditory, or olfactory stimulus, occurring at a critical/sensitive period during development, that influences the behavior of the animal, retained in the memory for long periods of time (Hasler et al. 1978; Immelmann & Suomi 1981). Elasmobranch fishes may use olfactory (Edrén & Gruber 2005; Heupel & Simpfendorfer 2005), visual (Schluessel & Bleckmann 2005a; Schluessel et al. 2015) and magnetic (Kalmijn 2000; Newton & Kajiura 2017) cues in orientation and navigation behaviors. Learned information has been shown to be retained in elasmobranchs for up to a year (Fuss & Schluessel 2015).

For an animal to use geomagnetic information as part of a cognitive map, it must be able to discriminate and recognize the magnetic characteristics of that environment, whether at a macro (local environment) or micro (specific landmark) scale. Although recent studies have demonstrated an ability of sharks to perceive a magnetic stimulus (Anderson et al. 2017) and to associate a magnetic stimulus with a food reward (Newton & Kajiura 2017), it is not known if these animals are capable of functionally differentiating/discriminating changes in the background magnetic field, or are able to resolve locations and landmarks by their magnetic signature.

This chapter describes behavioral experiments based on operant conditioning (on voluntary behaviors) designed to (i) examine the functional use of magnetoreceptive capability in scalloped hammerhead sharks, and (ii) further examine the sensory mechanisms by which magnetic information is perceived using sensory deprivation techniques. It was hypothesized that trained sharks would successfully enter a testing arena and locate a specific magnetic landmark from a choice of 2-4 visually identical landmarks to receive a food reward. Of the three generally accepted magnetoreceptor mechanisms, the optical/radical pairs mechanism is perhaps the least likely to function in elasmobranch fishes (Anderson et al. 2017). It was therefore hypothesized that in sensory deprivation trials, a significant change in orientation behaviors would be seen when sharks

were deprived of electrosensory information, whereas no significant difference in behaviors would be seen when animals were deprived of the blue wavelengths of light required according to the principles of the radical pairs mechanism.

3.3 *Materials & Methods*

3.3.1 *Animal Training Regime*

Captive juvenile *S. lewini* were housed in one half of a 7 m diameter circular tank divided by a median fence, with a central 2m wide gate (see figure 3.1). In the other half of the tank (the testing arena) visually identical targets (landmarks) were randomly placed during testing and training. Up to three sharks at a time were held and trained together to learn to recognize the magnetic signature/characteristics of a specific target, as studies suggest that sharks learn more efficiently in ego-allocentric, social situations (Guttridge et al. 2013; Guttridge & Brown 2014; Schluessel & Bleckmann 2005). In all training, sharks were given sensory experience of the specific (correct) target, and a visually identical blank (non-magnetic) target.

Figure 3.1. *Training and housing arena used in conditioned behaviour magnetic field discrimination experiments*. Sharks were exclusively kept in one side of the arena, and only allowed into the experimental half of the tank during training and testing.

Initially sharks were co-presented three separate stimuli as cues to enter the other (testing) side of the arena – an auditory stimulus (a bell that would sound for one minute), an olfactory stimulus (squid/fish rinse) and a visual stimulus (the raising of the gate). In early training, the squid rinse was presented first to motivate a feeding response in the sharks. Sharks were monitored closely. The bell was rung, and the gate raised as soon as sharks displayed any response to the olfactory stimulus (accelerated swimming rate/tail beat frequency). Pieces of food (squid &/or capelin) were placed at the center of the correct target. By feeding over the target (and over the magnet) sharks passively gained experience of the magnetic characteristics of the target, and learned to associate the target as a point in the tank at which it was fed. Sharks were trained once every day, over a maximum period of four weeks. As behavioral response and feeding performance improved (judged according to the time taken to come through the gate and seek out a food reward), provision of food was progressively delayed, from being provided at the outset, to when

sharks made a pass over the correct target, to not being provided until sharks produced a series of orientation behaviors (see table 3.1). Sharks were judged to be sufficiently trained when they could produce a series of orientation behaviors over the correct target for a period of at least 15 seconds before being given a food reward, and could repeat this over at least 5 consecutive training sessions.

Table 3.1. Ethogram of *S. lewini* experimental behaviors.

Behavior	Definition of Behavior
Normal swimming	Perimeter and cross-sectional use of non-testing side of tank.
Accelerated swimming	Swim rate > than 0.5 body lengths/s (Guttridge et al. 2013).
Arena entry	Passing through the gate within 120 seconds auditory stimulus.
Pass	Shark swims directly over the target without any deviation (Kajiura & Holland 2002).
Turn	A change in direction towards the target greater than 20 degrees from the initial swim path (Kajiura & Holland 2002).
Spiral	One or more concentric spiraling turns toward the center of the target, often biting at the field emanating from it (Kajiura & Holland 2002).
Overshoot	Shark swims over and past the center of the target, before doubling back on itself (Kajiura & Holland 2002).

Kajiura and Holland (2002), described a suite of orientation behaviors exhibited by scalloped hammerhead sharks in orientations to dipoles that simulated bioelectric prey fields. It was noted during training observations that similar behaviors were produced when sharks began to associate the magnetic target as being a feeding location. The behaviors described by Kajiura and Holland (2002) were therefore used as behavioral metrics in this study (Table 3.1). Thus, the shark could demonstrate when it had identified the feeding location. As it was impossible to determine if a pass over the target was an orientation behavior, rather than a random movement, passes were not included as a considered behavioral metric in testing, but were noted nonetheless as a basis for comparison. Similarly, determining if a “turn” was a random change in direction, or orientation behavior was considered too subjective, thus was not used as a behavioral metric.

3.3.2 *Testing*

Although sharks were trained in groups of two or three, testing was carried out on an individual basis. Each shark underwent two series of behavioral trials to examine magnetic field discriminative ability. The first series of trials were similar to the training regime. All trials were video recorded from an aerial perspective and analyzed post completion. Sharks were required to enter the arena within 120 seconds of the onset of co-presentation of the auditory and visual stimuli, to receive a food reward by locating the correct/magnetic target, from a choice of two visually identical targets (one magnetic, one blank), placed randomly in one of four fixed sites in the test arena. Maximum trial time was 5 minutes. Counts were made of the number of passes, spiral behaviors, and overshoot behaviors over each target. Once a shark began producing orientation behaviors over the correct target, a maximum time of 30 seconds was allowed before a food reward was provided, and the trial was considered to be over. In contrast, a shark could make continued orientation behaviors over the non-magnetic target up until the 5-minute maximum time period of the trial, so long as no orientation behaviors had been produced over the correct/magnetic target. Thus, the study was weighted toward producing more orientations over the non-magnetic target. A total of seven sharks were tested in this series of trials, each shark completing ten trials over a maximum period of fifteen days.

Upon successful completion of this first series of trials, sharks were then presented with a more complex problem to solve. Specifically, they were required to identify the same specific magnetic stimulus from a choice of four visually identical targets, one of which was a blank (no magnets embedded). The three remaining targets (landmarks) had embedded magnets, of different sizes, in different physical arrangements (see figure 3.3). Targets were again placed randomly among the four fixed sites in the test arena (figure 3.2). The placement of each target, in each trial was decide via a random sequence generator.

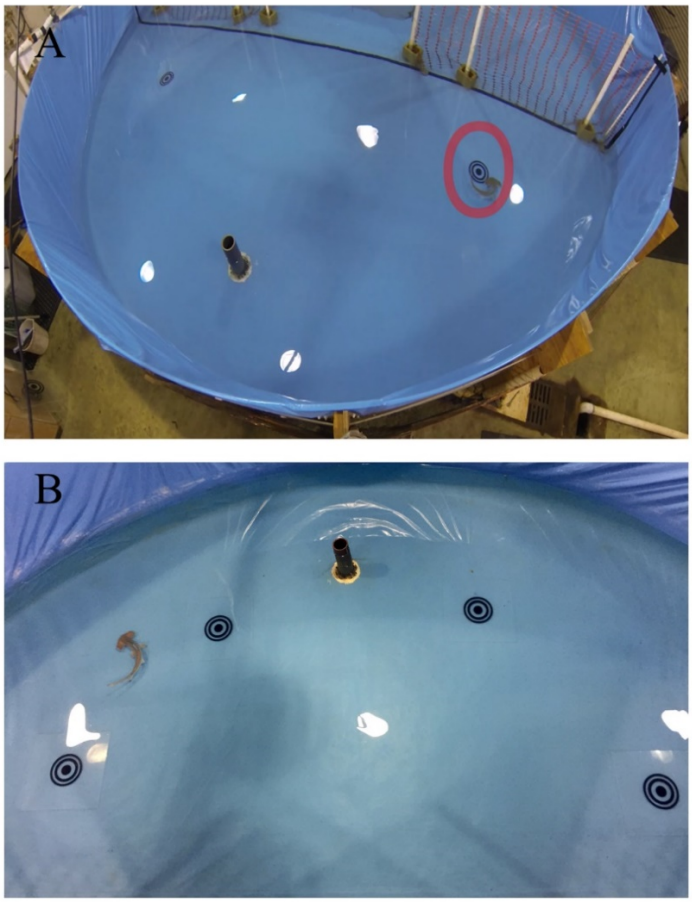

Figure 3.2. *Arrangement of visually identical landmarks*. In the two-target set up shown in (A), targets may be placed in any one of the four approximate locations shown in (B), as assigned by the random sequence generator. Red circle in (A) indicated the correct target (landmark), the shark can be seen orienting to the target (in this case the behavior produced was an overshoot).

Each target was assigned a reference letter for use in the random sequence generator. (A) was the correct target that sharks were required to identify. Two neodymium bar magnets were arranged in series, in the center of the target to create a dipole field (figure 3.3A). (B) represented the blank target, with no magnets embedded in it (figure 3.3B). (C) was assigned to a target where seven small cube shaped neodymium magnets were arranged (a heptapole) in an approximate circle, within the center of the target. Magnetic fields associated with the arrangement are governed by the spacing of the magnets, the arrangement of the poles and the magnetic interactions between individual magnets

(figure 3.3C). (D) was assigned to a target with four small cube shaped neodymium magnets arranged as a square, again in the center of the target. The alignment of the poles of the four magnets, and the lack of space between all magnets, results in an effective dipole field. The interaction of between the magnets and the difference in the width of the combined poles (compared to arrangement A) produces a field with stronger overall intensity, and greater spacing field lines emanating from, and returning to the poles (figure 3.3D).

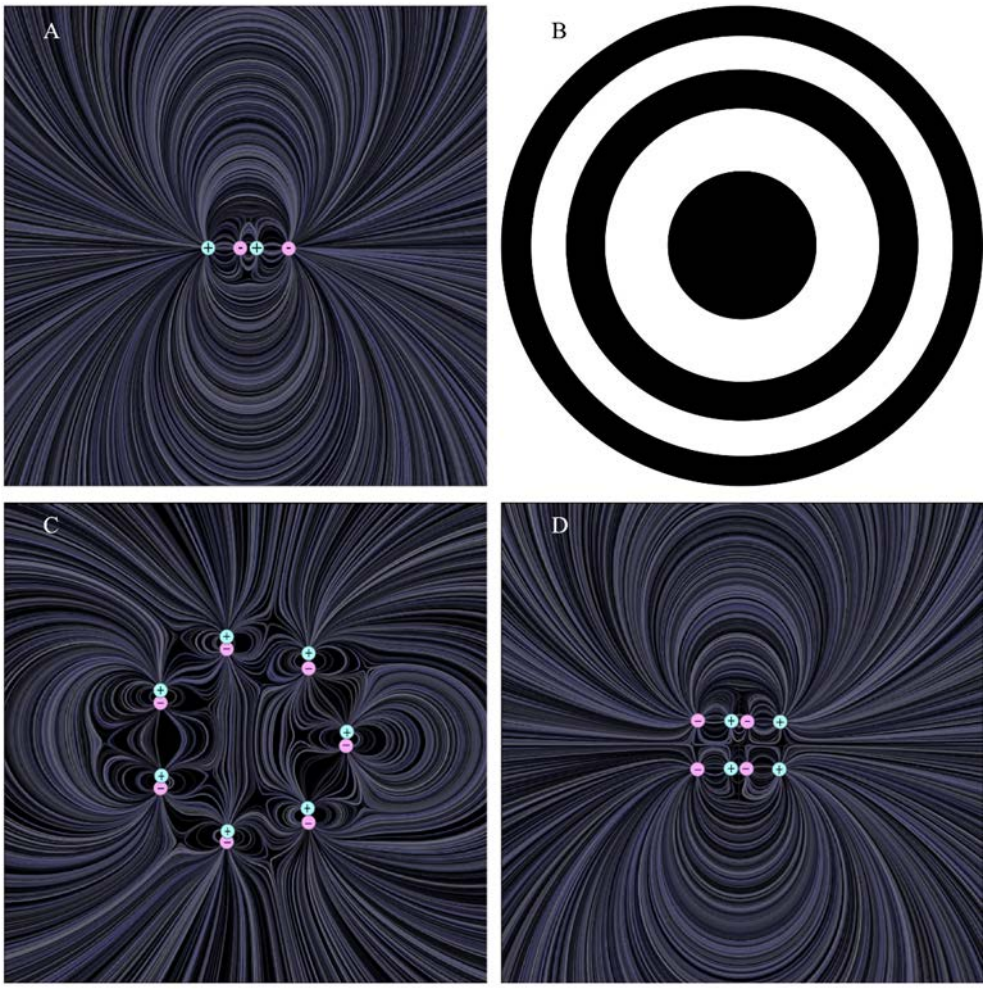

Figure 3.3. *Arrangement of magnets and associated modelled field lines of the four visually identical landmarks*. Each north (+) and south (-) pole represent a magnet. (A) Field lines produced by two neodymium bar magnets arranged in series. This configuration was embedded into the "correct" target sharks needed to identify to receive a food reward. (B) The blank target. (C) Magnets with heptagonal/heptapole arrangement. (D) Four cube magnets arranged as a square (weaker dipole).

All seven sharks (that had previously completed the two-target series) were subsequently tested in the four-target series of trials, each shark completing ten trials over a maximum period of fifteen days, using the same experimental protocols as in the two-target series. Sharks were not given time to learn/experience the new choices of magnetic landmarks.
Following successful completion of these two series of behavioral trials, six sharks underwent further testing series' using the two-target arrangement, each series incorporating a different sensory deprivation measure, designed to elucidate the sensory mechanisms used in orientation behaviors to a magnetic stimulus. First, the entire pore field of the ampullae of Lorenzini covering the cephalofoil of sharks was covered with a non-conductive, hydrophobic gel to impair the function of the electrosensory system in perception of any electrical fields induced as sharks swam through the magnetic field associated with a landmark. This method was successfully used by Ambrosino (2012) to block or impair the function of specific ampullae clusters in dipole simulated prey-field behavioral orientation experiments. Per the protocol of Ambrosino (2012), sharks were removed from the water, the head quickly dried, and the gel applied, making sure to cover the entire pore-field. Animals were returned to the water and allowed twenty-four hours to recover. A maximum of two trials was carried out over the course of a day. Gel was re-applied after every second day of testing to ensure pores remained blocked.
Sharks completed a series of ten trials (five for the 1st two sharks), carried out over a maximum period of fifteen days. Upon completion, gel was carefully cleaned from the sharks' cephalofoil, and the sharks allowed a five-day rest/recovery period. During this period, sharks continued to have training/reinforcement once a day.
Following the rest period, sharks underwent one final series of testing, in the dark under infra-red illumination. An CMOS camera (BlueFish, USA) with infra-red (λ 840nm) led's was mounted to a gantry above the center of the tank, directed toward the center of the testing arena, giving an aerial perspective. A second infra-red illuminator (λ 840nm) (SuperCircuits, Austin, TX) was mounted on a post to one side of the arena to ensure sufficient illumination of the peripheral target locations for the camera sensors. The same protocols as for all the two target trials were followed. Sharks completed a series of ten trials (five for the 1st two sharks), carried out over a maximum period of fifteen days.

3.3.3 *Data Collection and Analysis*

Table 3.2. *Metrics considered for analyses*. For each shark, in every trial, across all series of trials, the following data was gathered for possible consideration as a performance metric.

Metric	Definition
Time through gate (trial start time) (s)	Time taken to respond to presented stimuli and enter testing arena.
Trial time (s)	Time take to identify correct target + 30 seconds allowed for orientation behaviors.
Pass	Number of passes made over each target (including a pass over the target during an orientation behavior), by each shark.
Spiral	Number of spiral orientations observed over each target, by each shark.
Overshoot	Number of overshoot/double-back orientations observed over each target, by each shark.
Orientations	Sum of all orientation behaviors produced by each shark over each target.

N.b., A spiral orientation was recorded when a shark oriented to the dipole in a concentric-circular fashion. A spiral orientation was also recorded when a shark made one or more 180° turns while already at the center of the target. This would often co-occur with the shark biting at the center of the target, each subsequent 180° turn was scored as an orientation. A pass was recorded if a shark moved across the center of the target in any way, whether as a direct approach, or during a spiral or overshoot behavior. If a shark passed over the target, doubled-back on itself, then passed over the target again, that would be considered one double back, but two passes. If a shark performed a spiral orientation to the target, that would similarly be scored as one spiral orientation, and one pass. Further passes would not be scored in concert with 180° turns while already at the center of the target.

Orientation performance (the ability to orient to the correct target) was analyzed on an individual and collective basis across each trial series. For each shark, summed observed behavioural responses for each trial series were plotted. In two-target trials (for all experimental groups), Wilcoxon rank sum/Mann-Whitney U tests were used in individual

sharks to compare the number of passes, spiral behaviors, overshoot behaviors and total orientation behaviors over each target. The same tests were also used to compare patterns of orientation behaviors by target type, as well as the total number of orientations compared with the total number of passes (allowing a measure of randomness vs deliberateness in orientation behaviors observed). On a collective basis, data was pooled, and paired Wilcoxon signed-ranks tests were then used to examine behavioral orientations to each landmark type. A mixed-model approach (generalized linear mixed models (GLMMs)) was used to explore relationships between the orientation behaviors, differing magnetic variables and sensory variables (control/gel/infra-red) using the R package lme4 (Bates et al., 2015). Aikaike's Information Criterion (the most parsimonious model) was used to select the best model, and Chi Square analysis compare our model with a reduced (null) model that only contains an intercept term. Paired Wilcoxon signed-ranks tests were then used to examine the influential variable. These analyses allow a measure of likelihood of production of orientation behaviors made to a magnetic dipole, and the influence of specific variables on behavioral production.

In four target trials, generalized linear mixed-models were used to analyze relationships between the orientation behaviors and the differing magnetic variables of the four different landmarks. Where model results showed a significant effect of predictor (landmark type) upon orientation behaviors, Chi square analyses were used to examine significance of predictor influence. Paired Wilcoxon signed-ranks tests were then used to examine the influential variable. Wilcoxon Rank Sum/Mann-Whitney U tests were further used to compare specific orientation behaviors between landmark types.
The variable of individual shark, was considered as a potential random effect.
All statistical analyses were carried out in R (freeware available at www.r-project.org).

3.4 *Results*

3.4.1 *Two-target trials.*

The overall intensity of dipole magnetic arrangement (Landmark A) used as the correct landmark was measured to be 195 μT, 1cm above the surface of the target. The measurable field extended 63 cm vertically, 89 cm from the north pole, and 57.2 cm laterally.

Eight sharks were trained according to the established protocol, and successfully met the learning criterion (exhibiting orientation behaviors to the correct landmark for a period of at least fifteen seconds, in five successive training sessions). However, in testing, one shark (shark 2) stopped responding to presentation of the conditioned stimuli, thus was removed from further experiments and analyses. The remaining seven sharks successfully completed the 1st series of ten trials. All sharks were able to correctly identify the magnetic landmark, and made significantly more orientations to the magnetic landmark than the blank/non-magnetic landmark (table 3.3). All sharks, with exception of shark 8 (p = 0.369) made significantly more passes over the magnetic landmark than non-magnetic. No difference was seen in the number of overshoots made over either landmark by sharks 7 & 8 (p = 0.27 & 0.08 respectively)

Table 3.3 *Comparison of orientation behaviors to magnetic & non-magnetic landmarks*. Table shows *p*-values from Wilcoxon signed-rank tests comparing orientation responses over the different landmarks. All significant results (marked with a *) pertain to a statistically higher number of orientations recorded over the magnetic landmark, unless otherwise indicated.

Behavioral Metric	Orientations	Passes	Spirals	Overshoots
Shark				
1	0.014^{*}	0.019^{*}	0.226	0.014^{*}
3	0.002^{**}	0.006^{**}	0.007^{**}	0.003^{**}
4	$9.83e^{-5***}$	0.0002^{**}	0.002^{**}	0.002^{**}
5	0.0002^{**}	0.016^{*}	0.0002^{**}	0.002^{**}
6	0.0002^{**}	0.004^{**}	0.0006^{**}	0.001^{**}
7	0.0008^{**}	0.011^{*}	0.0003^{*}	0.27
8	0.01^{*}	0.369	0.008^{**}	0.080

Individual performances (in terms of the number of orientations observed, as well as the differences in types of orientation behaviors produced) were variable. When considering total orientations and passes across both targets over the series of tests in each shark, only shark 8 did not exhibit significantly more passes over the correct landmark (Wilcoxon signed-rank Test, Test, W = 76.5, p = 0.0455, table 3.4).

Table 3.4 *Comparison of combined (total) orientations vs passes by landmark type*. Table shows mean and median orientations and passes for each shark over the 10, two-landmark trials. p-values taken from Wilcoxon signed rank tests to compare orientation vs random movement (passes) over each landmark in each shark across the trial series. The number of orientations and passes observed were greater over the magnetic target.

Target Type		Magnetic			Blank		
Orientation Type		Orientations	Passes		Orientations	Passes	
Shark	Metric			p-value			p-value
1	median	2	3	0.582	0	0	0.722
	mean	2.8	3.6		1.3	1.7	
3	median	7	8	0.907	0	0	0.889
	mean	6.7	6.1		1.9	2.6	
4	median	3	3	0.690	0	0	0.361
	mean	3.5	4		0.1	0.4	
5	median	12	11	0.323	0	1	0.481
	mean	13.2	11.9		2.3	4.5	
6	median	10	10	0.701	1	1	0.873
	mean	10.2	10.8		1.7	3.1	
7	median	7.5	8	1	0.5	1	0.415
	mean	7.8	7.6		2.1	3	
8	median	12.5	4	0.0455*	1	3.8	0.412
	mean	11.8	4.1		1.5	2	

In general, spiral orientation behaviors were most commonly produced, although no differences were seen between the number of spiral & overshoot orientations produced in sharks 1, 3 & 4 (table 3.5). No difference in production of either type of

orientation behavior was seen in individual sharks over the non-magnetic landmark (table 3.5). When comparing overshoot vs spiral behaviors across both landmarks combined, sharks 7 & 8 produced significantly more spiral behaviors (Wilcoxon Signed Rank Test, Test W = 123.5 & 76.5, p = 0.036 & 0.045 respectively).

Table 3.5 *Comparison of orientation behaviors produced in individual sharks by landmark type*. Mean and median are shown for observed orientation behaviors produced in each shark, according to landmark type. p-values taken from Wilcoxon signed rank tests. * = significant difference, ** = highly significant difference.

Landmark Type		Magnetic			Blank		
Orientation Type		Overshoots	Spirals		Overshoots	Spirals	
Shark	Metric			p-value			p-value
1	median	1	1	0.582	0	0	0.654
	mean	1.4	1.4		0.3	1	
3	median	3.5	2.5	0.591	0	0	0.690
	mean	3.7	3		0.9	1	
4	median	1	2	0.510	0	0	0.669
	mean	1.5	2		0	0.1	
5	median	5	7.5	0.004*	0	0	0.790
	mean	4.8	8.4		1.2	1.1	
6	median	3.5	6.5	0.040*	0	0.5	0.212
	mean	3.9	6.3		0.6	1.1	
7	median	1.5	6.5	0.0003**	0	0.5	1
	mean	1.6	6.2		1.1	1	
8	median	1	10.5	0.0131*	0.5	0.5	0.345
	mean	1.4	10.4		0	1	

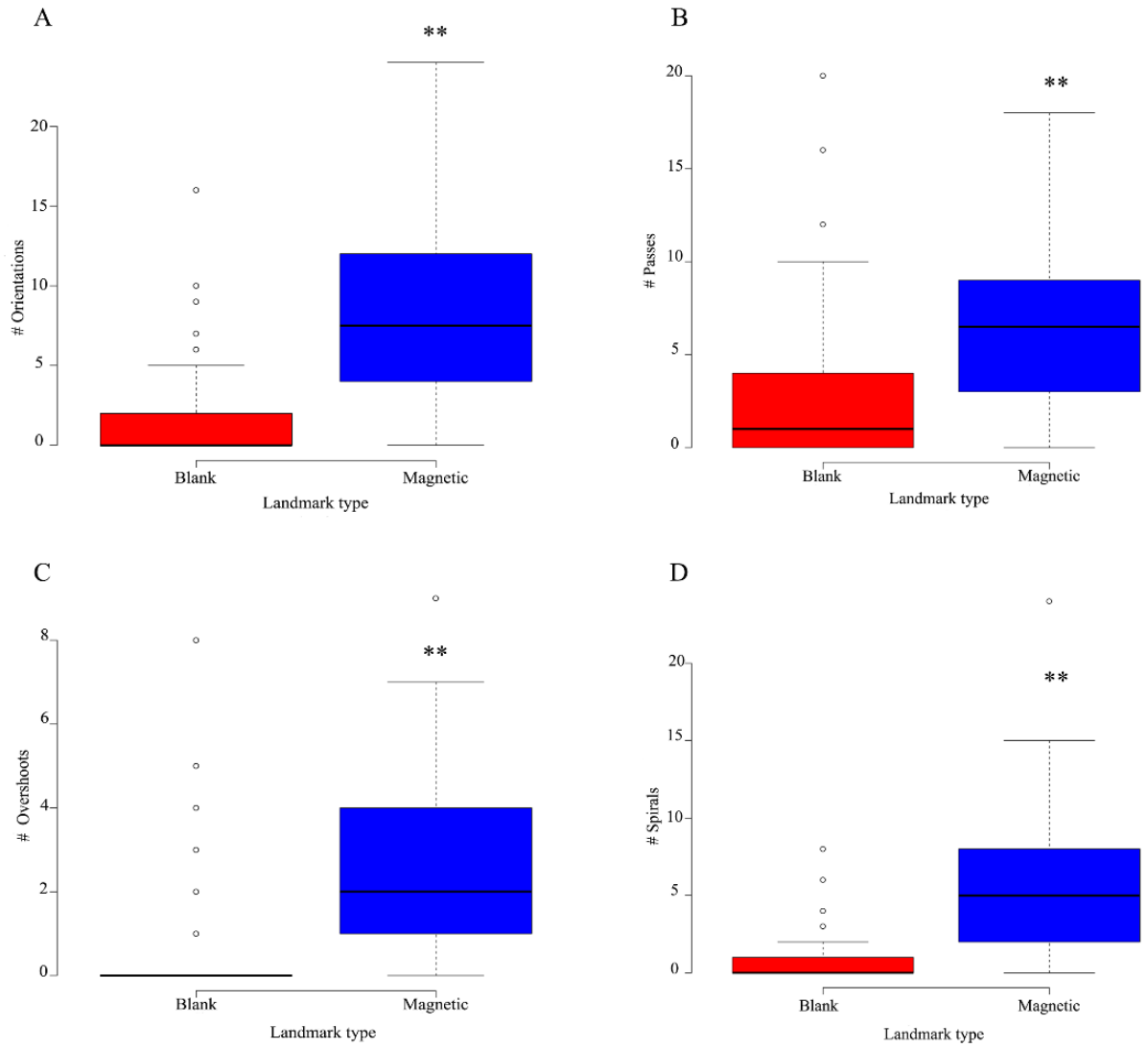

Figure 3.4 *Box plots of orientation behaviors by all sharks over magnetic and non-magnetic landmarks*. (A) Combined orientation behaviors to landmarks. Orientations to magnetic landmark were significantly higher (paired Wilcoxon signed-ranks test, V = 96.5, p = <0.0001). (B) Passes over landmarks – passes include any movement over the target, oriented or otherwise. Sharks showed preference to the magnetic landmark ((paired Wilcoxon signed-ranks test, V = 181, p = <0.0001). (C) & (D) Overshoot and spiral orientations. *N.b.* the difference in y-axis scale between (C) & (D). Both forms of orientation behaviors were exhibited significantly more often over the magnetic landmark (paired Wilcoxon signed-ranks test, V = 167.5 & 71 respectively, p = <0.0001 for both). Open circle = outliers, ** indicates significant difference, whiskers show variation in sample.

Analyzed collectively, sharks demonstrated a distinct association of the magnetic landmark as the location to receive food, and thus could readily identify the magnetic landmark in

behavioral trials. Across the trial series, sharks performed significantly more orientations and passes over the magnetic landmark than the non-magnetic landmark (figure 3.4). Median number (± S.D) of orientations (overshoots & spirals combined), passes, overshoots and spirals (to/over the magnetic landmark) were 10 ± 5, 8 ± 5, 3 ± 2 and 7 ± 5 respectively.

Spiral orientation behaviors were exhibited significantly more than overshoots both as a whole (over both landmarks) (Wilcoxon Rank Sum test, W = 8189.5, p = 0.013), and over the magnetic landmark (Wilcoxon Rank Sum test, W = 1503.5, p = <0.0001). No difference was seen between combined/total orientations compared with passes.

Evaluated collectively, sharks' performance over the series of ten trials did not improve or show signs of continued learning. The number of orientations and passes to the non-magnetic landmark showed a slight, but steady increase over the trial series (figure 3.5A). Overall orientations and passes to/over either target showed a similar pattern of increase, with the exception of an apparent pronounced spike in passes over the non-magnetic landmark in the 8th trial of the series. However, when considering orientation type, spiral orientation behaviors over the magnetic landmark showed a clear trend of improvement, while overshoot behaviors showed a negligible positive trend. The variation seen in the time taken to identify the correct target also demonstrates that orientation performance did not improve over the trial series (figure 3.5B).

Shark orientation distances to the target could not be quantified as the camera used to record trials was not aerially centered over the experimental arena, and the orientation angle/field of view of the lens was not the same across each trial. However, based upon observations the mean orientation distance observed (spiral tracking orientations) was approximately 1.5 body lengths (~60-80 cm). This compares with maximum recorded distances of ~30 and 32cm in electric dipole orientation studies in the species (Kajiura and Holland, 2002; Ambrosino, 2012).

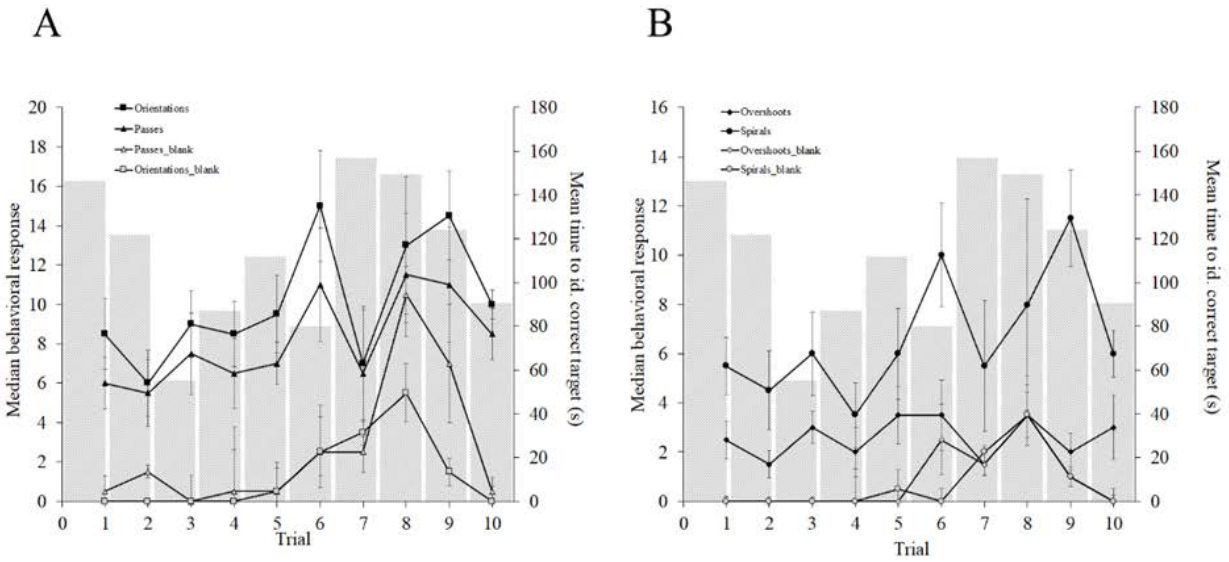

Figure 3.5 *Median behavioral orientations for all sharks in two target trials.* (A) Orientations and passes can be seen to be notably higher over magnetic landmark. Gradient of a trendline through both orientations & passes (m= ~ 0.5), indicates negligible performance improvement. A similar trendline through Passes_blank would have a gradient (m) of 0.6. (B) Overshoot and spiral orientation behaviors. Both forms of orientation were produced more over the magnetic landmark. Spiral behaviors were produced significantly more over the magnetic landmark than any other orientation type over either landmark type, and also showed a negligible increasing trend across trial series (m = 0.45). Grey bars (scale = z axis) show mean time taken to identify correct landmark.

3.4.2 *Four-target trials.*

Having completed the two-target series of trials, sharks were tested to explore their ability to solve a more complexed problem, which required them to discriminate between visually identical landmarks with contrasting magnetic characteristics.

The magnetic characteristics of the landmarks were measured as per the previous experiments. Magnetic field intensity associated with landmark C (heptapole) (measured 1cm above the center was 170 μT. Fields extended 19cm vertically. Horizontal fields were not symmetrical (due to magnet arrangement and spacing), but examined as orthogonal

cross-sections of the circle, extended 16.5 cm and 12.5 cm from the center in one plane, and 24.5cm and 14cm from the center in the other.

Landmark D (weak dipole) had an overall intensity of 170 μT. Vertical fields extended to 31cm. Horizontal fields extended 13.5 cm from the center (north and south), and 12cm laterally.

All sharks exhibited significantly higher orientations to the correct landmark (configuration A) than any other landmark arrangement. The exception to this was shark 4, for which no difference was seen in number of orientations made to landmarks when comparing configuration 'A' (dipole) with configuration 'D' (weak dipole) (table 3.6).

Table 3.6 *Orientation behaviors of individual sharks in 4-target trials.* Landmark arrangements: A = dipole, B = blank, C = heptapole, D = weak dipole.

Orientations								
Landmark		A	B	C	D	A vs B	A vs C	A vs D
Shark	Metric					*p*-value	*p*-value	*p*-value
1	median	8.2	1.2	0.7	1.3	0.008*	0.009*	0.008*
	mean	9	0	0	0			
3	median	4.7	0.6	0.4	1.4	0.008*	0.008*	0.049*
	mean	3.5	0	0	0.5			
4	median	2.3	0.1	0.4	1.5	0.009*	0.02*	0.351
	mean	2.5	0	0	0			
5	median	6.3	0.6	0	0.4	0.006*	0.009*	0.006*
	mean	6.5	0	0	0			
6	median	9.4	0.7	0.6	1.2	0.006*	0.006*	0.006*
	mean	9	0	0	0.5			
7	median	9.4	1.2	0.7	1.3	0.008*	0.008*	0.009*
	mean	9	0	0	0			
8	median	13.9	0.8	1.2	1.7	0.009*	0.009*	0.009*
	mean	15	0	0	0			
Passes								
Landmark		A	B	C	D	A vs B	A vs C	A vs D
Shark	Metric					*p*-value	*p*-value	*p*-value
1	median	6.5	3.6	1.4	3.3	0.07	0.009*	0.12
	mean	6.5	4	0.5	2			
3	median	3.6	2	1.6	2.4	0.09	0.06	0.26
	mean	3	1.5	0.5	2.5			
4	median	6.4	1.7	1.4	1.5	0.009*	0.009*	0.009*
	mean	5	1	0.5	0.5			
5	median	6.6	1.9	1.9	2	0.006*	0.006*	0.006*
	mean	6	2	1.5	2			
6	median	8.4	1.3	2.3	1.7	0.006*	0.009*	0.006*
	mean	8.5	1	1	1			
7	median	6.2	3	1.7	2.3	0.17	0.028*	0.04*
	mean	6.5	0.5	0.5	1.5			
8	median	4	0.9	1.7	2.1	0.017*	0.14	0.37
	mean	4	0	0	0			

Table 3.6 (cont.) *Orientation behaviors of individual sharks in 4-target trials.* *p*-values from paired Wilcoxon signed-ranks tests comparing behavioural orientations between landmark types.

Overshoots Landmark		A	B	C	D	A vs B	A vs C	A vs D
Shark	Metric					*p*-value	*p*-value	*p*-value
1	median	2.6	0.5	0.3	0.3	0.017*	0.02*	0.027*
	mean	2.5	0	0	0			
3	median	3	0.4	0.2	1	0.015*	0.015*	0.07
	mean	3	0	0	0.5			
4	median	1.4	0.1	0.1	0.9	0.02*	0.02*	0.34
	mean	1	0	0	0			
5	median	2.7	0.1	0	0.1	0.008*	0.009*	0.009*
	mean	2	0	0	0			
6	median	4.7	0	0.6	0.6	0.006*	0.006*	0.009*
	mean	5	0	0	0			
7	median	2.6	0.5	0.3	0.6	0.017*	0.027*	0.02*
	mean	2.5	0	0	0			
8	median	1.7	0.4	0.3	0.5	0.05*	0.02*	0.06
	mean	1	0	0	0			
Spirals Landmark		A	B	C	D	A vs B	A vs C	A vs D
Shark	Metric					*p*-value	*p*-value	*p*-value
1	median	5.6	0.7	0.4	0.7	0.009*	0.006*	0.033*
	mean	5	0	0	0			
3	median	1.7	0.2	0.2	0.4	0.021*	0.019*	0.033*
	mean	1.5	0	0	0			
4	median	0.9	0	0.3	0.6	0.03*	0.1	0.6
	mean	1	0	0	0			
5	median	3.6	0.5	0	0.3	0.009*	0.009*	0.009*
	mean	3.5	0	0	0			
6	median	4.7	0.7	0	0.6	0.006*	0.006*	0.009*
	mean	5	0	0	0.5			
7	median	5.6	0.7	0.4	0.7	0.009*	0.008*	0.006*
	mean	5	0	0	0			
8	median	12.2	0.4	0.9	1.2	0.021*	0.019*	0.033*
	mean	13	0	0	0			

The same observation can be made for passes, where shark 4 only showed a greater number of orientations to the correct landmark in comparison to 'B (blank) (table 3.6). Three of the seven sharks exhibited no difference in overshoot orientations between configurations 'A (dipole)' and 'D (weak dipole)'. Shark 4 was again the only shark not to exhibit significantly higher spiral orientations to configurations 'C' (circle) and 'D' (table 3.6). Thus, it was apparent that configuration 'D' provided the greatest challenge in discriminating differences between the magnetic configurations, with shark 4 exhibiting notably poorer orientation performance to the correct magnetic landmark across behavioural orientation metrics. This is exemplified in figure 3.6.

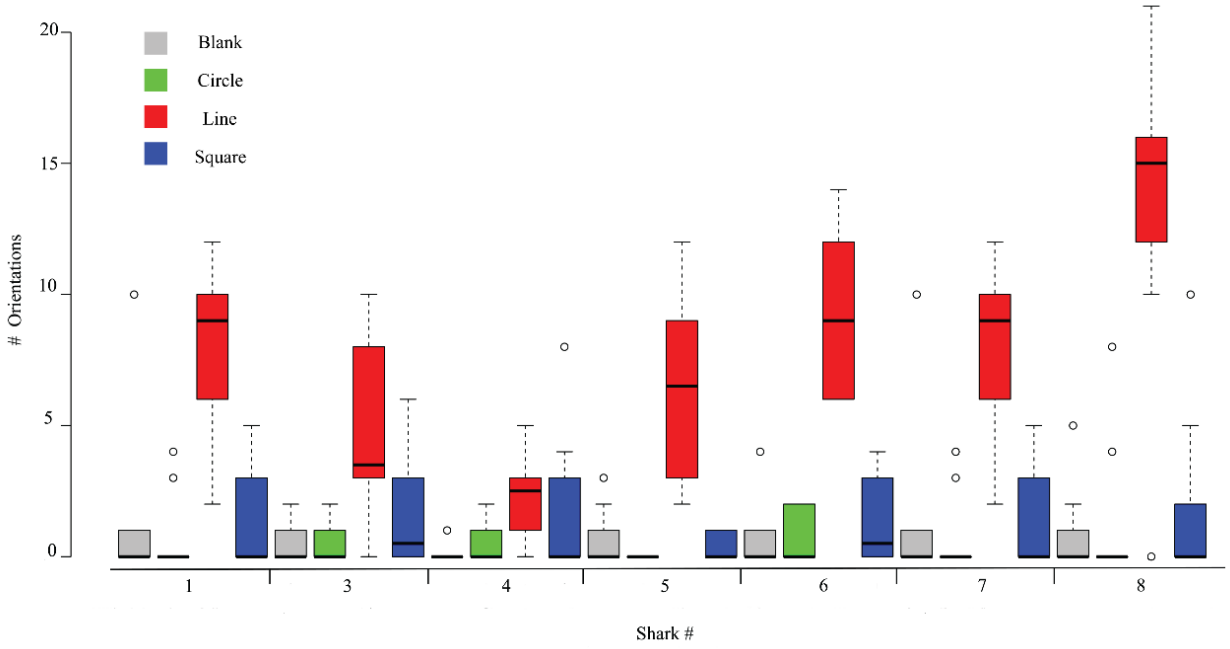

Figure 3.6 *Box plot of total orientations (overshoot & spiral combined) for individual sharks according to landmark configuration*. All sharks produced significantly more orientations to the correct configuration (see table 3.6). Although overall performance was variable, particularly shark 4, results indicate sharks could recognize and distinguish the magnetic characteristic of the correct configuration. Line = dipole. A, Blank = B, Circle = heptapole, Square = weak dipole.

Generalized linear mixed-models with Poisson distributions were used to explore relationships between magnetic configuration of landmarks and the orientation behaviors exhibited by sharks in the study.

Table 3.7 *Ranked generalized linear mixed-effects models of magnetic landmark on probability of behavioral orientation to a landmark*. Models with a lowest ΔAIC_c are shown. df = degrees of freedom; logLik = maximum log-likelihood; %DE = percent deviance explained.

Model	df	logLik	AIC_c	ΔAIC_c	%DE
Orientations					
Orientations ~ Target + Shark + Target*Shark +(1|Shark)	251	-505.9	1069.9	0.00	45.90
Orientations ~ Target + (1|Target:Shark)	275	-540.5	1091	21.1	42.21
Passes					
Passes ~ Target + Shark + Target*Shark +(1|Shark)	251	-641.2	1340.4	0.00	27.9
Passes ~ Target + (1|Target:Shark)	275	-353.5	1342.4	2	28.76
Spirals					
Spirals ~ Target + (1|Shark)	275	-327.7	665.3	0.00	51
Spirals ~ Target + (1|Target:Shark)	275	-387.5	785	119.7	41.51
Overshoots					
Overshoots ~ Target + (1|Target:Shark)	275	-326.4	662.8	0.00	27.9
Overshoots ~ Target + (1|Shark)	275	-327.7	665.34	2.54	27.62

The best-fitting, four target GLMMS's indicated probability of an orientation to a target was significantly influenced by target type, specifically configuration 'A' (the dipole), indicating sharks were able to recognize and discriminate this (correct) configuration from other choices (table 3.8). Models revealed that shark 4 was significantly less likely to produce an

orientation behavior to the correct landmark, and had a higher probability of orienting to an alternative configuration, most likely configuration 'D' (weak) (table 3.8). Final models explained 27 % to 51% of deviance in orientation behaviors produced.

Table 3.8 *Effects of highly influential variables in mixed model analyses*. Standardized model -averaged coefficients ± standard error are followed by the associated *p*-value in parenthes es (i.e. Pr(>|Z|)). significance codes: 0 = ***; 0.001 = **; 0.01 = *

	Fixed effects:					
		Estimate	Std. Error	z value	Pr(>|z|)	
Orientations						
	TargetLine	1.92	$3.09e^{-01}$	6.218	$5.02e^{-10}$	***
	SharkShark4	-2.49	1.	-2.387	0.017	*
	TargetSquare:SharkShark4	2.63	1.11	2.373	0.0177	*
Passes						
	TargetCircle	-0.94446	0.31497	-2.999	0.0027	**
	TargetLine	0.590868	0.20776	2.844	0.0045	**
	SharkShark3	-0.58779	0.27889	-2.108	0.0350	*
	SharkShark4	-0.75031	0.29428	-2.55	0.0108	*
	SharkShark5	-0.63908	0.28357	-2.254	0.0242	*
	SharkShark6	-1.01857	0.32358	-3.148	0.0017	**
	SharkShark8	-1.38629	0.37268	-3.72	0.0002	***
	TargetLine:SharkShark4	0.734801	0.34295	2.143	0.0321	*
	TargetCircle:SharkShark5	0.944462	0.45219	2.089	0.0367	*
	TargetLine:SharkShark5	0.654347	0.33309	1.964	0.0495	*
	TargetCircle:SharkShark6	1.515006	0.46862	3.233	0.0012	**
	TargetLine:SharkShark6	1.274999	0.36331	3.509	0.0005	***
	TargetCircle:SharkShark8	1.58045	0.51879	3.046	0.0023	**
	TargetLine:SharkShark8	0.900787	0.42341	2.127	0.0339	*
	TargetSquare:SharkShark8	0.934309	0.46563	2.007	0.0448	*
Overshoots						
	TargetLine	2.2354	0.2346	9.529	$< 2e^{-16}$	***
	TargetSquare	0.7655	0.2699	2.836	0.00466	**
Spirals						
	TargetLine	2.372	0.1842	12.878	$< 2e^{-16}$	***

Models suggest the probability of a shark making a pass (non-oriented movement) over a target was highest for configurations 'A' and 'C', and that all sharks (with the exception of

shark 7) where highly likely to perform a non-oriented pass over any landmark (table 3.8), which may reflect searching patterns. Configurations 'A' and 'D' (the dipole configurations) were highly influential in the likelihood of overshoot orientations being exhibited. A comparison of overshoot orientations to both configurations by all sharks showed significantly more overshoot orientations were exhibited over configuration 'D' compared with configurations 'B' & 'C' (Wilcoxon signed-ranks test, V = 50 & 67, p = 0.022 & 0.016 respectively). However, significantly more overshoot orientations were made to configuration 'A' compared with configuration 'D' (Wilcoxon signed-ranks test, V = 1726, p = <0.0001).

Across the trial series, sharks oriented to the correct landmark (configuration A) significantly more than any other landmark configuration (p = <0.0001 for all comparisons, Wilcoxon signed-ranks tests). Median number (± S.D) of orientations by landmark configuration were 7.71 ± 4.8 (A), 0 ± 1 (B), 1.07± 1.8 (C), 0.5 ± 0.7 (D). Similarly, spiral and overshoot orientations to the configuration 'A' were seen significantly more than to any other configuration (p = <0.0001 for all comparisons, Wilcoxon signed-ranks tests). Median overshoot and spiral orientations (± S.D) respectively, by landmark were 2.7 ± 1.96 & 4.3 ± 4.3 (A), 0 ± 0.48 & 0.3 ± 0.77 (B), 0 ± 0.51 & 0 ± 0.56 (C), 0.2 ± 0.8 & 0.1 ± 0.41 (D). No difference was seen in the number of overshoot and spiral orientation behaviors produced across all landmarks (Wilcoxon rank sum test, W = 37010, p = 0.189). However, significantly more spirals than overshoots were exhibited over landmark 'A' (Wilcoxon rank sum test, W = 1727, p = 0.002), no differences in these two orientation behaviors were seen over any other landmark configuration.

As in two-landmark trials, sharks' performance over the series of ten trials did not improve or show signs of continued learning. Mean time to orient to the correct target showed marked reduction across the course of the first three trials, but showed distinct subsequent fluctuation (grey bars – figure 3.7). Overall, orientation behaviors to the correct landmark did not show an increasing trend over the series of trials (angles of trend-line applied to orientation, overshoot and spiral plots in figure 3.7 are 0.04, 0.01 & 0.02 respectively). Behavioral orientations to the incorrect (all remaining) landmarks also fluctuated across

trial series', however, these again did follow any notable positive or negative trend. Thus collectively, sharks demonstrated a clear ability to recognize and discriminate a specific magnetic stimulus.

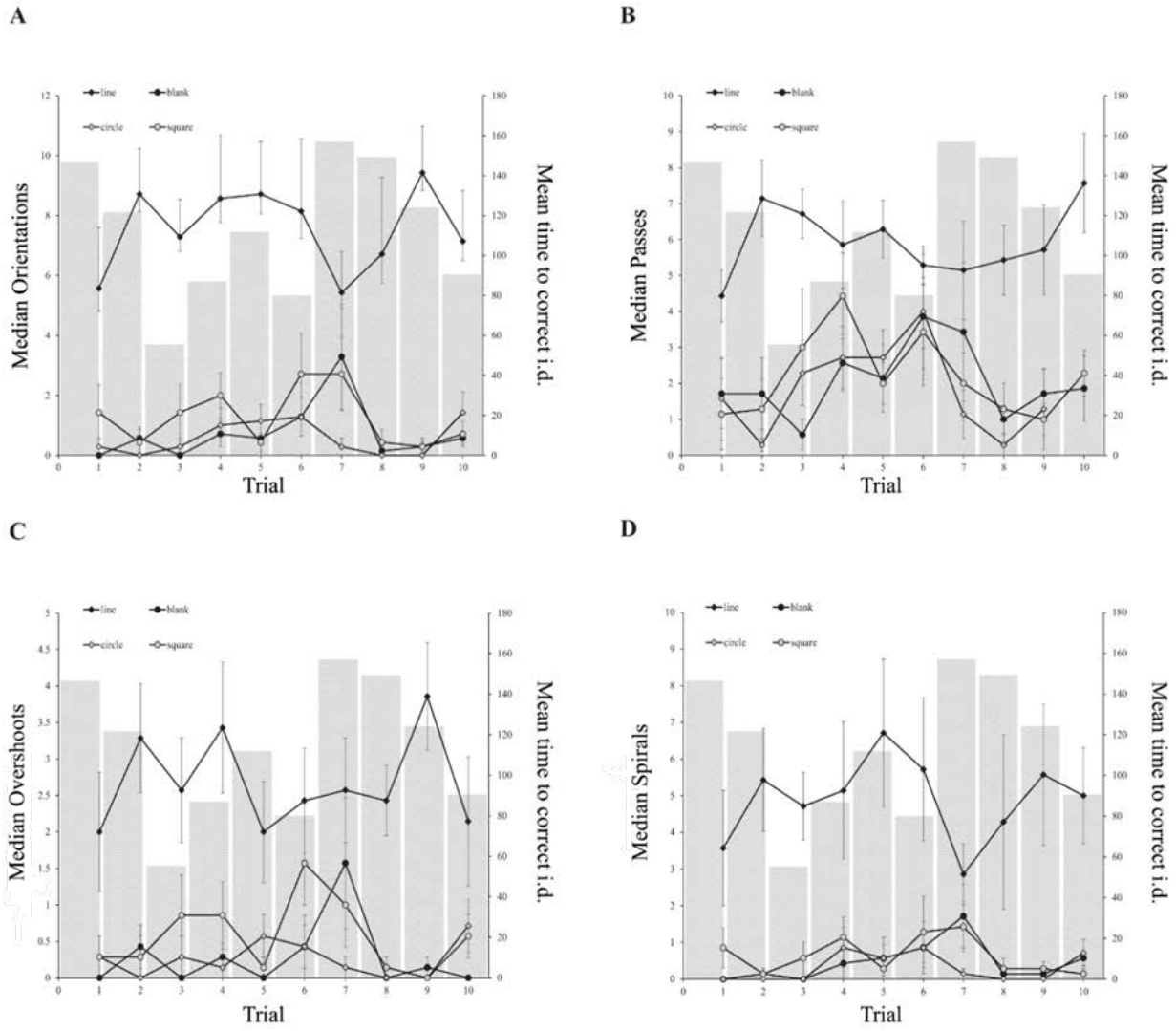

Figure 3.7 *Median behavioral orientations for all sharks in four-target trials.* All sharks oriented to the correct magnetic landmark significantly more times than any other configuration. Median passes (not classed as an orientation) over configurations B, C & D were noted to be higher B, C & D, as well as over significantly higher over configuration A (p = <0.001). A = Orientations, B = Passes, C = Overshoots, D = Spirals. Grey bars (scale = z axis) show mean time taken to identify correct landmark.

3.4.3 *Two-target sensory trials.*

Having completed the two and four target trial series, six sharks were tested in two further series of trials designed to examine the sensory mechanisms used in magnetic field perception. As with the previous two trial series', individual performances across the two sensory trial series' were variable. All sharks were able to discriminate the magnetic landmark, regardless of the sensory deprivation treatment, making significantly more orientations to the magnetic landmark than the blank, with the exception of shark 3 in, in the non-conductive gel treatment group (figure 3.8A).

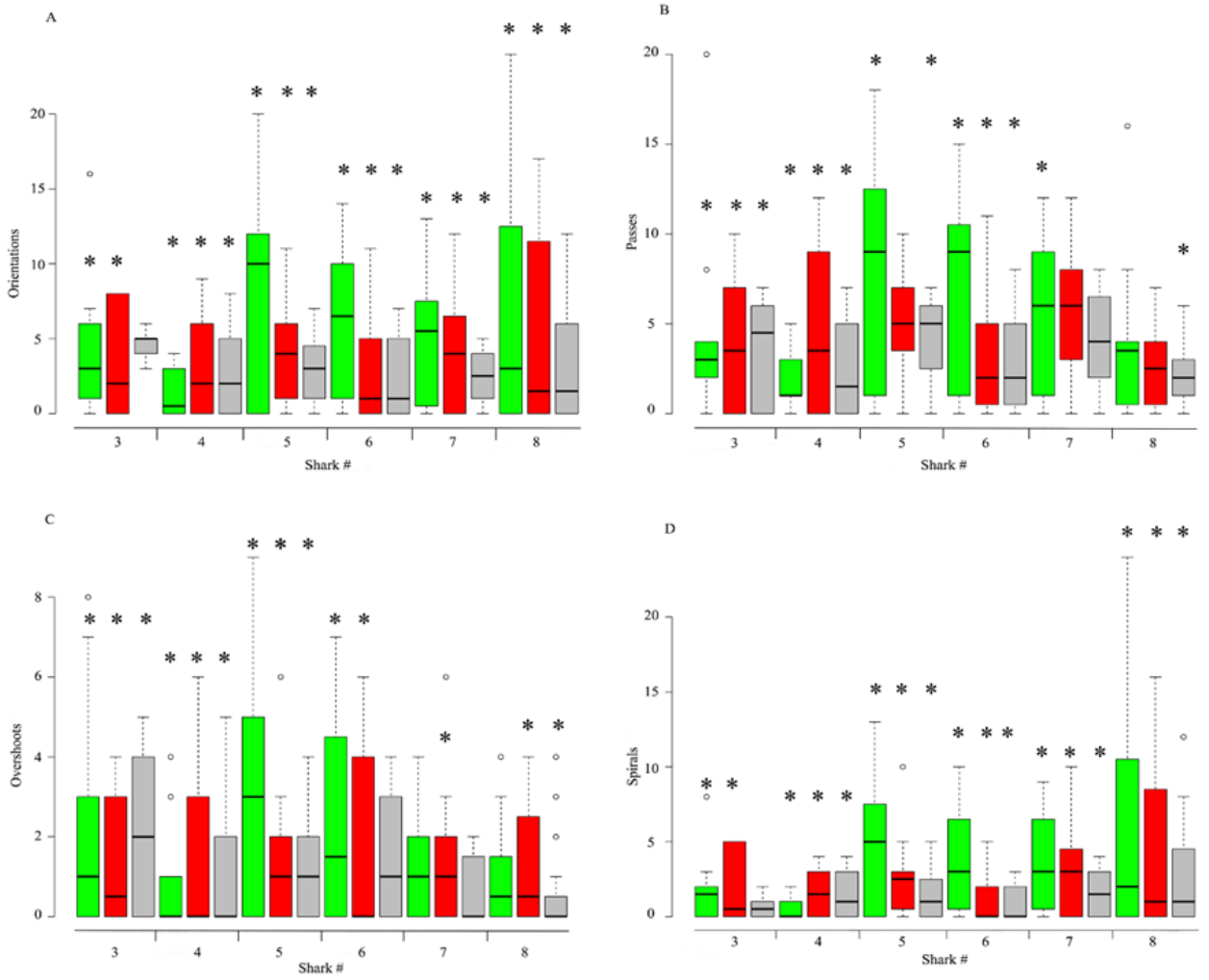

Figure 3.8 *Orientation behaviors in two-target sensory trials*. Panel shows behavioral orientations and passes to/over both targets according to treatment. green = control; red = infra-red; grey = non-conductive gel. *'s indicate significantly higher production of behaviors over magnetic than non-magnetic landmark.

As a general trend, a reduction in behavioral orientations was seen across both series of sensory treatment trials, although this again varied by individual shark (figure 3.8). Within treatment groups few sharks exhibited stark contrasts in the frequency of different behavioral orientations (spiral and overshoot behaviors) to the magnetic target (table 3.9).

Table 3.9 (A) *Behavioral orientations to landmarks according to treatment groups*. *p*-values from paired Wilcoxon signed-ranks tests in individual sharks to compare responses by behaviour type according to landmark type.

Gel											
Landmark type	Shark	Spirals	Overshoots	Sig. Diff?	*p* value	Which?	Passes	Orientations	Sig. Diff?	*p* value	Which?
Magnetic	3	6	21	**y**	0.011	**Overshoots**	30	22	x	N/A	N/A
Blank	3	1	1	x	N/A	N/A	5	23	**y**	0.049	**Orientations**
Magnetic	4	16	12	x	N/A	N/A	24	28	x	N/A	N/A
Blank	4	0	0	x	N/A	N/A	1	0	x	N/A	N/A
Magnetic	5	24	21	x	N/A	N/A	55	45	x	N/A	N/A
Blank	5	5	8	x	N/A	N/A	25	13	x	N/A	N/A
Magnetic	6	19	27	x	N/A	N/A	49	46	x	N/A	N/A
Blank	6	0	1	x	N/A	N/A	9	1	**y**	**0.04**	**Passes**
Magnetic	7	27	5	**y**	**0.01**	**Spiral**	55	32	x	N/A	N/A
Blank	7	11	5	x	N/A	N/A	36	16	x	N/A	N/A
Magnetic	8	24	21	x	N/A	N/A	55	32	**y**	**0**	**Orientations**
Blank	8	5	8	x	N/A	N/A	25	13	x	N/A	N/A

Infra-red Landmark type	Shark	Spirals	Overshoots	Sig. Diff?	P value	Which?	Passes	Orientations	Sig. Diff?	P value	Which?
Magnetic	3	20	14	x	N/A	N/A	37	35	x	N/A	N/A
Blank	3	0	0	x	N/A	N/A	3	0	x	N/A	N/A
Magnetic	4	16	12	x	N/A	N/A	24	28	x	N/A	N/A
Blank	4	0	0	x	N/A	N/A	1	0	x	N/A	N/A
Magnetic	5	24	21	**y**	**0.04**	**Spiral**	55	45	x	N/A	N/A
Blank	5	5	8	x	N/A	N/A	25	13	x	N/A	N/A
Magnetic	6	19	27	x	N/A	N/A	49	46	x	N/A	N/A
Blank	6	0	1	x	N/A	N/A	9	1	**y**	**0.01**	**Passes**
Magnetic	7	27	5	**y**	**<0.001**	**Spiral**	55	32	x	N/A	N/A
Blank	7	11	5	x	N/A	N/A	36	16	x	N/A	N/A
Magnetic	8	24	21	**y**	**0**	**Spiral**	55	32	**y**	**0**	**Orientations**
Blank	8	5	8	x	N/A	N/A	25	13	x	N/A	N/A

Table 3.9 (B)

GLMMs with a negative-binomial distribution were used to explore relationships between the orientation behaviors, differing magnetic variables and sensory variables (control/gel/infra-red) (table 3.10). The best-fitting models indicated probability of an orientation to a target was significantly influenced by landmark type, specifically configuration A (magnetic landmark), indicating sharks were able to recognize and discriminate the magnetic landmark regardless of the sensory deprivation treatment imposed (table 3.11). Models help emphasize the variability in individual performance, but also help reveal the influence of treatment type upon the probability of production of specific behavioral orientations in individual sharks. For sharks 5-8, the probability of any type of orientation behavior being produced was significantly influenced (diminished) by

non-conductive gel treatment (table 3.11). Testing under infra-red light significantly reduced the likelihood of spiral orientation behaviors being produced by shark six (table 3.11, figure 3.8D).

Table 3.10 *Ranked generalized linear mixed-effects models of magnetic landmark on probability of behavioral orientation to a landmark*. Models with the lowest AIC_c are shown. df = degrees of freedom; logLik = maximum log-likelihood; %DE = percent deviance explained. Final models explained 27 % to 51% of deviance in orientation behaviors produced. This suggests variables not considered in models also influenced the likelihood of orientation to a specific landmark, as well as the nature of the behavioral orientation produced.

Model	df	logLik	AIC_c	ΔAIC_c	%DE
Orientations					
Orientations ~ Target + Treatment + Treatment*Shark +Target*Shark + (1|Shark)	274	-605.7	1263	0.00	19.54
Orientations ~ Target + Treatment + (1|Shark)	294	-659.5	1331	68	19.54
Passes					
Passes ~ Target + Treatment + Treatment*Shark + Target*Shark + (1|Shark)	274	-673.7	1347	0.00	11.23
Passes ~ Target + Treatment + (1|Shark)	294	-702.5	1417	70	7.43
Spirals					
Spirals ~ Target + (1|Shark)	274	-480.5	1013	0.00	23.28
Spirals ~ Target + (1|Target:Shark)	294	-519.1	1050	27	17.12
Overshoots					
Overshoots ~ Target + (1|Target:Shark)	274	-405.4	862.7	0.00	18.15
Overshoots ~ Target + (1|Shark)	294	-437.9	887.9	25.2	18.15

Table 3.11 *Effects of highly influential variables in mixed model analyses of two-target sensory trials*. Standardized model-averaged coefficients ± standard error are followed by the associated *p*-value in parentheses (i.e. Pr(>|Z|)).

	Fixed Effects	Estimate	Std. Error	z value	Pr(>|z|)	
Orientations						
	TgtMag	0.70192	0.25549	2.747	0.00601	**
	Shark6	-1.06739	0.36624	-2.914	0.00356	**
	Shark8	-1.14251	0.36105	-3.164	0.00155	**
	TreatIR:Shark4	1.27283	0.53018	2.401	0.01636	*
	TreatVas:Shark5	-1.01372	0.36673	-2.764	0.00571	**
	TreatVas:Shark6	-1.15746	0.386	-2.999	0.00271	**
	TreatVas:Shark7	-0.84737	0.37827	-2.24	0.02508	*
	TreatVas:Shark8	-0.89413	0.37764	-2.368	0.0179	*
	TgtMag:Shark5	0.67642	0.31858	2.123	0.03373	*
	TgtMag:Shark6	1.80303	0.37751	4.776	1.79E-06	***
	TgtMag:Shark8	1.98627	0.365	5.442	5.27E-08	***
Passes						
	TargetMagnet	1.04965	0.28497	3.683	0.00023	***
	Shark4	-2.26443	0.55312	-4.094	4.24E-05	***
	TreatIR:Shark4	1.31004	0.52007	2.519	0.01177	*
	TgtMag:Shark4	1.36454	0.52309	2.609	0.00909	**
Overshoots						
	TgtMag	1.621	0.3762	4.309	1.64E-05	***
	Shark8	-1.1504	0.5707	-2.016	0.0438	*
	TreatIR:Shark4	1.3756	0.6298	2.184	0.0289	*
	TgtMag:Shark7	-1.0549	0.4656	-2.266	0.0235	*
Spirals						
	TgtMag	1.17712	0.37865	3.109	0.001879	**
	TrtVas:Shark4	2.24717	0.74503	3.016	0.002559	**
	TrtIR:Shark6	-1.24113	0.47536	-2.611	0.009029	**
	TgtMag:Shark6	1.11284	0.51082	2.179	0.029367	*
	TgtMag:Shark8	1.75847	0.48595	3.619	0.000296	***

Significance codes: 0 = ***; 0.001 = **; 0.01 = *

In terms of specific orientation behaviors in individuals, models suggested shark seven was significantly more likely to produce an overshoot orientation to the magnetic target, while shark eight was significantly less likely to produce an overshoot behavior over either landmark (table 3,11, figure 3.8C). Sharks six and eight were both significantly more likely to produce a spiral orientation to the magnetic landmark (table 3,11, figure 3.8D). Shark 4, which was seen to perform least optimally in the initial (control) two-target trial series, was demonstrated by the model to be most influenced by treatment type, for all orientation forms.

Considered collectively, orientation performance in sharks tested was impacted by sensory deprivation treatment. Orientation performance in control trials showed a general trend of improvement, with an increase in orientations across the series (figure 3.9). No similar trend was seen in orientation performance in the non-conductive gel or infra-red treatment groups.

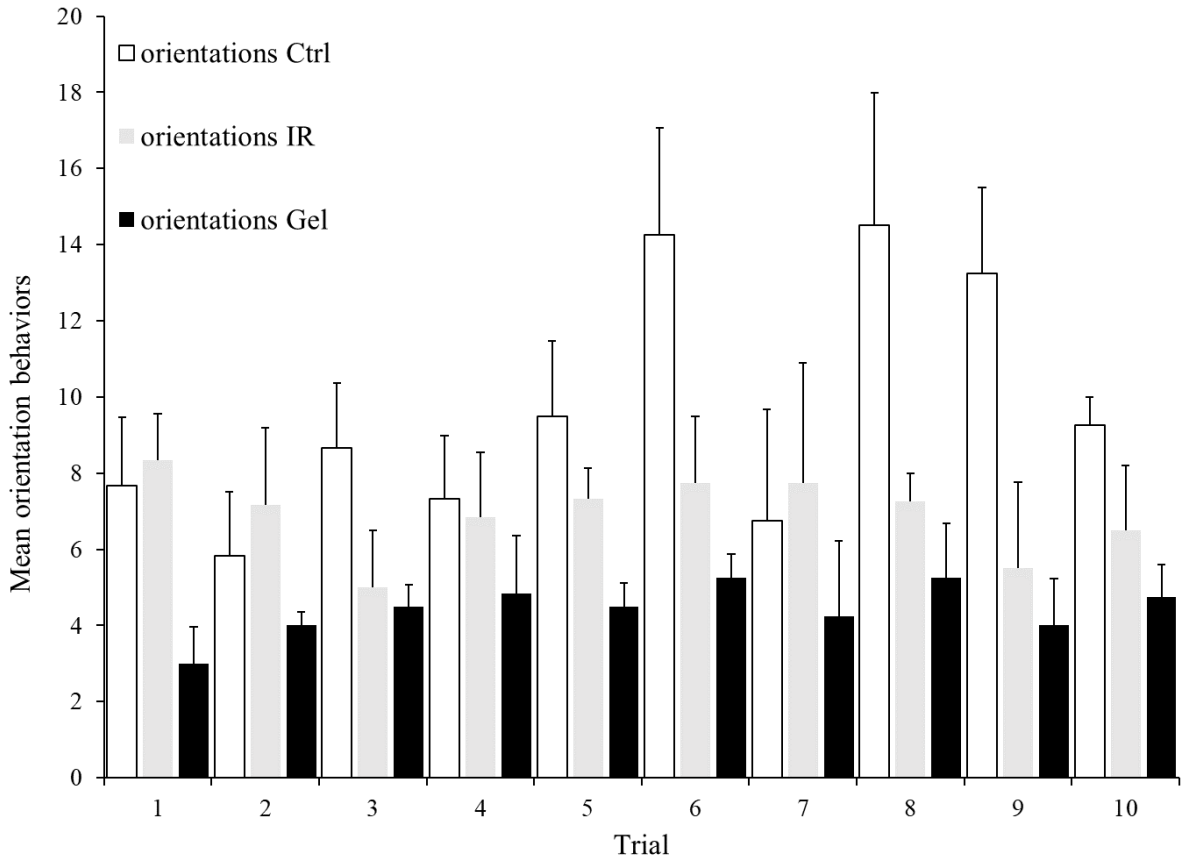

Figure 3.9 *Mean orientations of all sharks to magnetic landmark across treatments in two-target trials.* Error bars show standard deviation.

Sharks made significantly more orientations to the magnetic landmark in the control series than in both the non-conductive gel (V = 114, p = <0.001, Wilcoxon signed-ranks test) and the infra-red (V = 342, p = 0.007, Wilcoxon signed-ranks test) treatment groups. Sharks oriented to the correct target significantly more in the infra-red trial series, than in the non-conductive gel trial series (V = 173.5, p = <0.001, Wilcoxon signed-ranks test).

Production of specific behaviors was also found to be affected by treatment group. Spiral orientation behaviors were much reduced in sensory treatment groups (figure 3.10).

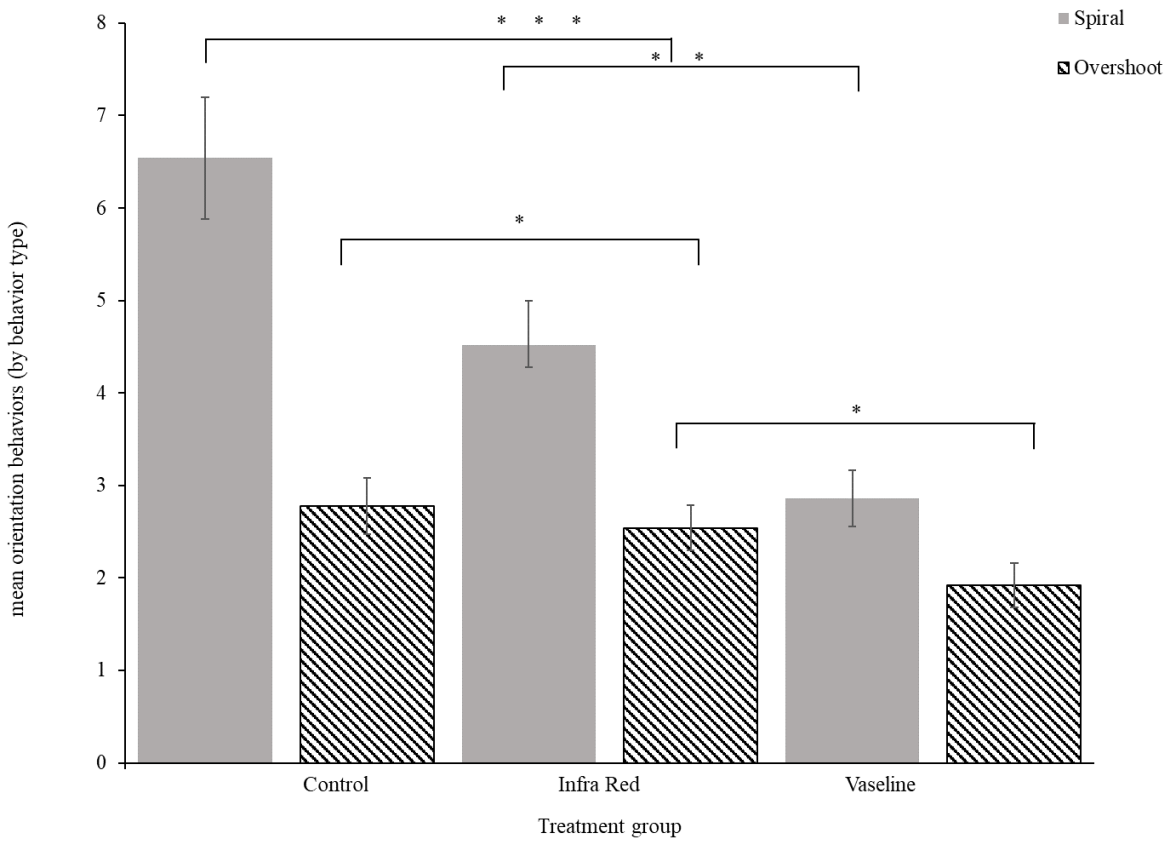

Figure 3.10 *Mean spiral and overshoot behavioral orientations across treatments in two-target trials*. Branches show where differences exist between groups, stars indicate level of significance.

Under control conditions, sharks exhibited significantly more spiral orientations to the correct target than gel (Wilcoxon signed-ranks test, V = 114.5, p = <0.001) or infra-red (Wilcoxon signed-ranks test, V = 308, p = 0.004) treatment groups. Significantly more spiral orientations were made by sharks under infra-red testing than under gel testing

(Wilcoxon signed-ranks test, V = 172, p = 0.001). By contrast, sharks produced significantly more overshoot orientations under control conditions compared to gel treatment (Wilcoxon signed-ranks test, V = 252, p = 0.01), but no difference was seen in overshoots between control and infra-red treatments. Under infra-red treatment, spiral orientation behaviors were produced significantly more than overshoot behaviors (Wilcoxon signed-ranks test, V = 733, p = 0.001), whereas no difference was seen under non-conductive gel treatment. Thus, it was apparent that the different sensory deprivation treatments had differing effects upon both the ability of sharks tested to locate the magnetic landmark, and the manner in which they oriented to the landmark.

3.5 *Discussion*

The experiments described here were designed to test the hypothesis that sharks could be trained to learn to associate a specific magnetic stimulus with the location at which they were fed. Thus, to receive food, they must be able to recognize and locate that specific magnetic signature. i.e., they need to be able to learn and memorize the sensory details of the magnetic stimulus. Newton & Kajiura (2017), demonstrated that yellow stingrays (*Urobatis jamaicensis*) could be trained to locate a magnet buried in the sand in order to receive a food reward. The magnetic characteristics of that magnet did not change however, thus no further light was cast on the discriminative capability of the elasmobranch magnetosense. In the two-landmark/target series of trials described here, scalloped hammerhead sharks demonstrated they were able to recognize the difference in magnetic signature of two visually identical landmarks, orienting to the magnetic landmark significantly more than the non-magnetic alternative (figures 3.4, 3.5). The importance of the visual system in orientation, learning and problem solving in elasmobranchs has been well documented (Fuss et al. 2014; Fuss & Schluessel 2015), thus it was important landmarks were visually identical, so as not to present any cues to orientation other than the magnetic stimulus. Similarly, it was equally important the landmarks were pseudo-randomly positioned before each trial, to control for the possibility that sharks might use landmarks within or outside of the tank as cues to orientation.

Spiral and overshoot orientations were used as behavioral metrics, demonstrating when a shark had identified the correct landmark. Across the trial series, all sharks (with the

exception of shark four) exhibited more spiral orientations to the magnetic landmark than overshoots (table 3.6). Kalmijn (2000) proposed that sharks orienting to both acoustic and bio-electric fields will follow field lines emitted from the source by maintaining a constant angle between it's body and the vective source. Kajiura and Holland (2002), noted that in behavioral experiments using prey-field simulating dipoles, scalloped hammerhead and sandbar sharks followed the electric field lines produced by the dipole, to the dipoles' center, as predicted by Kalmijn (2000), often biting at the dipole. These descriptions bear a striking resemblance to the spiral orientations to the magnetic landmark (which itself is a magnetic dipole). It is quite probable sharks followed the magnetic field lines (whether via their electrosensory system, or another means) to the center of the magnet, thus emulating behaviors described by Kajiura & Holland (2002). While the number of overshoot orientation behaviors produced across the trial series showed a relatively static trend, spiral orientations showed an increasing trend (figure 3.5B). It is hypothesized from this that overshoot behaviors reflect searching behavioral patterns, where the location of an object, or source of signal is not known, or is uncertain. Spiral behaviors therefore reflect positive identification of an object or signal source. Kajiura and Holland (2002) hypothesized these (overshoot) behaviors may have occurred because sharks were moving too fast (which is less likely in this scenario – sharks were not in a "frenzied" state due to the presence of olfactory stimulants in the water), or because sharks may have failed to identify the location of the stimulus, but recognized a localized electrical field anomaly having moved out of the dipole field, and detected and inverse field polarity. The latter hypothesis is certainly possible, and supports the concept that these behaviors are produced when the location or source of the signal is not known.

Sharks that had successfully completed the initial two target series of trials were tested again to assess their ability to discriminate and recognize the same magnetic landmark from a range of magnetically contrasting, visually identical landmarks. Again, landmark placement was randomly selected among the four fixed sites in the test arena. This, combined with sharks only being allowed to experience the individual landmark arrangements during trials (sharks were kept on the other side of the median partition to the testing area), was the best proxy for habitat disruption that could be feasibly achieved in this environment. Scalloped hammerhead sharks are a coastal-pelagic

species, utilizing inshore and pelagic waters, thus are likely to use both egocentric and allocentric orientation strategies. Animals with well-defined home ranges, or that demonstrate high levels of site-affiliation, are likely to utilize egocentric (idiothetic) strategies (that rely on recognition of specific features in the environment (Odling-Smee & Braithwaite 2003), focusing on local landmarks as directional cues, and orienting relative to their position within the environment (Andreano & Cahill 2009)), as well as allocentric strategies (that rely on cognitive spatial representation of objects or features in relation to other objects (Filimon 2015)). The hypothesis of a cognitive magnetic map requires that animals not only learn & memorize the spatial relationship of geomagnetic phenomena, but can also use that knowledge to extrapolate the heading/bearing required when the location of a destination is not known (Gould 2015). Thus, an animal can proceed to a goal from an unknown starting point. Egocentric orientation strategies are detrimentally affected by habitat disruption (Rodriguez et al. 1994), thus the pseudo-random placement of targets, and the occlusion of sharks from the testing arena outside of testing was designed to prevent or deter sharks from using egocentric orientation strategies. Although not a perfect proxy, the design of the experiment aimed to demonstrate use of non-egocentric (therefore allocentric or ego-allocentric) strategies, as are hypothesized to be used in the navigation by cognitive (and magnetic) maps.

Sharks in the study again demonstrated a clear aptitude to recognize and identify the correct magnetic landmark. All sharks produced significantly more orientations (total orientations, spirals & overshoots) to landmark 'A' (dipole arrangement) than landmark 'B' (blank. Three of the seven sharks tested exhibited no difference in overshoot orientations to landmark 'D' (cube/square) compared to landmark 'A'. On the surface, it might be considered these sharks had greater difficulty in discriminating the magnetic field characteristics of landmark 'A' from landmark 'D'. Certainly, modeling their associated magnetic field lines showed these two landmarks have very similar characteristics, although landmark 'D' has a more complexed field associated with its center due to magnetic interactions between the four magnets arranged in its' center (figure 3.3A & D). However, analysis and interpretation of the individual responses suggests the most likely reason for this apparent reduced overshoot orientation performance is because these sharks (sharks three and eight) exhibited high spiral orientations to landmark 'A' compared to landmark 'B'. Assuming the hypothesis that

overshoot orientations prevail when the object or signal source is unknown, and spiral orientations indicate more assured identification, the lack of a difference in overshoot orientations between the two landmarks in these two sharks appears to indicate the sharks were 'confident' of identification of the correct signal, as evidence by the high corresponding spiral behaviors.

Overall, sharks tested demonstrated they possess the functional capability to locate and identify a specific magnetic stimulus, and could discriminate between contrasting magnetic stimuli in doing so. Further, these data are the first empirical data to demonstrate this functional capability. This capability describes the fundamental requirement of orienting or navigating using geomagnetic field information, whether as part of a piloting strategy, or path integration strategy. The results suggest that sharks were capable of learning and memorizing the magnetic characteristics of the landmarks, that might form part of map-step in orientation and navigation behaviors, although it is difficult to even speculate as to whether they may have been attending to the magnetic "topographic" patterns, the overall intensity, or the dynamics of the field lines associated with each target. Certainly, this experiment does not provide evidence of a magnetic compass sense, nor evidence for capability for true navigation. A magnetic map sense, based on intensity and/or inclination of the geomagnetic field has been demonstrated in invertebrates, e.g. spiny lobsters (Boles & Lohmann, 2003), and in several vertebrate taxa, including newts (Fischer et al., 1993), salmon (Putman et al., 2014) and turtles (Lohmann, 2004). However, it is probable that animals in these studies used a bi-modal map system, i.e. they formed an understanding of the spatial relationships of features in their environment through a combination of the magnetic field, and some other environmental characteristic. These data lend support to Klimley's hypothesis of geomagnetic topotaxis in the species in as much as they demonstrate the functional capacity of the species to orient to magnetic features. Klimley speculated that sharks in his study may have used both the geomagnetic maxima and minima as reference points, as well as the gradient of the magnetic field associated with those maxima and minima. This could be argued to represent a bi-modal topographic map. As we cannot say which characteristics of the landmarks magnetic fields sharks in this study attended to, we cannot provide supporting evidence of a bi-modal capability. While experiments were designed to prevent, or at least discourage the use of egocentric orientation strategies, it is impossible to actually

determine the strategy in use from these data. Freshwater stingrays (*Potamatrygon* motoro) in spatial orientation experiments have been shown to place greater importance on the overall environmental or geometric arena than on specific landmarks (Schluessel et al. 2015). Discrimination of the correct magnetic landmark certainly required knowledge of it's magnetic characteristics, as well as those of the alternative configurations. However, the design of the experiment cannot conclude with any confidence whether sharks used egocentric or allocentric strategies. Sharks were observed to orient directly to the correct landmark on repeated occasions, but they were also regularly observed to move from one landmark to the next, until the correct landmark was found. This latter observation is akin to taxon strategies, which many animals will use in addition to allocentric strategies (O'Keefe & Nadel 1978; Schluessel & Bleckmann 2005), essentially moving from one familiar object to the next. Thus, it is probably likely tested sharks used a combination of the two strategies (ego-allocentric). This does not preclude use of allocentric geomagnetic orientation strategies, as required in the formation of a cognitive magnetic map.

In fish, cognitive maps are thought to be retained within the telencephalon in a region homologous to the human hippocampus, the pallium (Rodríguez et al. 2002). More specifically, the lateral pallium (Portavella et al. 2002). In elasmobranchs, the medial and dorsal pallium have been shown to be involved in acquisition and retention of spatial information pertaining to allocentric, but not egocentric orientation strategies (Fuss et al. 2014a; Fuss et al. 2014b). Based on morphometric studies, scalloped hammerhead sharks could certainly be argued to possess the physical structures required for cognitive map acquisition. Elasmobranchs in general exhibit brain to body size ratios comparable to most higher vertebrates (Yopak et al. 2007b; Yopak 2012). Sphyrinid sharks in particular exhibit pronounced enlargement of the telencephalon (Yopak 2012) which may confer increased capacity to acquire and retain (spatial) information.

Sensory deprivation treatments were incorporated into two-target/landmark testing, designed to examine the sensory mechanisms potentially used in magnetic field perception in sharks. Electrosensory capability in sharks tested was impaired or disrupted through covering the pores of the ampullae of Lorenzini with a non-conductive hydrophobic gel. This technique was incorporated into electrosensory

behavioral orientation experiments using prey-simulating dipole fields (Ambrosino 2012). These experiments, designed to test the functional sub-unit hypothesis (Tricas 2001), demonstrated that such gels could be used to occlude specific clusters of ampullae of Lorenzini and elicit a subsequent change in the nature of behavioral orientations produced.

The role of the electrosensory system in magnetic field perception has been much debated, but is generally accepted (Kalmijn 1966; Kalmijn 1981; Kalmijn 2000; Paulin 1995; Molteno & Kennedy 2009). Ambrosino's methods were therefore incorporated into two-target magnetic field orientation experiments to occlude the electrosensory system in identification of the magnetic target. Ambrosino concluded that occlusion of the superficial ophthalmic pore cluster (SOA) resulted in a reduction in spiral orientation behaviors, and a subsequent increase in overshoot orientation. Thus, it was concluded that SOA pore cluster were directly responsible for mediating the source of electrical stimuli, and orienting to the location of those stimuli through spiral behaviors. The increase in overshoot behaviors represented a compensatory (redundancy) mechanism.

In these magnetic field experiments, sharks treated with non-conductive, hydrophobic gel exhibited significantly less spiral orientations to the magnetic landmark than in control trials. Spiral orientation behaviors were still exhibited however. It was notable that in contrast to the results of the Ambrosino (2012) study, overshoot orientation behaviors did not show an increase corresponding with compensation for the spiral behaviors. The Ambrosino study only occluded one pore cluster (on either side of the cephalofoil) at a time, which probably facilitated behavioral compensation using an alternative pore cluster (Ambrosino hypothesized the buccal cluster). Although it can only be confirmed through electrophysiology, it is assumed that in these (magnetic field) experiments, compensation through another pore cluster was not possible, as all pores, and their associated clusters, were inactivated. The reduction of overshoot behaviors seen in the gel-treatment trials compared to control trials serves to support this notion. Thus, continued perception of magnetic stimuli must be derived via an alternative mechanism.

An iron (magnetite) based system may facilitate both overshoot and spiraling behaviors. A magnetite based could possess sufficient thermal energy to be used in perception of magnetic field direction and inclination, as well as magnetic field intensity (magnitude)

(Walker et al. 2006). Overshoot orientation behaviors could therefore function in a searching strategy. When the shark perceives an anomaly in the intensity of the local magnetic field (in this case the magnetic landmark), it can double-back upon itself, and narrow in on the source of the magnetic anomaly, following the field lines associated with the anomaly/landmark. This could explain how and why orientation behaviors continue to be produced even though the electrosensory system has been occluded. Alternatively, an optically based system, such as that proposed in some avian species (Wiltschko & Wiltschko 2006) allows the animal to "see" the lines of magnetic field information. If such sensory capability does exist in sharks, they could, potentially "see" the field lines associated with the magnetic landmark, and thus follow them into the center of the landmark in a spiral fashion. Whether or not this is likely is a separate question.

This question was addressed via the infra-red treatment two-landmark/target testing. The optically based radical-pairs mechanism requires blue wavelengths of light to excite the singlet state electrons within cryptochrome molecules in the retina (Wiltschko & Wiltschko 2006). Thus, magnetic field orientation in the absence of blue light wavelengths cannot be facilitated via the radical-pairs mechanisms. Peak sensitivity to light under scotopic conditions in scalloped hammerhead sharks was recorded at λ 530 and 480 nm (McComb et al. 2010). Infra-red illuminators used in the study project light at λ 840nm. It was hypothesized that no significant difference would be seen in orientation performance by sharks tested under infra-red light. Scalloped hammerheads make regular dives to depths of over 800m, presumably to forage. White and blue light attenuates long before these depths are reached. Thus, it was expected that sharks would be able to seek out the stimulus they had been trained to associate with food (i.e. forage) under infra-red light.

Results of trials showed that sharks tested could indeed successfully identify and locate the magnetic target under infra-red conditions, and made significantly orientations to the magnetic target. However, a significant general reduction in orientations was seen in comparison to control trials, although orientations produced were still significantly higher than in the non-conductive gel treatment (figure 3.9). Significantly more spiral behaviors were exhibited in control trials compared to infra-red trials, but no difference was seen in overshoot behaviors (figure 3.10). The reduction in orientation behaviors seen is likely a function of the removal of a primary sensory resource otherwise used in

these trials. That no difference was seen in overshoots likely reflects this, as overshoots in lit (white light) conditions likely constitute a deliberate behavioral choice as part of a searching strategy, i.e., it would not be expected that overshoot behaviors would increase, as the deliberate nature of producing an overshoot orientation to a visual landmark is precluded. Unlike the orientation behaviors demonstrated by Kajiura & Holland (2002) and Amrosino (2012), the orientation behaviors seen in this study likely do not reflect natural behaviors that one might expect to observe in orientation and navigation under natural/normal conditions. Rather, the spiraling and overshoot orientation behaviors observed and described here are a proxy for measuring functional capability, and are borne from the learned association of the magnet stimulus as a food resource.

The sensory treatment experiments described provide support to the likely use of the electrosensory system in orienting to magnetic field stimuli, as evidenced by the significant reduction in total orientation behaviors in the non-conductive gel treatment trials. Based on Ambrosino's findings, there is no reason to suspect that sharks maintained a functional electrosense post non-conductive gel treatment. Thus, the continued (although reduced) ability to orient to the magnetic landmark in the gel trials lends support to the use of alternative mechanism for magnetic field perception, which could involve putative iron-based mechanisms, or an optically based mechanism, or both. The reduction in orientation behaviors seen can be explained as resulting from the decreased signal experienced by the shark. If sharks had principally relied (not necessarily consciously) on magnetic-electric induction as the means of transducing magnetic stimuli, it's sudden removal would likely confer a reduction in orientation capability.

The subsequent infra-red treatment trials demonstrate that sharks can perceive magnetic field stimuli in the absence of the blue wavelengths of light it is proposed to function by. This does not demonstrate that sharks (and by proxy elasmobranchs) do not have or do not use an optical magnetoreceptor mechanism, it simply demonstrates that such a mechanism is not critical in perception of magnetic field stimuli, particularly when other mechanisms are apparently available.

Future studies should therefore look to find support for an iron-based mechanism. Such studies may take the form of behavioral experiments, such as those detailed in chapter 2

(although any such efforts should concentrate on knocking out/ablating proposed neural mediation pathways proposed to be involved, and examining subsequent behavioral responses). Combining the gel and infra-red treatments may be a useful means to find further support for an iron-based magnetoreceptor, however, it may be best used with an alternative species. Scalloped hammerhead sharks, juvenile or adult, are highly susceptible to stress related mortality, whether from acute of chronic stress sources (pers. obs.; Gallagher et al. 2014), thus would have been unlikely to survive a further series of handling and manipulation, followed by testing. Supporting evidence should also be gathered from physiology based studies. Neurophysiology to examine the function of specific nerves proposed to be used in mediation of magnetic field information from iron/magnetite based receptors would significantly advance the iron-based magnetoreceptor hypothesis. Of-course, any such studies would be well complemented by complete description and characterization of magnetite containing structures, and quantification of their occurrence.

Chapter 4 – *Searching For An Olfactory Magnetoreceptor*

4.1 *Abstract*

The results presented, and conclusions drawn in chapters two and three suggest that the elasmobranch electrosense may not be the only mechanism used in magnetic field perception. Of the two generally accepted alternative hypotheses, an iron based magnetoreceptor mechanism, perhaps homologous to that described in some teleost fish, may also function in elasmobranch fishes. There is continuing debate regarding the means and mechanisms by which an iron based magnetoreceptor works in both teleost fishes and birds, with questions raised over the findings of previous studies, and no single methodology seemingly able to unilaterally define a receptor and its' structural components. Thus, correlative approaches are required to sequentially draw out the critical information needed to determine whether or not sharks possess the physical means and mechanisms necessary for an iron based magnetoreceptor.

This chapter presents the results of just such an approach, designed to investigate and describe the principal required components of an olfactory magnetoreceptor in scalloped hammerhead and sandbar sharks. In these investigations, scalloped hammerhead and sandbar sharks were found to have the fundamental structures required to support an iron-based magnetoreceptor hypothesis, similar to that described in the rainbow trout *Oncorhynchus* mykiss. Olfactory tissues were found to receive widespread supply from superficial ophthalmic ramus of the trigeminal nerve, as has been described in *O.* mykiss. Iron-oxide (magnetite) containing cells were found throughout olfactory tissues and occurred in sufficient quantities and concentrations to potentially function in magnetoreception. Analysis of the magnetic nature of iron found suggest single-domain magnetism, as is required for the physical transduction of magnetic field information. The ultrastructure of iron containing cells was not described. Feasible suggestions are made for continued investigation.

The methodologies incorporated into these investigations present a reproducible, multi-faceted, correlative approach that can be used to screen for, identify and describe iron/magnetite containing structures that may function in magnetic field perception.

4.2 *Introduction*

As discussed in the previous chapters, it is well acknowledged that more than one sensory mechanism is employed across different taxa in the perception and use of magnetic field information. It is similarly possible, if not probable, that species' may integrate information regarding the geomagnetic field from different sources in the formation of cognitive magnetic maps (Lohmann, Lohmann, et al. 2008). The evidence presented in chapter 2 suggested the ability to use a non-electrosensory means of magnetoreception, and it was subsequently argued that the impairment methods applied supported a hypothetical olfactory based magnetoreceptor. In chapter 3, results of the behavioral experiments and sensory deprivation experiments reported supported shark electrosensory system involvement in magnetoreception, but also demonstrated a continued magnetoreceptive ability when deprived of electroreceptive capability. Further, the reduced, but continued responses seen under infra-red lighting suggest a limited (if any) role of a cryptochrome magnetoreceptor mechanism, at least in the species tested (*Sphyrna lewini*). It follows therefore, that a third sensory receptor mechanism is involved in magnetoreception in these fish. On the basis of the generally accepted magnetoreceptor hypotheses (see chapter 1), an iron-particle based receptor mechanism may well be used in sharks (or again, at least in this species). The debate about the means and mechanisms by which an iron based magnetoreceptor continues unabated, with no single methodology seemingly able to unilaterally define a receptor and its' structural components. Thus, a correlative approach that combines and integrates techniques to succinctly describe and characterize the necessary components of a such a magnetoreceptor is needed (Shaw et al. 2015). This chapter presents the results of just such an approach, designed to investigate and describe the principal required components of an olfactory magnetoreceptor in scalloped hammerhead and sandbar sharks.

Studies have suggested that in salmonids, the olfactory rosette serves as the magnetoreceptor structure, housing cells containing single domain magnetite (Walker et al. 1997; Diebel et al. 2000). It is further proposed that the superficial ophthalmic branch (SOA) of cranial nerve V (CNV) (Trigeminal) innervates the olfactory rosettes, and is the pathway of information transduction to higher processing regions of the brain (Walker et al. 1997; Hellinger & Hoffmann 2009).

4.2.2

The trigeminal nerve relays somatosensory information to the brain from receptors around the head and mouth. In teleost fish, trigeminal receptors are sensitive to mechanical (pressure, stretch, vibration), thermal, and chemical stimuli (Sneddon 2003). CNV also functions in nociception (detection of a noxious or tissue-damaging stimulus) (Sneddon 2002) and has a functional role in olfaction (Belousova et al. 1983; Bouvet et al. 1987). The role of the trigeminal system in olfaction in teleosts has received much attention (Hara 1975; Belousova et al. 1983; Puzdrowski 1988), and free nerve endings of the CNV have been described in the olfactory epithelium of a range of teleosts. If follows therefore that sensory afferents from CNV may well serve to convey magnetosensory information as suggested by Walker (1997) and supported by the findings of Hellinger & Hoffman (2012). Essentially, trigeminal receptors sensitive to pressure, stretch and vibration are likely to be sensitive to physical forces exerted upon iron/magnetite containing cells and tissues as the magnetite crystals within them experience torque induced by a change in the local magnetic field. Studies of trigeminal function in elasmobranchs did not identify a nociceptive function (specifically as a pain receptor) (Snow et al. 1993). This does not, however, preclude trigeminal innervation to the elasmobranch olfactory rosette, or its' function as a mechanoreceptor. Thus, *in* & *ex vivo* tract tracing techniques were incorporated into this study to examine putative trigeminal innervation of the olfactory rosette. The lipophilic stain Oil Red 'O' was used to examine gross morphology and nerve pathway structure, and to identify candidate CNV sites for application of neuro-tracers (Biotinylated Dextran Amine (BDA), DiI and Neurobiotin^{+}™).

4.2.3

If elasmobranchs do indeed possess and use a magnetite based magnetoreceptor homologous to that proposed and described in their teleost cousins, the presence of magnetite is required in the tissues of the olfactory rosette. A form of magnetite (titanomagnetite) was described in association with the sacculus in guitarfish (O'Leary et al. 1981; Vilches-Troya et al. 1984). However, due to the size of the crystals, and their subsequent domain structure, it is presumed their magnetic axes would not align with an external magnetic field, and would therefore not function in magnetoreception. Magnetite is thought to be incorporated into cells through biogenic processes, although

these processes have only been studied in magnetotactic bacteria (MTB) (Blakemore 1975; Frankel et al. 1979; Schüler 2008; Faivre & Schüler 2008). Essentially, iron is actively transported in the cell, and is converted into magnetite via reduction and oxidation reactions. Invaginations of the cell wall of the MTB are formed during this process, eventually resulting in a membrane bound, magnetite containing organelle, termed a magnetosome (Komeili et al. 2006). The species-specific size and shape of the magnetite crystal within a magnetosome is thought to be under direct genetic control (Schüler 2008). These magnetosomes are arranged within the MTB, and held in place through actin-like protein filaments known as MamK. Thus, although MTB's are prokaryotes, their organelles are considered to share many characteristics of eukaryotic cells (Komeili et al. 2006). It is broadly held that magnetite formation in other taxa may be under similar genetic control (Shaw et al. 2015), rather than being a byproduct of environmental exposure.

In the rainbow trout (*Oncorhynchus mykiss*), cells containing single-domain magnetite particles are 10–12 μm in length, have a distinctive multilobed shape, and are consistently located near the basal lamina of the olfactory epithelium. The chain of magnetite crystals in each cell is about 1 μm long (Diebel et al. 2000). Magnetite containing cells in *O. mykiss* were reported to be quite rare, with an average 4 cells per 10000 being identified. Such cells were reported to contain clustered chains of magnetite crystals, made up of 70-1700 crystals (Eder et al. 2012).

4.2.4

To test the elasmobranch olfactory magnetoreceptor hypothesis, a multi-faceted approach was adopted, incorporating techniques including histology (Perls Prussian Blue), magnetic resonance imaging (MRI), flow cytometry, Raman spectroscopy and electron microscopy (SEM & TEM). This approach was designed to examine shark olfactory tissues for the presence of iron/magnetite; characterize the structures in which magnetic or magnetite-containing cells occur; characterize magnetic or magnetite containing cells; examine the size of magnetite crystals; and examine the arrangement (e.g. clusters/chains) in which magnetite crystals occur. Perls Prussian Blue technique has been used to identify putative magnetite containing cells in tissues from the upper beak of the homing pigeon (*Columba livia*) (Fleissner et al. 2003). It presents a valid way to identify the presence of non-haem iron. In the presence of Fe^{+3} and HCl^{+} potassium

hexacyanoferrate turns into dark blue ferric ferrocyanide (Fleissner et al. 2003), thus can be used to locate potential magnetite (Fe^3O^4) clusters.

The identification of regions of interest was attempted using a combination of magnetic resonance imaging (MRI) and serial sectioning with histological staining using Perl's Prussian blue. This part of the approach was designed to qualitatively and quantitatively determine the presence of iron oxide and magnetic material within the olfactory tissues. MRI, is a unique technique that can non-invasively acquire high-resolution, 3D digital data of soft tissue structures. Although this technique is extensively developed for applications in human brain research, it's utility in comparative neurobiology remains largely under-used. Iron deposits in soft tissues such as the olfactory epithelium are detectable using MRI, but the miniscule amounts such as those that occur in macrophages would not be resolved. Thus, the combination of MRI & Prussian Blue to co-localize iron containing cells presents a novel means of identifying potential magnetite containing structures/regions within the olfactory rosette.

Flow cytometry (FCM) is a means of measuring certain physical and chemical characteristics of cells or particles as they pass in a fluid stream by a beam of laser light. Flow sorting (separation of cell populations according to a given metric) can also be used. This process compliments FCM by using electrical or mechanical means to divert and collect cells (for example based upon emission or reflectance spectra). Following dissociation of the olfactory rosette into a single-cell suspension, FCM was used to characterize and quantify magnetic cells.

Spectroscopic methods used in elemental analysis are based on emission, absorption, fluorescence or scattering of energy from matter, and can be used for qualitative (identification of an element via measurement of radiation frequency) and quantitative (concentration of an element via measurement of radiation intensity) analysis of a sample (Bumbrah & Sharma 2016). Raman spectroscopy relies on the inelastic scattering of monochromatic (i.e. a specific source wavelength) light. Any given molecule has a specific vibrational frequency, and thus scatters light at specific wavelengths (Raman effect). A Raman spectrum is a plot of the intensity (per unit counts) of Raman scattered radiation as a function of its frequency difference from the incident radiation (usually in units of wavenumbers, cm^{-1}). This difference is known as the *Raman, shift*, and is independent of the frequency of the incident radiation. Magnetite has its own specific Raman shift (Shebanova & Lazor 2003), and Raman

spectroscopy has been used to identify magnetosomes in MTBs (Watanabe et al. 2008; Eder, Gigler et al. 2014), but has not been used to identify magnetite containing cells from any other taxa.

TEM has been a definitive tool in characterizing magnetosomes and magnetite crystals from a variety of species. However, the difficulties of locating microscopic deposits of magnetite make TEM a particularly inefficient (and expensive) means of screening tissues for magnetite crystals. The impracticality of combining screening histological techniques such as Prussian Blue with TEM was noted by Shaw et al (2015), who summarized that the only way to combine these methods was to adopt semi-correlative Prussian blue and TEM approach, taking alternate semi-thin and ultra-thin sections for optical and electron microscopy. This study incorporates a directly correlative approach that combines these two techniques to screen for putative magnetite deposits using histology, then directly examine the region of interest using TEM.

4.3 *Methods*

4.3.1 *Cranial Nerve Pathway Tracing*

The heads of juvenile scalloped hammerhead and sandbar sharks caught as bycatch in other research activities were removed and fixed in 10% formalin, then stored in 50% isopropanol. To examine the gross anatomy and pathways of cranial nerves, with particular attention to CNV, repeated dissections were made to determine the locations of the main trunks of cranial nerves, and their pathways toward their terminal points of innervation. To aid in tracing finer processes and projections, the lipophilic dye Oil Red O was applied to candidate nerves, and allowed time to migrate before continued investigation. Labelled nerve fibers (which turned red/pink) were carefully traced to their receptor fields, or the most distal extent possible.

The heads of two further juvenile sandbar sharks were fixed in 4% paraformaldehyde. Following fixation, DiI (1,1'-Dioctadecyl-3,3,3',3'-Tetramethylindocarbocyanine Perchlorate), a long-chain lipophilic carbocyanine dye, was applied to a cut portion of the superficial ophthalmic branch of the trigeminal nerve using an insect pin, a short distance before it passed over the cartilaginous capsule that encases the olfactory rosette (see figure 4.1). DiI crystals were applied to the cut nerve stump until discolored. Parafilm was placed over each cut stump, then crimped to the stump using tweezers. A surgical sponge was then placed over the

parafilm and compressed into place. Vaseline was then smeared over the top of the surgical sponge to act as a hydrophobic barrier. The heads were then stored in 4% paraformaldehyde (PFA) made up with 0.1M PBS and kept in a dark environment for a year.

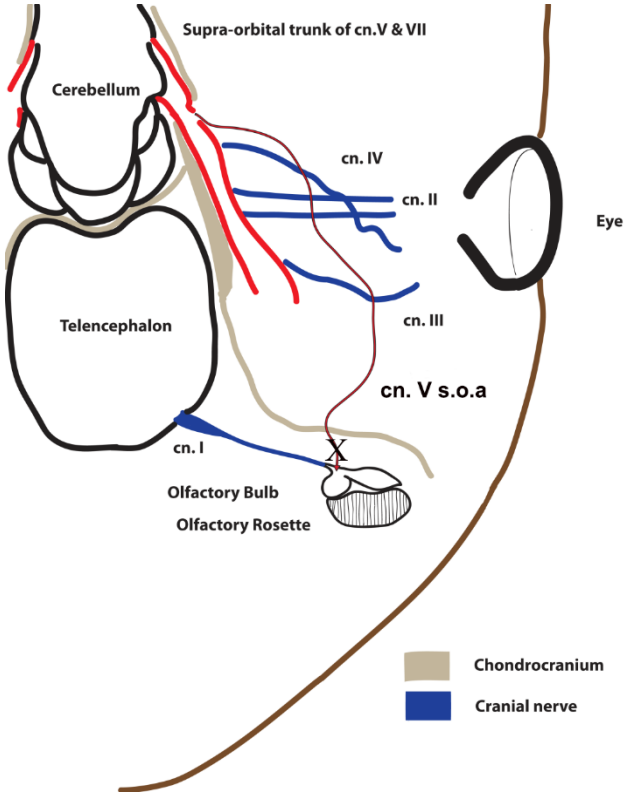

Figure 4.1 *Schematic of CNV s.o.a., showing surgical locus* (X) *of DiI application*. From its apparent source at the trigeminal ganglion the nerve descends rostrally, passing over CNIV and CNII coursing medially to the. The nerve then passes under CNIII before again coursing slightly medially. At the level of the anterior telencephalon, approximately parallel to the origin of CNI, the nerve penetrates the cartilage 'wall' that descends from the chondrocranium toward the rostrum coursing toward the olfactory capsule, which is penetrated by rami of the nerve near to the medial lobe of the olfactory bulb.

In juvenile scalloped hammerhead sharks, the lateral expansion of the head results in its unique cranial morphology. As a result, the distance between the dorsal and ventral surfaces of the head is comparatively small when compared to most other shark species. Accessing the cranial nerves is considerably less intrusive as a result. Thus, applications of two neural tracers were made *in vivo* to the same branch of the CNV (figure 5.2). Following surgery (see surgical preparation and procedure), animals were revived, and

given a period of up to seven days for the dyes to migrate, before being euthanized and prepared for histological investigation (see histological investigation).

4.3.2 *Surgical preparation and procedure.*

Juvenile *S. lewini* (n = 10) were collected from Kaneohe Bay, Oahu, HI using handlines, then held in aquaria at the Hawaii Institute of Marine Biology, before undergoing surgery. Sharks were sedated using MS-222 at a concentration of (0.5 g/L^{-1}) through an oral ventilator, powered by a 12-volt battery. Sharks were deemed sedated when a lens reflex no longer occurred if gentle pressure was applied to the eye. Once sedated, sharks were kept under sedation using a "maintenance" dose of MS-222 (0.5 g/L^{-1}) in a recirculating system.

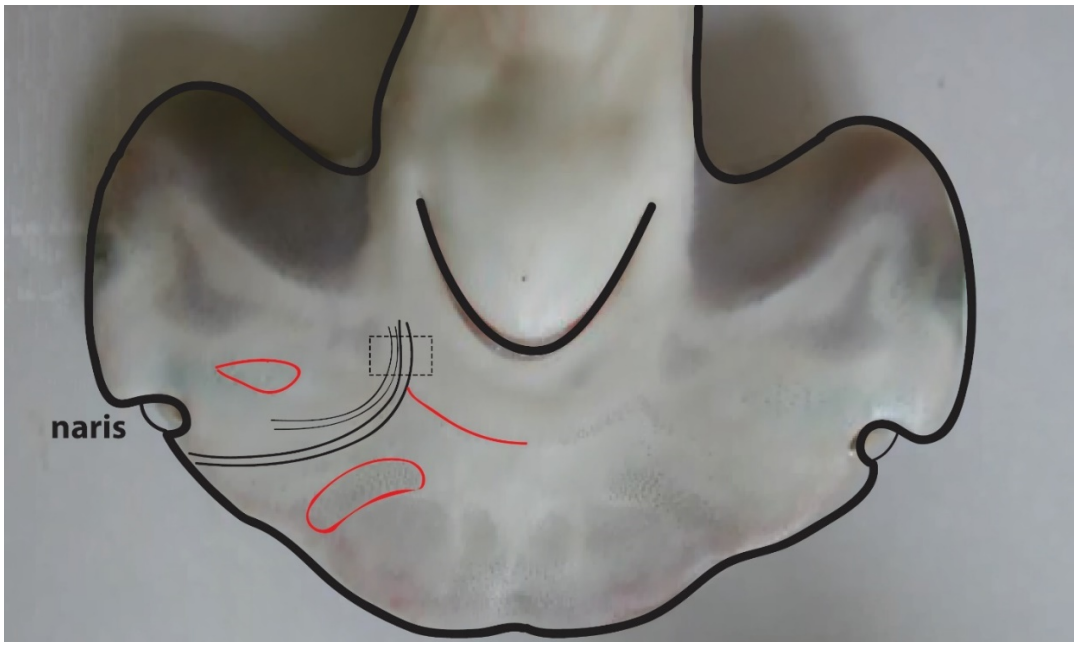

Figure 4.2 *Schematic of candidate nerve pathway, showing surgical locus* (boxed area). For reference, the location of ventral ampullary clusters are also shown (in red). Approximate location of the SOA branches of CNV and aLLN (beneath the integument) shown in black. Application of BDA or Neurobiotin^{+} was made to the distal/rostral end of the severed ramus of CNV – assumed to be the SOA ramus due to its close association to the SOA ramus of the electrosensory anterior lateral line.

Sharks were placed on their dorsal surface, on a foam pad, with a slit cut to accommodate the dorsal fin. A neoprene shield was fitted around the end of the of the ventilator in order to seal the buccal cavity and prevent water spilling out over the ventral surface of the sharks head. Three incisions were made at the site of the surgical

locus (see figure 4.2). The incisions were connected to make 'flap', which could be peeled back, then held in place using an insect pin. Ampullary canals between the flap and the target nerve branches were carefully excised using iris scissors, thus exposing the ophthalmic branches of the anterior lateral line and trigeminal nerve.

As with the DiI application in fixed *C. plumbeus* heads, a cut was made to the candidate nerve branch before either BDA (NeuroTrace® BDA-10,000 Neuronal Tracer Kit) (5 sharks) or Neurobiotin^{+} (5 sharks) were applied to the cut nerve stump. Parafilm was placed over each cut stump, then crimped to the stump using tweezers. A surgical sponge was then placed over the parafilm, then compressed into place. Vaseline was again smeared over the top of the surgical sponge to act as a hydrophobic barrier. The 'flap' of skin was then folded back into place, and the cut edges glued together using VetBond (3M, Minnesota, U.S.A). Sharks were then returned to holding aquaria where they were revived and monitored until such as time as they were deemed to be swimming normally. Sharks subsequently held for up to seven days to allow for migration of the tracer, before being euthanized for histological analysis.

4.3.3 *Euthanasia and histological procedure.*

Following seven days post-surgery, sharks were again sedated using MS-222 at a concentration of (1 g/L^{-1}). If sharks did not regain 'normal' behavior patterns at any point after surgery, or looked to deteriorate in general condition, survival period was cut short (n=3). Anesthetized sharks were trans-cardially perfused with physiological saline to exsanguinate the body, before perfusing with 4% PFA in 0.1M PBS. The olfactory rosettes were then excised, before being post-fixed in the same fixative solution.

Tissues were serially sectioned using a freezing microtome, sections ranged from 10-40 µm thickness, and placed on glass slides.

Sectioned tissues that had been labeled with BDA were bathed in 1% Hydrogen peroxide in PB for 10 min (e.g. 6.6 ml stock 3% H_2O_2 in 13.4 ml PB) as a quenching step, then rinsed in phosphate buffer for a further 10 minutes. Sections were then transferred to 0.4% Triton-X in 0.05M PBS for at least 30 min (30 ml PBS + 120µl Triton-X). Following this, sections were bathed in Vector Elite ABC solution (10 ml PBS + 2 drops solution A + 2 drops solution B) containing an avidin-biotin-peroxidase complex.

Transported BDA was then visualized using 3, 3′-diaminobenzidine tetrahydrochloride (DAB) as a chromogen (Vector Laboratories). Any persisting reaction was stopped by bathing sections in 0.1M PB for 10 minutes. Finally, sections were either counterstained with cresyl violet, or left 'as is', before being cover-slipped and analyzed with a Zeiss Axioskop 2 Fluorescence Microscope.

4.3.4 *Prussian Blue histological preparation.*

Olfactory rosettes from *C. plumbeus* (n=5) & *S. lewini* (n=5) were prepared and excised following the protocols described in section 5.3.3. Titanium scalpels were used for rosette excision to control for the possibility of introducing iron to rosettes via the excision process.

Fixed rosettes were transferred through a series of sucrose solutions (30%, 20%, 10%) to cryoprotect tissues. Rosettes were then embedded in optical cutting temperature compound (OCT), then frozen in a -80°C freezer. Rosettes were sectioned (10-40 μm thickness) on a Leica CM1950 cryostat (Leica Biosystems, Wetzlar, Germany), using titanium coated blades to control for possible introduction of iron to sectioned tissues. Slides with sectioned tissues were washed in dH_2O for 10 minutes to remove residual OCT. Sections were then bathed in a solution containing a 2:3 ratio of 2% Potassium Ferrocyanide & 1% Hydrochloric Acid, followed by 3 separate dip baths in dH_2O. Finally, sections were bathed for 2 minutes in nuclear fast red solution, rinsed again and coverslipped. Sections were examined using either a Zeiss Axioskop 2 Fluorescence Microscope, or an Olympus BX51 light microscope.

4.3.5 *Magnetic Resonance Imaging*

Two juvenile *C. plumbeus* and three *S. lewini* were captured in Kaneohe Bay, brought back to HIMB, then sedated and trans-cardially perfused per the established. The olfactory bulbs and rosettes were excised from each specimen and post fixed in 4% PFA in 0.1 M phosphate buffer. After fixation, rosettes were transferred to 1 x PBS + 0.01% sodium azide for at least 14 days to remove excess fixative before transferring to fresh 1 x PBS + 0.01% sodium azide, with the addition of 5 mM of a gadolinium-based contrast at 4°C (Magnevist ®). Equilibrating the tissue in this contrast agent achieves a significant reduction in the longitudinal relaxation time (T1) of the sample and a corresponding increase in the SNR efficiency of the data acquisition.

Rosettes were removed from the contrast agent solution and placed in vacuum chamber to remove all exogenous fluids and air bubbles. Imaging was performed on a Bruker 9.4 Tesla small animal magnet and an Avance 16.4 Tesla micro-imaging scanner. Both magnets are housed in the Centre for Advanced Imaging at the University of Queensland, Australia, a part of the National Imaging Facility. Investigatory MR imaging consisted of high-resolution (10-20 μm), T1-weighted anatomical acquisition using a gradient recalled echo with no RF spoiling. MR acquisition time were run overnight to maximize signal to noise ratio. Three-dimensional data, acquired from high-resolution MRI, were digitally segmented using MicroDicom image viewer. In each rosette, total counts of iron signal sites/r.o.i$_s$ were made, the location of visualized iron signal within the tissues was noted, as was the number of digital slices (sections) in which each individual site of signal occurred. Separately, localization of particles in the MR data were compared to serial sections of the same tissues (stained with Perls Prussian Blue) to co-localize deposits of ferric-iron in tissues.

4.3.*6 Tissue dissociation and flow cytometry*

Six olfactory rosettes were collected from juvenile *S. lewini*. Animals were sedated and exsanguinated via the perfusion methods described, although no PFA or any other fixative was used. Individual rosettes & bulbs were cut into approximately 0.5cm x 0.5cm pieces using a titanium scalpel before being immersed into a gentleMACS ™ 'C' tube and incubated in a solution of collagenase (Liberase ™; SigmaAldrich, MO, USA) at 37°C for 20 minutes. Tissues were then mechanically dissociated to a single cell suspension using a gentleMACS™ dissociator (Miltenyi Biotec, Bergisch Gladbach, Germany), until no chunks of tissue could be seen. The suspension was then centrifuged at 4000 g to pelletize the cells.

The supernate was pipetted out, and the equivalent volume of PBS substituted. Pelletized cells and PBS were then vortexed to re-suspend the cells and wash them. This process was repeated a further two times. The final suspension was first filtered through a 100 μm filter, followed by a 70 μm filter. The number of cells in the suspension was then estimated using a haemocytometer.

Single cell suspensions were then separated into magnetically positive M+ and magnetically negative populations using an LS column with a QuadroMACS ™ separator. LS columns contain a matrix composed of "cell-friendly" ferromagnetic

(superparamagnetic) spheres, for fast and gentle separation of cells. Under the external magnetic field of the separator, the spheres amplify the magnetic field (up to 10,000x) inducing a high gradient within the column. Magnetic cells (30 μm in size) are held in suspension within the column, without binding to the column matrix. The enriched (M+) population can then be harvested by removing the LS column from the separator and flushing with a volume of PBS. The M+ cell population was then estimated using a hemocytometer.

A BD FACSCalibur™ (BD Biosciences, NJ, USA) flow cytometer was used to qualitatively describe the M+ cell population. The M+ single cell suspension was vortexed to make it homogenous, a 1ml sample pipetted from it, then added to the flow stream. Cells added to the flow were counted and qualified according to size (forward scatter – FSC) and granularity (side scatter – SSC). This allows for gating (sorting) into sub-populations FSC and SSC.
A separate 1ml aliquot was taken from the homogeneous M+ population, and an 1μl aliquot of a solution containing microscopic (mean size = 0.35μm), fluorescent magnetic beads added (Spherotech Inc, Lake Forest, IL). This suspension was again vortexed, then allowed to settle to provide sufficient time for the magnetic beads to bind to magnetic/iron containing cells. Cells and beads were again re-suspended before being added to the flow stream. This cell+bead population was counted analyzed using the fluorescent-activated cell sorter (FACS). By qualifying according to fluorescence, size and granularity, cells bound to beads can be distinguished from beads alone, or from cells alone. The cell+bead population was further gated into sub-populations based upon FSC & SSC.

4.3.*7 Raman spectroscopy*
A Kaiser 785nm micro-Raman system (Kaiser Optical Systems Inc, MI, USA) was used to examine tissues and cells for the presence of magnetite. Tissues were first sectioned then stained with Perls Prussian Blue to screen for iron. Sections with blue stain (positive for iron) were set aside, then rehydrated in dH_2O. A ring around the region of interest (ROI) was cut using a titanium scalpel, then the ROI gently floated off the glass slide, before being collected onto an aluminum slide (glass slides cannot be used in Raman). Collected sections were allowed to dry before analysis.

M+ single cell suspensions were prepared from olfactory tissues per the described methodology and pelletized. A micropipette was used to resuspend cells before being pipetted onto an aluminum slide. Pipetted cells were dried before analysis.
One M+ pellet was allowed to dry with a falcon tube. A strong neodymium magnet was used to draw magnetic material out of the dried cellular debris, which was then deposited onto an aluminum slide. Samples were measured using a 785nm laser focused at 5x or 10x, at power varying between 0.5 and 12 milliWatts (mW). Exposure times (to the laser) ranged between 2-30 seconds, while the number of acquisitions (for signal averaging) ranged from 5 to 150.

4.3.*8 Electron microscopy*

Olfactory tissues prepared for histology as previously described, sectioned at 20 μm, then screened for iron using Perls Prussian Blue. Select ROI's were subsequently using SEM & TEM. For SEM analysis, sections containing ROI's remained on glass slides. Sections were sputtered with gold/palladium (Au/Pd) in a Hummer 6.2 sputter coater to prevent charging, reduce beam damage and enhance electron transmission. ROIs were viewed screen for apparent inorganic structures with a Hitachi S-4800 Field Emission Scanning Electron Microscope at an accelerating voltage of 5kV. Candidate structures were subsequently compositionally analyzed using energy-dispersive x-ray spectroscopy (EDS) to confirm presence of iron.
For TEM, the methodology described by Jones (2016) was adapted to prepare ROI's for analysis. Slides were laid in a glass dish (sections facing up) and bathed in a 1:1 mixture of LX-112 epoxy resin and propylene oxide, then left to allow infiltration of sections. After 12 hours, excess propylene oxide/embedding mix was drained from slides. Slides were again laid flat in a glass dish and bathed in a freshly propylene oxide/embedding mix (bubbles removed from the mix in a vacuum oven). Slides and section were placed in a vacuum oven at 20°C and again left for 12 hours, after which excess propylene oxide/embedding mix was drained off, before slides were laid in a foil tray.
An embedding capsule (hinged lid removed) was filled ~ half way with fresh embedding resin, inverted, then placed on top of each ROI. The foil tray containing slides and capsules was placed in an oven at 20°C for 48 hours. Slides were removed, allowed to cool, then placed in a Dewar containing liquid nitrogen for ~ 3 minutes. Slides were

then removed with tongs, and the embedding capsule grasped with forceps to remove it from the surface of the slide. The capsule and the embedded ROI should come away together. The capsule was then carefully cut with a razor blade to remove it from the resin block, and the block then trimmed. Ultrathin (60-80 nm) sections were obtained on a RMC Ultratome ultramicrotome (Boeckeler Instruments, Az, USA) double stained with uranyl acetate and lead citrate, then viewed on a Hitachi HT7700 transmission electron microscope at 100 kV.

4.4 *Results*

4.4.1 *Trigeminal Nerve Pathway Tracing*

Having removed the integument, connective tissues and ampullary canals of heads, the gross anatomy of the cranial nerves was examined to locate the pathways of CNV. The chondrocranium was carefully removed to reveal the points at which the various cranial nerves arise from the brain. CNV stems from the antero-lateral medulla oblongata, forming a sensory ganglion that serves all three CNV branches (maxillary, mandibular, ophthalmic) between the medulla and the chondrocranium. The ophthalmic and maxillary branches are purely sensory, while the mandibular branch (primarily innervating the lower jaw) has both sensory and motor functions and fibers, the latter having both afferent and efferent functions. From the ganglion, CNV courses anteriorly as a trunk, in association with the primary trunks of the facial nerve (CNVII) and the anterior lateral line (aLLN).

In *C. plumbeus*, the deep ophthalmic ramus of CNV (*opthalmicus profundus*), which is sensory in nature, passes over CNIV and CNII coursing medially to the orbit, though not through it as described in *O. mykiss* by Walker et al. (1997) (see Figure 4.1). The nerve then passes under CNIII before again coursing slightly medially. At the level of the anterior telencephalon, approximately parallel to the origin of CNI, the nerve penetrates the cartilage 'wall' that descends from the chondrocranium toward the rostrum.

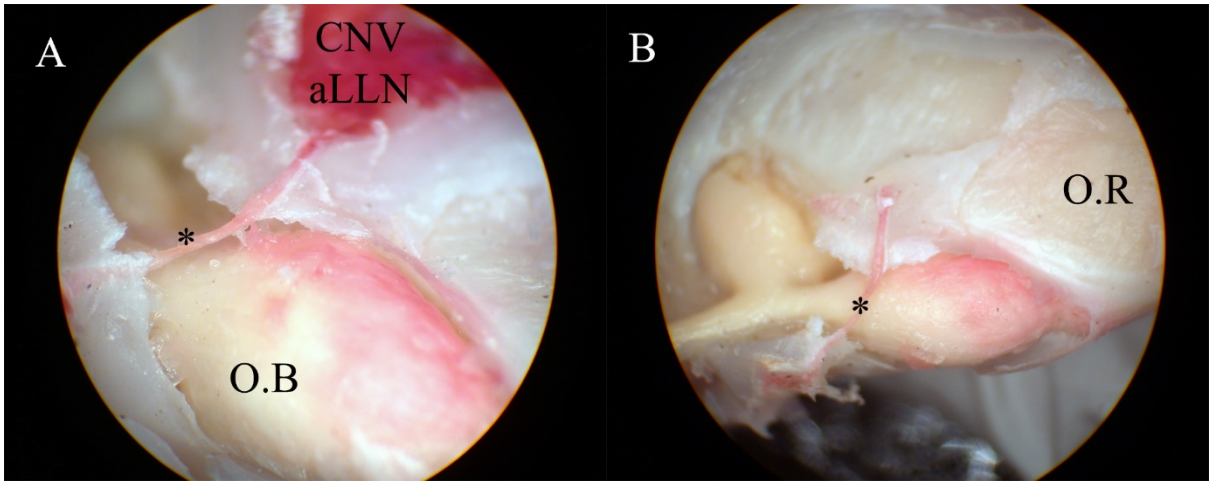

Figure 4.3 *Deep ophthalmic CNV supply to olfactory organ in C. plumbeus*.
A) Photograph taken at 25x showing deep ophthalmic branch of CNV (starred) labelled with Oil Red "O". Red mass toward top of photo is the remains of the principle trunk of CNV and aLLN. Fibers can be seen coursing over the top of the medial portion of the olfactory bulb (O.B) toward the olfactory rosette (not shown). (B) Photograph (at 25x) showing bifurcation of olfactory bulb, and path of deep ophthalmic branch of CNV. Labelled fibers do not supply the lateral portion of the bulb. The cartilaginous capsule covering the olfactory rosette (O.R) has been partially removed to show the olfactory rosette. Labelled fibers do not envelop the olfactory rosette, but instead course anteriorly along the medial and medial-ventral surface of the rosette.

After passing through the cartilage wall, the nerve courses directly toward the olfactory capsule, which it penetrates near to the medial lobe of the olfactory bulb. The nerve appears to ramify, with fibers descending over the olfactory bulb and toward the rosette (figure 4.3). The olfactory bulb in *C. plumbeus* is bifurcated, and only the medial branch of the bulb appears to receive any fibers from this branch of CNV (figure 4.3b). The main path of the nerve continues anteriorly, rejoining the common trunk of CNV and ALLN, then innervating the skin of the dorsal surface of the snout.

DiI was used to examine the projections of the deep ophthalmic CNV fibers into the tissues of the olfactory rosette. Rosettes were serially sectioned on a freezing microtome and examined under a fluorescent microscope using a 620nm wavelength light source. DiI migrated from the point of application toward and into the olfactory organ. DiI signal was seen in tissues of the olfactory rosette, the olfactory bulb, and in the sheath of connective tissue that envelops the olfactory rosette (figure 4.4, 4.5).

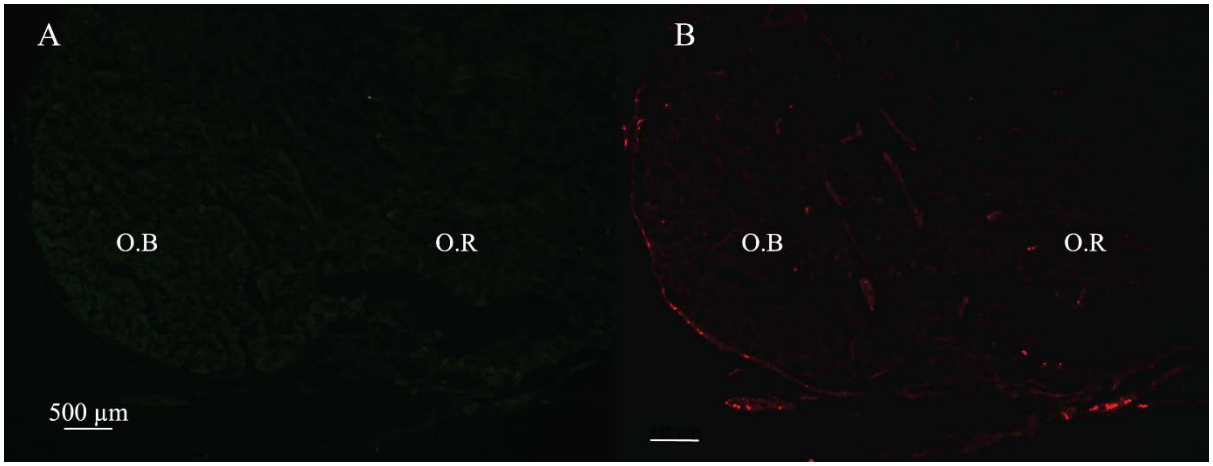

Figure 4.4 *Sagittal section of DiI labelled C. plumbeus olfactory organ*. (A) Section viewed under 488nm light source at 5x magnification. (B) Section viewed under 620nm light source at 5x magnification. O.B = olfactory bulb, O.R = olfactory rosette. DiI signal is seen in the olfactory bulb, and in the connective tissue sheath of the rosette.

Neither broad scale labelling across functional regions, nor fine scale labelling of specific structures was commonly seen through DiI labelling. Auto-fluorescence was also apparent in both lamella and lamina propria tissue layers (figure 4.5)

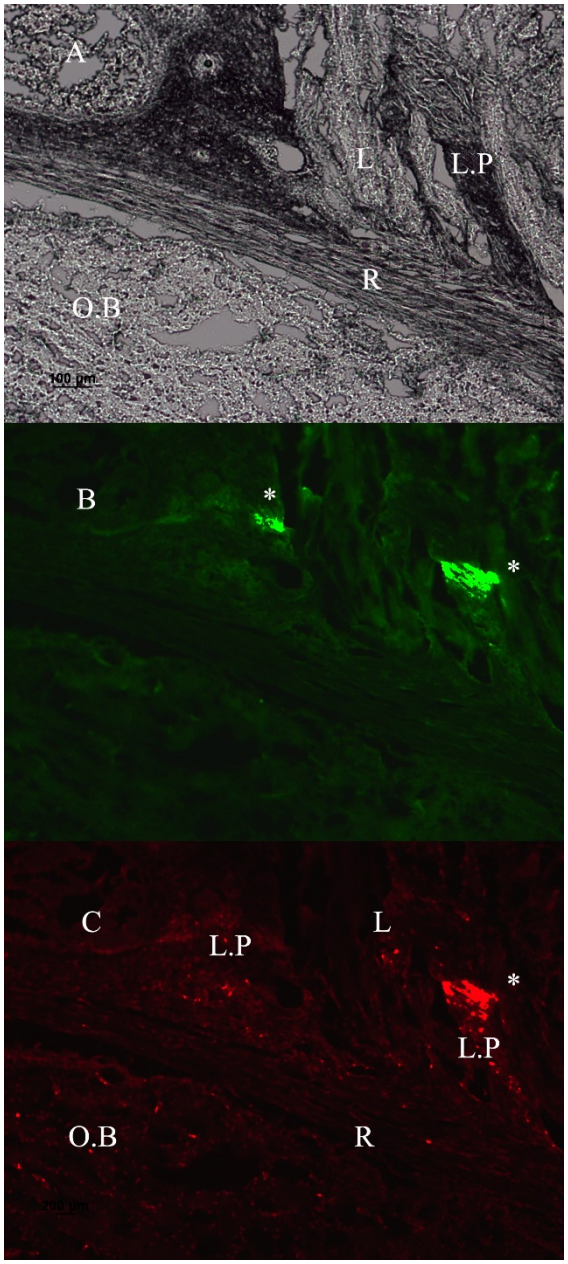

Figure 4.5 *Panel showing 10x sagittal section olfactory bulb and rosette.* (A) Unstained section under brightfield illumination. Olfactory bulb = O.B, central raphe = R, lamella = L, lamina propria = L.P. (B) Section illuminated under 488 nm wavelength light. *N.b.* regions of autofluorescence (starred). (C) Section illuminated under 620 nm wavelength light. Weak DiI labelling can be seen in the olfactory bulb and the lamina propria.

Extensive labelling of axon bundles was seen in the filia olfactoria, lamina propria, epithelium and the tips of the secondary folds of lamella in a few sections (figure 4.6).

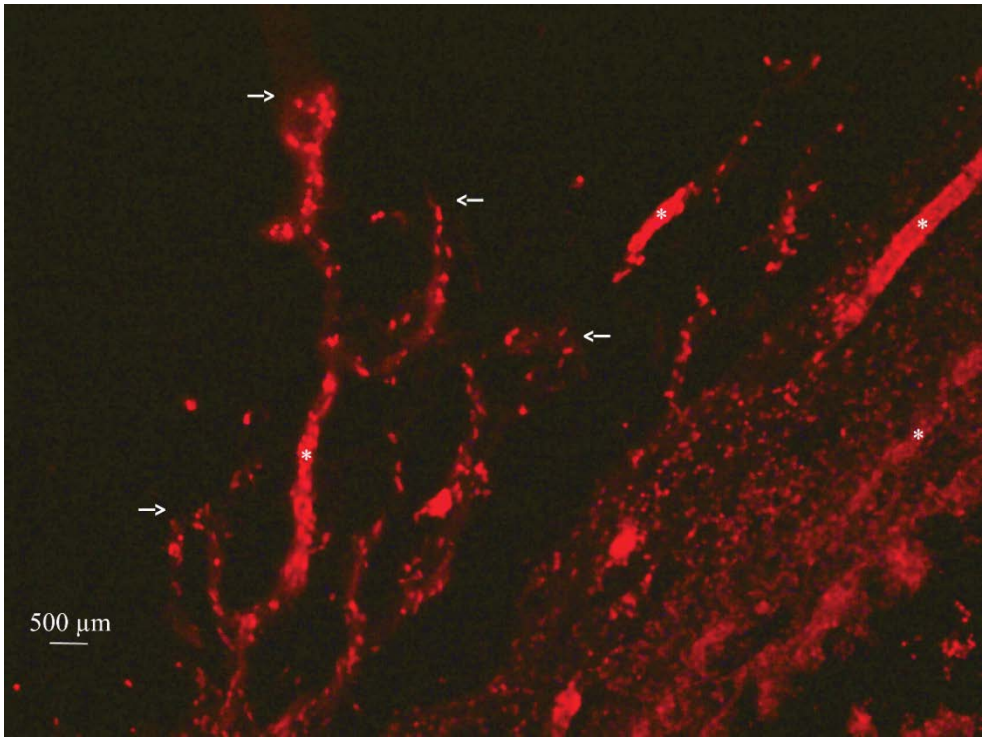

Figure 4.6 *20x section showing DiI labelling in secondary lamellae and lamina propria.* Labelling can be seen in axon bundles of the lamina propria (starred) as well as the tips of the secondary folds of the lamella (arrows).

In *S. lewini*, dissection and pathway tracing with Oil Red 'O' led to the identification of a candidate branch of CNV SOA that appeared to penetrate the olfactory capsule on the ventral side of the head.

Figure 4.7(A) highlights cranial nerves V, VII & ALLN, which course in close association as a large trunk, descending from the region of the anterior medulla rostrally, following the chondrocranium. At approximately the level of the mid telencephalon, the trunk rammifies into a series of branches spreading laterally as well as dorso & ventro-rostally. One of these ventro-rostral rami consists of a candidate superficial opthamic branch of CNV and ALLN, as shown in figure 4.7(C) with a star. One of the depicted rami in figure 4.7(C) courses close to the superficial opthalmic ampullary cluster (shown in depicted in figure 4.2) , and projects rostro-laterally toward the naris. The other courses over the posterior region of the olfactory capsule, projecting toward both orbit and the naris.

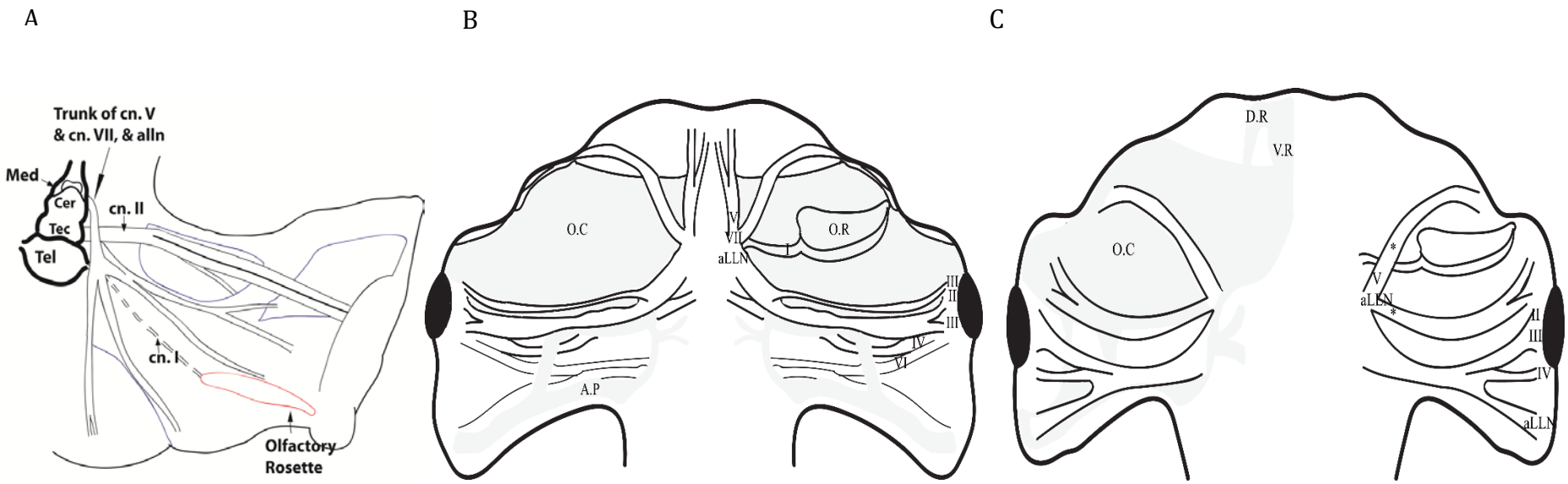

Figure 4.7. *Schematic representation of select cranial nerve pathways in S. lewini*. (A) Dorsal perspective showing origins and projections of cranial nerves I, II, V, VII and aLLN. (B) Dorsal perspective showing pathways of cranial nerves I-VII and aLLN. Grey shaded regions represent cranial cartilage structures. (C) Ventral aspect showing pathways of cranial nerves I-V and aLLN. Representations of these cranial nerves are approximate and do not convey detail of the smaller and finer branches that may ramify from the main trunks of the nerves. They also do not show the finer processes and ultimate projections of these nerves & branches. The olfactory rosette (shown on the right side of the diagram) is encapsulated within the anterior cranial cartilage.
Med = medulla oblongata, Cer = cerebellum, Tec = tectum, Tel = telencephalon, O.C = olfactory capsule, A.P = auditory process, O.R = olfactory rosette, O.C = olfactory capsule, D.R = dorsal bar of rostrum, V.R = ventral bar of rostrum.

In BDA labelled tissues, widespread labelling was seen in the central raphe, filia olfactoria and the lamina propria (figure 4.8). peripheral projections approximately terminate in the basal lamina, which is the same tissue layer demonstrated to contain magnetite containing cells in *O. mykiss* (Diebel et al. 2000). Labeled axons course along the central nerve bundle (*filia olfactoria*). The filia olfactoria is largely made up from the convergence of axons stemming from sensory olfactory receptor neurons, and ultimately synapse with the olfactory bulb. Whilst the labeled axons can also be see coursing with the *filia olfactoria* containing tissues, they can also be seen innervating the *lamina propria,* the thin layer of loose connective tissue which lies beneath the epithelium. The sensory and non-sensory epithelial tissues can be seen as the grey/brown margins that surround the labelled fibers in each secondary fold (branching to the side of the lamella). Labelled fibers appear to remain within the lamina propria, and do not extend into the epithelium.

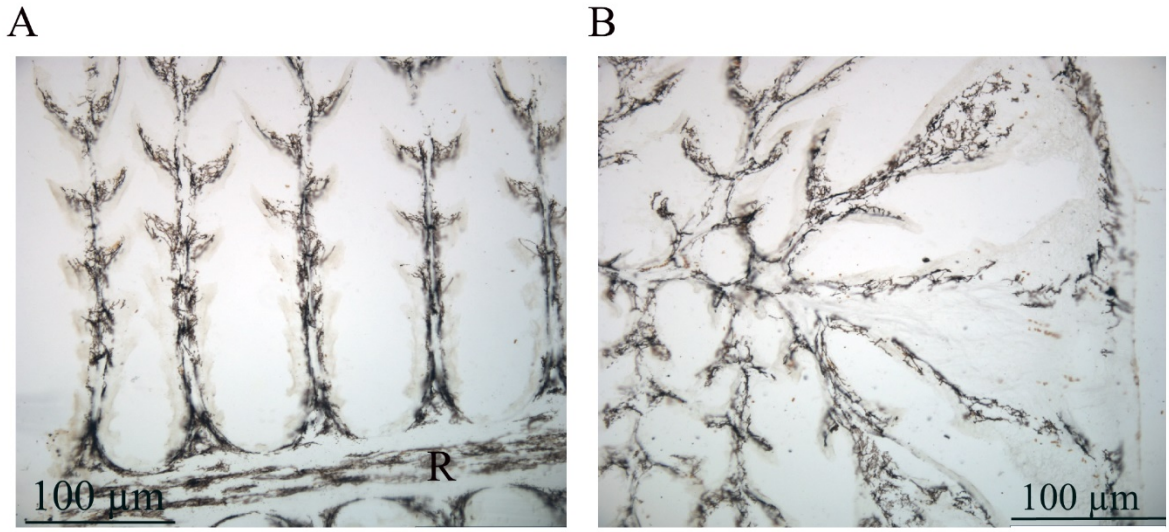

Figure 4.8. *Frontal/transverse section (10 µm, 5x) of a BDA labelled olfactory rosette.* (A) Central portion of rosette showing distinct labelling of axon bundles in the central raphe (R), the lamina propria (the layer between the epithelium and the connective tissue of the vertical columns in the center of each primary lamella), with labelled fibers extending into the tip/secondary folds of the lamellae. (B) Distal/lateral portion of rosette demonstrating widespread labelling through to periphery.

Unlabeled olfactory tissues were section at 10µm and stained with H&E to examine the morphology of the tissues, and better identify terminal projections of labelled trigeminal fibers. Figure 4.9(A) show several rows of lamellae rising from the olfactory

bulb. Light brown coloration (melanin and possibly reticular connective tissue fibers) can be seem at the confluence of the lamina propria with the olfactory epithelium. While the melanin (light brown) is widespread throughout the lamellae, it cannot be mistaken for the labelling (black) shown at the same magnification (5x) in figure 4.8. Figure 4.9b is a higher magnification image (40x) of a single lamella, with the different cell/tissue regions identified. Ciliated cells can be seen in the apical layer of the secondary folds of the lamellae, supported by surface layer of sustentacular cells (colored pink by the staining process). Beneath these lie two to three layers of (microvillar) olfactory receptor neurons.

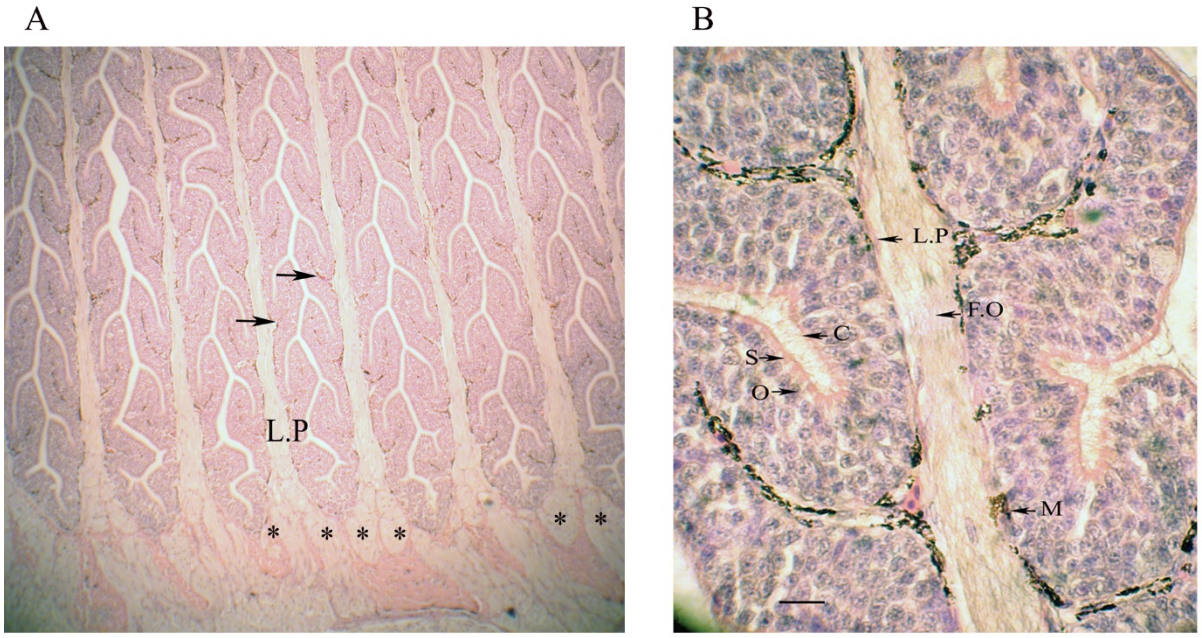

Figure 4.9. *Horizontal sections of S. lewini olfactory rosette (no BDA label), stained with H&E.* (A) 5x magnification showing basal aspect of rosette. The olfactory bulb, glomeruli (starred) lead to the filia olfactoria. Examples of melanin deposited within tissues is highlighted with black arrows. Gaps between lamella are the ventilatory channels for flow of water over the sensory epithelium. (B) 40x magnification of a single lamella, showing fine structure within. C = ciliated cells, S = sustentacular cells, O = olfactory receptor neurons, M = melanin deposit, F.O = filia olfactoria, L.P = lamina propria. Scale bar = 20 µm.

Neurobiotin $^{+}$ was used to further examine projection of labelled fibers in *S. lewini* olfactory tissues. Sections were cut on a freezing microtome and visualized under 488 nm wavelength light. Labeling extended into the central raphe (figure 4.10(A)), non-

sensory epithelium (4.10(B & C)), and the lamina propria layer (figure 4.10(D). Distinguishing signal from noise was made complicated due to auto-fluorescence within tissues. However, strongly labeled cells and axons can be identified by their sharper definition and brighter coloration (figure 4.10 (D)). Labeling was not seen to be uniform across rosettes, with no apparent trend or pattern observed in labeling in peripheral/lateral or medial regions. The extent of labeling observed did not mirror the labeling seen through BDA.

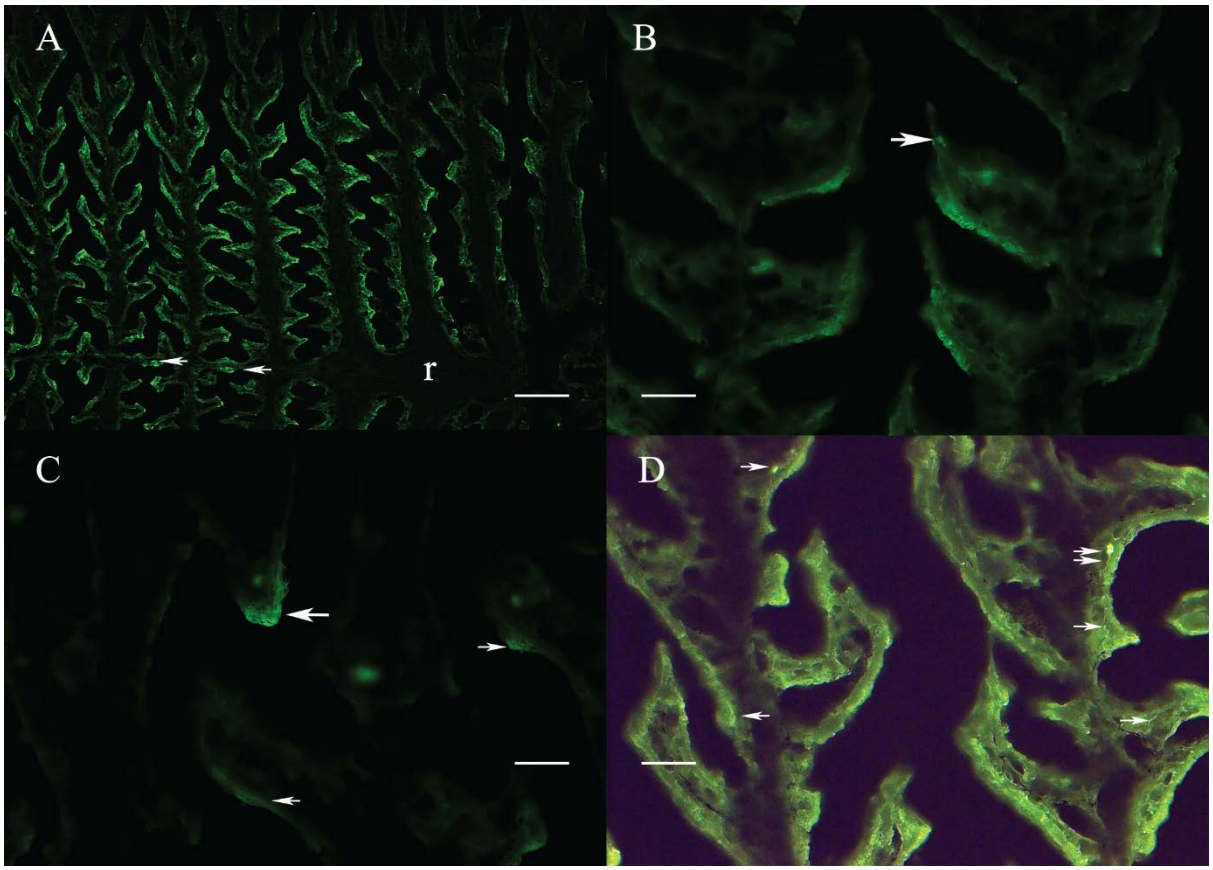

Figure 4.10. *Neurobiotin⁺ labelling in S. lewini olfactory tissues.* (A) Horizontal section at 5x magnification, showing central raphe, olfactory lamellae and secondary folds. Weakly labeled fibers can be seen in the central raphe (white arrows). Scale bar = 200 µm, r = central raphe. (B) 20x magnification showing labeled axon bundles, as well as labeled cells (white arrow). Scale bar = 50 µm. (C) 40x magnification of labeled axon bundles in non-sensory epithelium (large white arrow) and lamina propria layer (small white arrow). Scale bar = 25 µm. (D) 20x magnification showing labeled axons and cells at approximate level of lamina propria layer (white arrows). Auto-fluorescence in epithelial tissues is apparent. Scale bar = 50 µm.

4.4.2 *Prussian Blue histology & MRI*

Olfactory organs from both *S. lewini* & *C. plumbeus* were sectioned on a freezing microtome, and Perls Prussian Blue stain used to look for the presence of non-haem iron. Olfactory tissues in both species were found to have a positive signal for iron (figure 4.11). Iron containing areas tended to be ~20-50µm wide (based upon blue signal observed). In *C. plumbeus* sections, positive staining could be found in 12 serial sections, comprising tissue ~500 µm in thickness. However, iron distribution did not appear to be ordered or uniform across rosettes, and no predictable loci could be found for its occurrence.

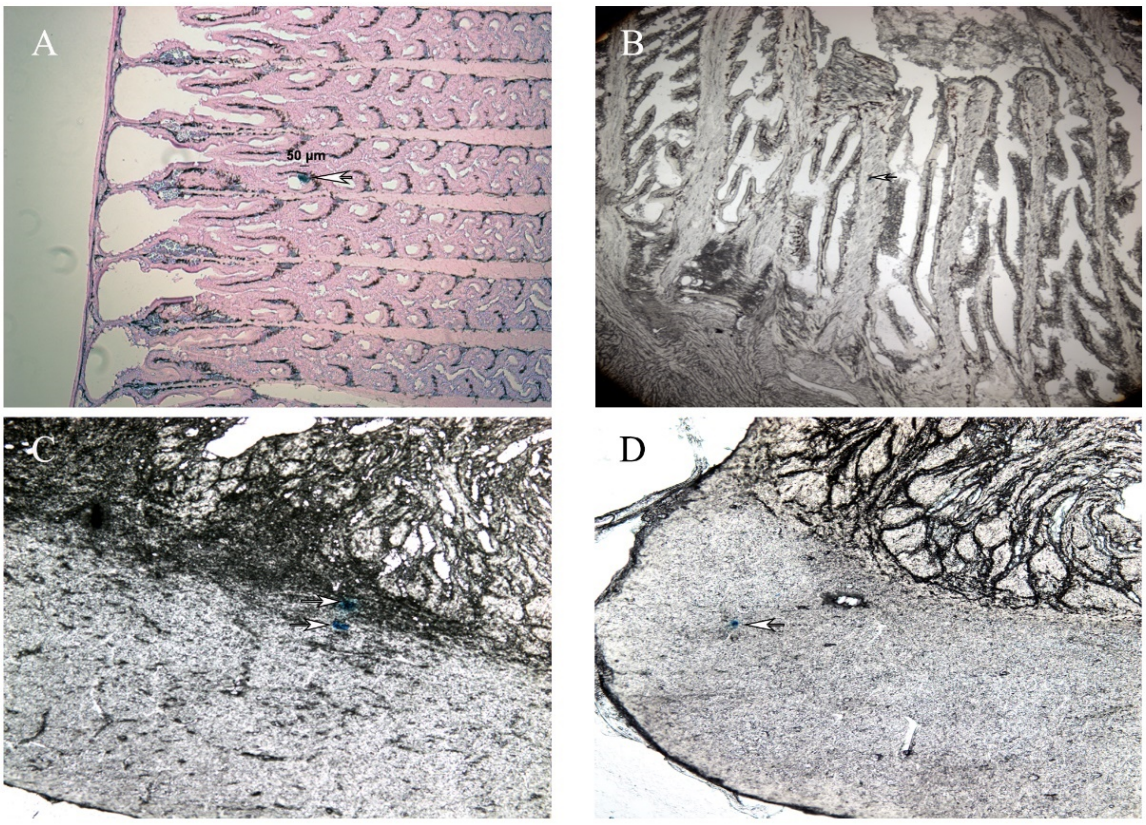

Figure 4.11. *Prussian blue labeling in shark olfactory tissues.* (A) *S. lewini* olfactory epithelium (5x magnification) showing Prussian Blue labeling (blue stain, white arrow) in a secondary lamella fold, at the approximate level of the lamina propria. Sections B-D are stained only with Potassium Ferrocyanide (not nuclear fast red), hence there no coloration to the tissues. (B) Iron signal in center of filia olfactoria (white arrow – 5x magnification). (C) Two sites of iron signal (two white arrows) occurring with a layer of olfactory axons (upper) and the glomerular layer of the bulb (lower), magnification at 10x. (D) Iron deposit at the level of the granule cell layer of the olfactory bulb (white arrow – 10x magnification).

In both species, positive signal was found across a range of tissue layers, including the epithelium (figure 4.11A), filia olfactoria/lamina propria (figure 4.11B), between the olfactory nerve and glomerular layer of the olfactory bulb (figure 4.11C), and the granule cell layer (figure 4.11D). Positive signal was also seen regularly at the layer of the connective tissue sheath that encapsulates the rosette (not shown).
The stain itself often masks the specific cells from which signal may originate, thus it was not possible to accurately describe the morphology of iron containing cells using light microscopy.

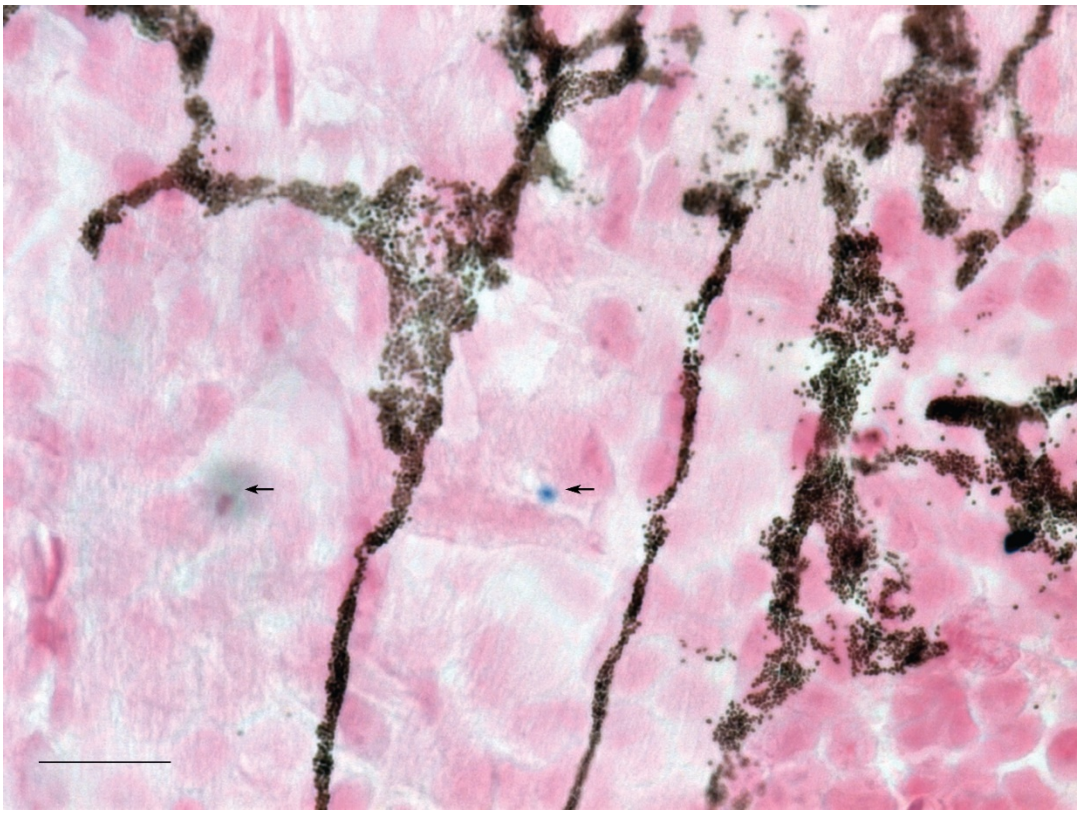

Figure 4.12. *Single epithelial cell with positive Prussian Blue labeling.* 20 µm section showing two sites of labeling (black arrows). In the stronger (right side) example, the site/source of signal can be seen at or proximal to the cell membrane. The darkened center of the site of signal (source of signal) is approximately 1 µm in diameter. The weaker (left side) signal likely comes from deeper within the section, thus, it not possible to characterize the source. Magnification = 40x, scale bar = 10 µm.

However, a reduced bathing time in potassium ferrocyanide solution did correspond to weaker labelling/staining of tissues, which, with careful scrutiny of stained tissues, did allow identification of single cells with a single site of signal (figure 4.12), although

identification of these cells was uncommon. Such cells were typically located within the epithelial layer, were approximately 10 µm in size (diameter), with a site of signal (iron deposit) approximately 1 µm in diameter (figure 4.12). Iron deposits appeared at or next to the cell membrane. It was not possible to distinguish if the site of signal was held within a membrane of its own, or was in any way attached/connected to the cell membrane.

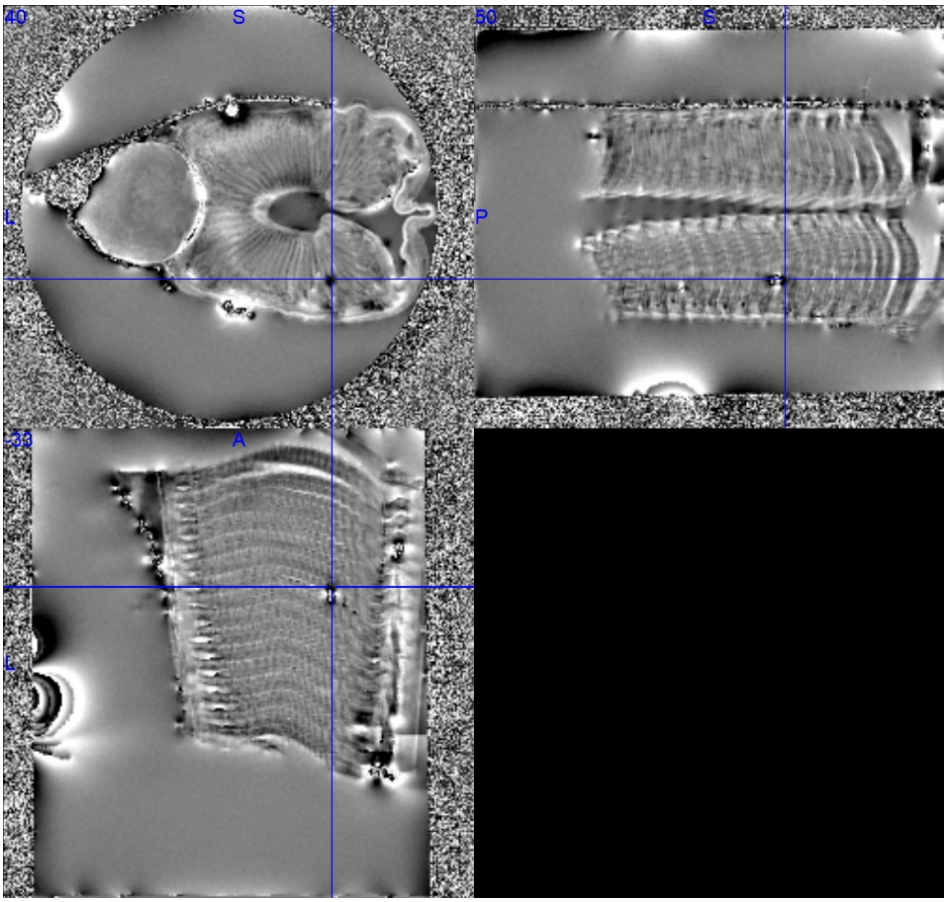

Figure 4.13. *3D rendering of Magnetic Resonance Imaging.* Optical slices (representing 10-20 µm) can be viewed in the x,y & z planes simultaneously. The above image shows iron signal occurring within the lamellae of a rosette (center of blue cross-hairs). Top left image shows the optical slice and signal in the sagittal plane (x). Top right shows the same region of interest/site of signal in the transverse (top down) plane (y). Bottom left image shows the coronal (frontal) plane. Through digital analyses, the r.o.i. can be mapped to a precise region of the tissue. In this example, it occurs in the seventh (from the right) lamella, approximately 3mm from the lateral periphery.

MRI allows for high definition 3D imaging of soft tissues (figure 4.13), presenting a means to examine whole organ or structure without the possibility of yielding false

positives through the extraneous introduction of iron via tissue preparation procedures. Optical slice resolution was between 10-20 μm, depending on the strength of the magnet used (9.4 Tesla/16.4 Tesla respectively).

Sites of potential iron signal were found to be widespread in the lamellae of both species. For the purposes of this analysis, only signal seen in clearly defined structure was considered. i.e., any signal seen at the periphery of the rosette, in the connective tissue & nerve fibers between the bulb and the rosette, or at the interface between the tissues and their surrounding medium. Signal was seen as black dots (figure 4.14) that varied in (voxel) size according to the strength of the signal, and potentially the size of the deposit/signal source.

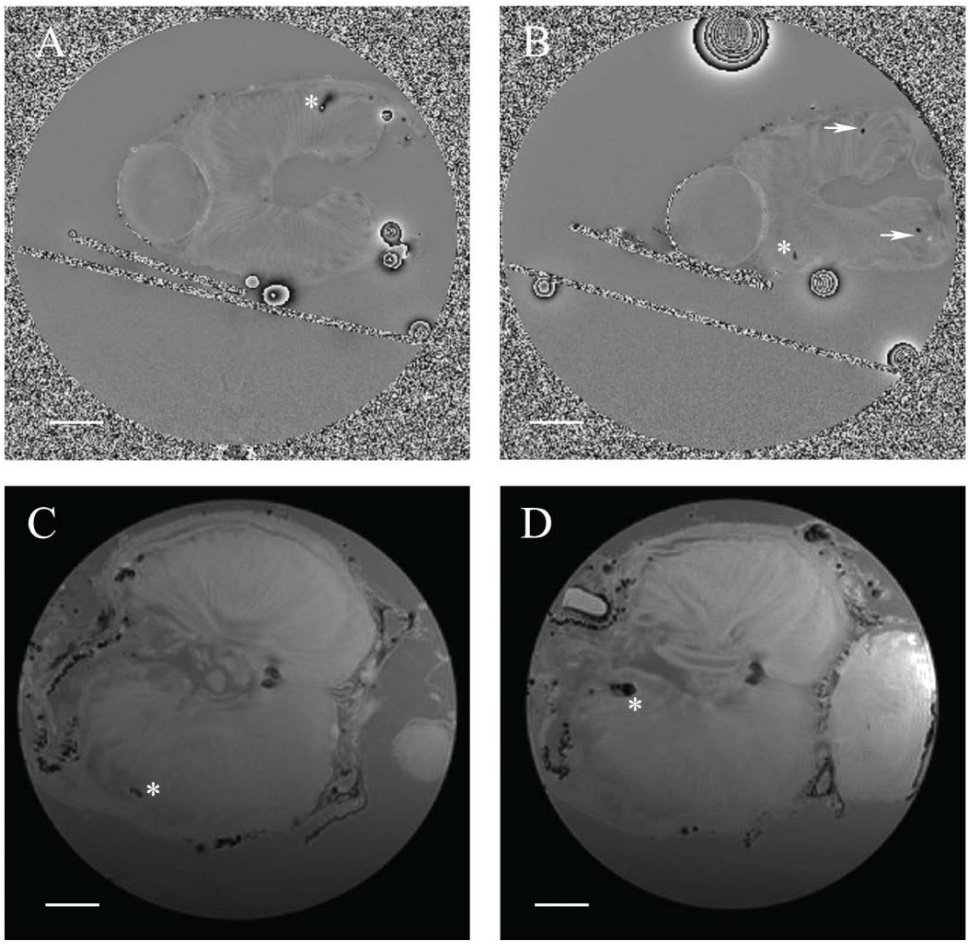

Figure 4.14. *Panel figure showing iron signal in olfactory tissues using MRI.* (A) & (B) Iron signal in *S. lewini* rosettes. (C) & (D) Iron signal in *C. plumbeus* Strong signal (white stars) was seen in various regions of the lamellae and could be seen in numerous serial optical slices. Weaker signals (white arrows) were smaller in size (fewer voxels), and typically in 1-3 (serial) sections. Scale bars = 2mm

As rosettes that were compared were not exactly the same size and conformation, it was not possible to stereographically map the precise location of each site of signal to examine whether iron deposits could be precisely co-localized across samples. However, as an alternative, the approximate location was mapped, incorporating reference to the strength and visual size of the signal. The number of optical slices in which each iron signal occurred was also noted. The mean number of sites of signal identified in *S. lewini* & *C. plumbeus* was 34 and 36 respectively. In *S. lewini* (n=3), signal sites were widely distributed throughout the organ with no visually obvious trends in occurrence locus (figure 4.15A). The small sample size meant that it was not possible to run any valid statistical analyses. Mapping of the signal locations identified one region where sizeable deposits were seen in all three samples (figure 4.15A). The maximum number of optical slices/sections in which a specific signal was seen was 14 (∴ ~ 140 µm region of tissue, while the mean of all three *S. lewini* rosettes analyzed was 49.5 µm.

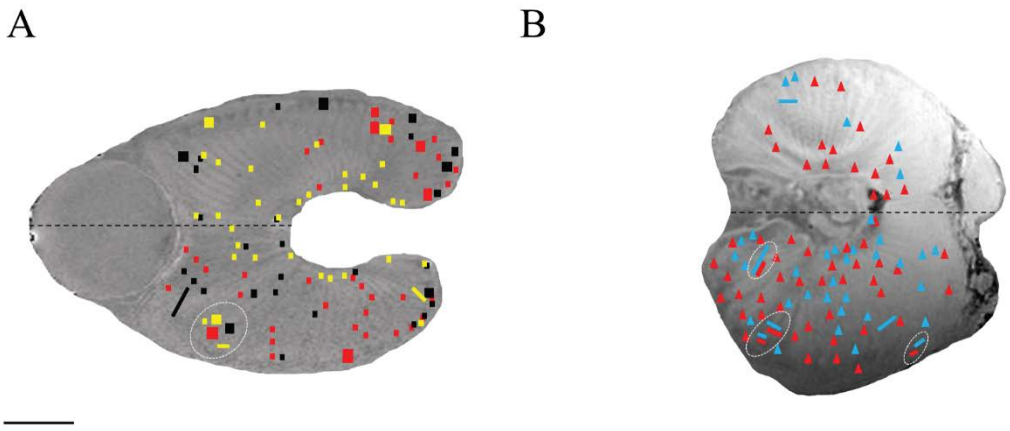

Figure 4.15. *Iron signal in shark olfactory rosettes as identified with MRI.* Signal strength (# of optical slices in which it occurs) represented by square size. Significant/large (in physical area) signal represented by bars/rectangles. Different colors represent different samples. Scale bar = 2mm. (A) Composite of sites of signal in *S. lewini*. Observed signal was widely distributed across lamella and was variable in size and strength. One region was identified where larger deposits appeared to occur in all three samples (broken white oval). Red = *S. lewini* 1, Yellow = *S. lewini* 2, Black = *S. lewini* 3. (B) Composite of sites of signal in *C. plumbeus*. Observed signal was widely distributed across upper and lower halves of the rosette in *C. plumbeus* 1 (red triangles), whereas observed signal was scant in the upper half of the rosette in *C. plumbeus* 2 (blue triangles). Three apparent regions of large signal co-occurrence were identified (broken white ovals).

In *C. plumbeus* (n = 2), wide distribution of signal was seen in one half of the rosette (when viewed from a sagittal perspective), with larger signal occurring in both rosettes in similar regions in three locations (figure 4.15B). Signal occurrence in the opposite (upper) half of the rosette initially appears scant. However, when the contributions from both samples are considered, it can be see that this is not a trend that is consistent across the two samples (Table 4.1). Variation of signal size and strength (in terms of serial sections signal occurred in) was low in comparison to *S.* lewini (mode = 2). Three regions of lamella were identified where large deposits/sites of signal appeared to co-occur (figure 4.15B – broken white rings/ovals). Maximum number of optical slices/sections in which a specific signal was seen was 8 (∴ ~ 160 μm region of tissue, while the mean of both *C. plumbeus* rosettes analyzed was 45.6 μm.

Table 4.1. *Signal strength and occurrence across olfactory rosette samples.* Counts are shown for individual samples, broken down by distribution with the upper and lower halves of each rosette (sagittal perspective). Mean deposit size is calculated by factoring magnet strength with the mean number of serial sections individual sites of signal occur within.

Sample	Magnet strength (Tesla)	Signal count (upper)	Signal count (lower)	Mean approx. deposit size (μm)
S. lewini 1	9.4	12	17	65.31
S. lewini 2	9.4	20	16	67.18
S. lewini 3	9.4	14	22	59.23
C. plumbeus 1	16.4	13	18	81.71
C. plumbeus 2	16.4	6	34	75.81

Following MRI analysis, one *S. lewini* rosette was sectioned at 20 μm (approximately twice the thickness of the MRI optical slices), stained with Prussian Blue, then examined to co-localize iron deposits. Identified iron signal in histological sections was correlated and compared with the equivalent MRI optical slice. Although less than 10% of the Prussian Blue labelled iron in histological sections could be co-localized with the

approximate corresponding optical section, it was possible to co-localize iron signal in both methods (figure 4.16). The two sites of signal identified in figure 4.16A were co-localized to epithelium. While the upper site of signal in figure 4.116B looks to be in a void within the epithelium, it can be seen upon closer inspection that it stems from a primary lamella in a deeper tissue layer (thus not all the layer is captured in the section) and is not in-fact in a void. The second site of signal is also located within the olfactory epithelium, occurring in the second layer of epithelial cells below the sustentacular layer, toward the tip of that lamella (figure 4.16E). Figure 4.16 (C) & (D) also show co-localization of iron signal. This would also appear to be within an epithelial layer, although again, there are mixed tissues from differing depths within the organ captured within the section (figure 4.16F).

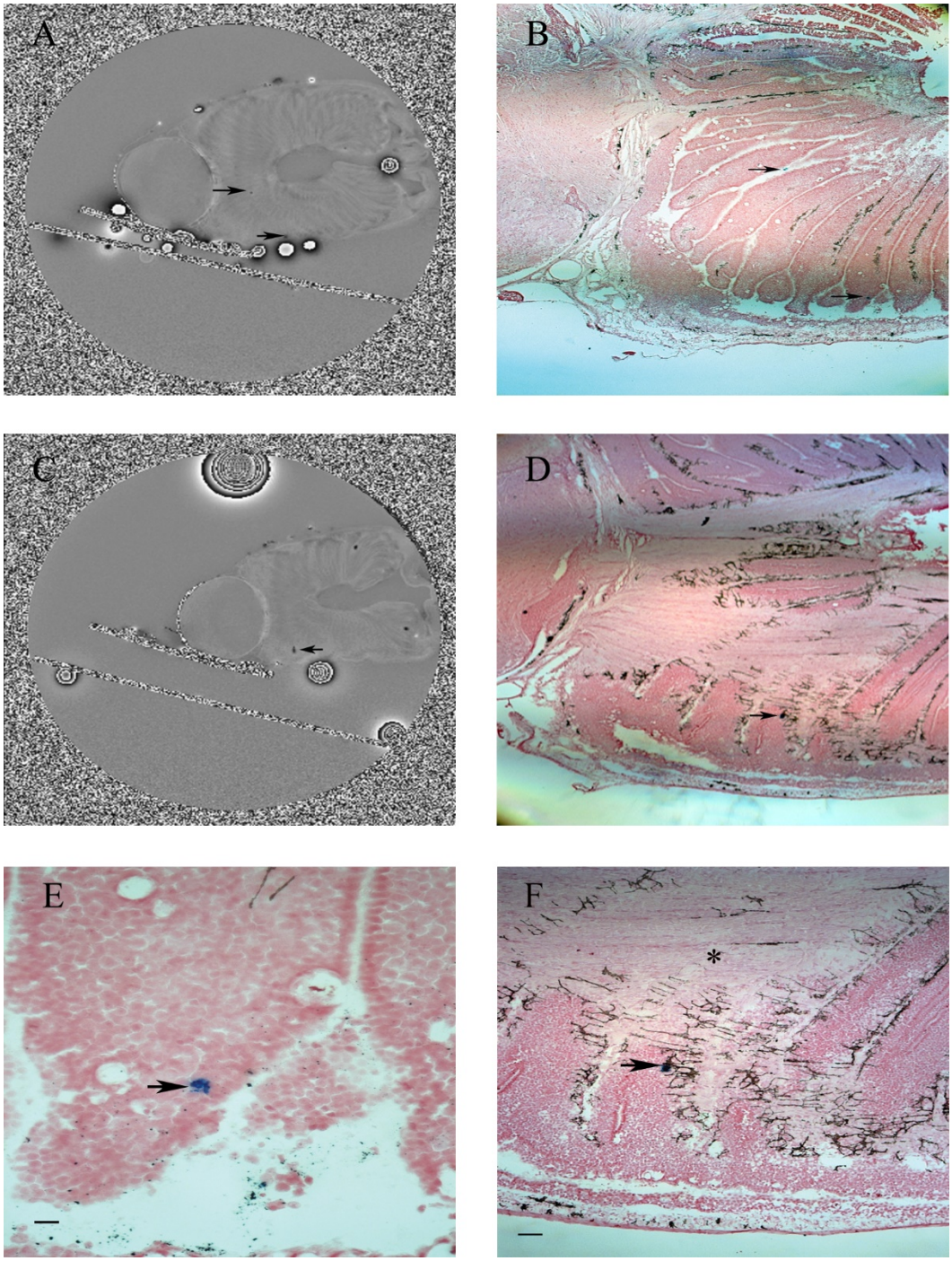

Figure 4.16. *Co-localization of iron in S. lewini olfactory tissues.* (A) MRI rendering showing two sites of signal (black arrows). (B) Prussian Blue stained histological section (5x magnification) at equivalent depth in tissue showing two signal sites in same approximate location as (A). (C) & (D) MRI rendering & Prussian Blue stained histological section (5x magnification) showing co-localized iron signal (black arrows). (E) 40x magnification of lower signal site in (B) showing signal site in epithelium below sustentacular layer. Scale bar = 20 μm. (F) 10x magnification of signal site in (D) (black arrow) showing location in tissue layer, and mixed tissue layers present in section (starred). Scale bar = 40 μm.

4.4.3 *Cell dissociation and flow cytometry*

Six *S. lewini* olfactory rosettes (olfactory bulb and tract removed) were dissociated to a single cell suspension, then separated into magnetically positive and negative fractions through filtration in an LS column with a 20 μm magnetic filter. Pre-filtration cell yield was variable (table 4.2), mean pre-filtration cell yield was estimated at ~ 6.67×10^5 cells. Mean cell harvest following magnetic filtration was approximately 10% of the original population (mean number of cells harvested per rosette was 7.16×10^4). One rosette (rosette 4) yielded a markedly larger magnetically positive fraction (17 % of original population). A volume of magnetically positive suspended cells was pipetted on to a petri dish and examined under a confocal microscope. At the same time, a bar magnet was placed above the petri dish and rotated. Fifteen cells, or clusters of cells, were observed to rotate in-line with the rotating bar magnet during a ten-minute observation period.

Table 4.2. *Cell counts and magnetic filtration yields from dissociated olfactory rosettes.* Estimates were made of the total number of cells <20 μm in size from six dissociated *S. lewini* olfactory rosettes. Magnetically positive cell yield was ~ 10% although the yield from rosette 4 may be anomalous.

Rosette	Cells pre-filter	Cells post filter	% Difference
1	668000	60480	9.05
2	698700	56025	8.02
3	71550	6310	8.82
4	865900	147800	17.07
5	537500	46000	8.56
6	1160000	113000	9.74

Magnetically positive (M+) and negative (M-) cell fractions were analyzed with a flow cytometer to characterize any apparent differences in composition and size. Cells and particles (debris) were grouped and color coded (see key/legend, figure 4.17). Live cells (pink colored points in the figures) in the M- fraction were identified and gated (black polygon – figure 4.17A), meaning everything outside the gated box corresponds to cellular debris. M+ fractions were then examined in the same way to compare the

physical characteristics of the live cells. Although there were more cells per 1ml aliquot in the M- fraction, live M+ and M- cell fractions were similar in size and composition (figure 4.17A,B), exhibiting a range of cell sizes (FSC). To confirm the magnetic properties of the M+ fraction, a 1 µl aliquot fluorescent magnetic beads (in solution) was added to separate 1ml aliquots from both the M+ and M- fractions and given time to bind to cells.

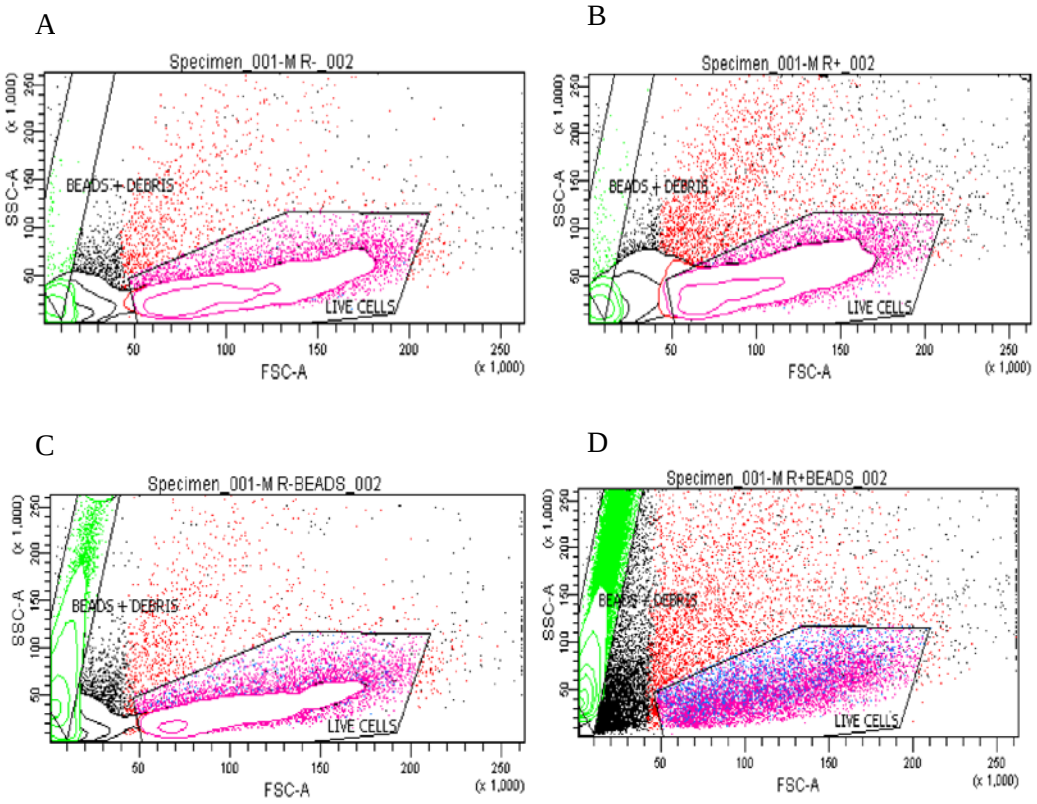

Figure 4.17. *Composition of populations from M+ and M- cell fractions as determined by flow cytometry.* (A) M- population. Live cells (pink) are gated (black polygon) and distinguished from cellular debris. (B) M+ population. Live cells were similar in size and composition to M- fraction. (C) M- population with fluorescent magnetic beads. Spectral characteristics clearly distinguish beads from lives cells and debris. (D) M+ population with beads. Beads are well described in their gated area, but also bind to both debris and live cells, which was not seen in M- population. Key: green = beads, black & red = debris (compositionally different), pink = live cells, blue = live cells + beads.

The spectral characteristics of the beads were characterized (green points - figure 4.17C,D). M+ and M- aliquots were then analyzed by the flow cytometer. The population of live cells with beads attached (characterized by composition/granularity and the

spectral characteristics of the beads) was notably different between the M+ and M- populations (blue points - figure 4.17C,D). It was notable too that not all the M+ fraction of live cells bound to beads.

The population of live cells from each group (M+, M-, with beads, without beads) was sorted (separated) and further compared. Again, M+ and M- fractions without beads were similar (figure 4.18A,B), indicating that live cells in both types are likely comprised of the same functional classes of cells (e.g. epithelial, sustentacular, orn's etc). Although the gated area seen in figure 4.18C shows some signal/events, much of this is likely just beads. The markedly larger number of events seen in the gated box in 4.18D demonstrates the strong affinity the M+ population of live cells shows to the beads, indicating they are magnetically attracted to them. Thus, the magnetic properties of these cells makes them fundamentally different to the rest of the cell population. This difference is not reflected in cell size, or composition (granularity) without enrichment by the beads.

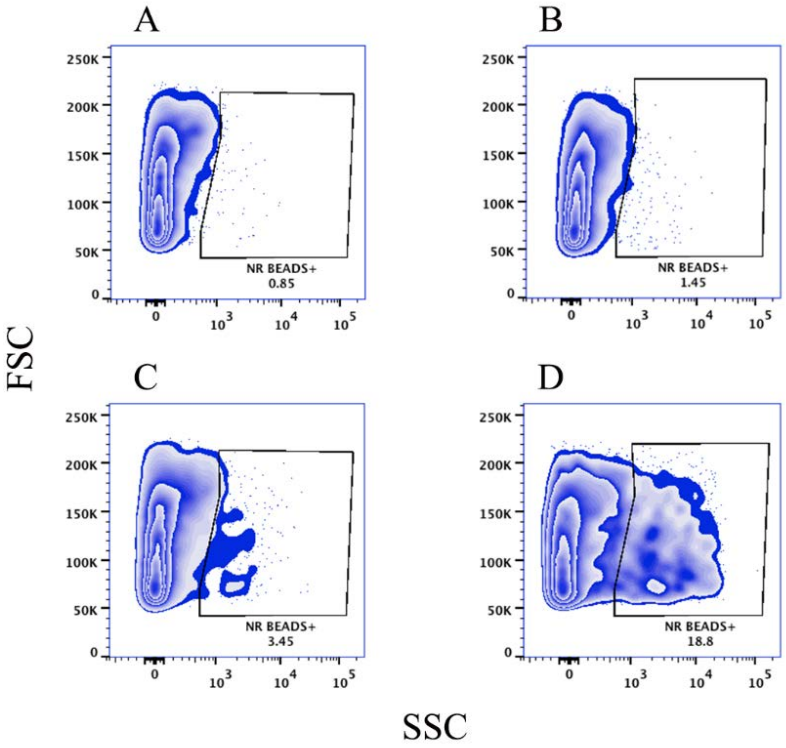

Figure 4.18. *Composition of live cells M+ and M- cell fractions.* Live cells from both fractions are compositionally similar, but only cells from the M+ fraction bind strongly to the magnetic beads. (A) M- population, no beads. (B) M+ population, no beads. (C) M- population + beads. (D) M+ population + beads.

To examine whether the magnetic properties of olfactory tissues were unique, or could be found in other epithelium containing structures, the heart of one *S. lewini* was prepared for flow analysis following the methodology used for olfactory tissue. As might be expected, spectral characteristics of heart tissues were different to those of the olfactory tissues, specifically their composition/granularity (figure 4.19). Little, if any binding of cells dissociated from the heart was seen, indicating cells dissociated from cardiac tissues did not have magnetic properties (figure 4.19B).

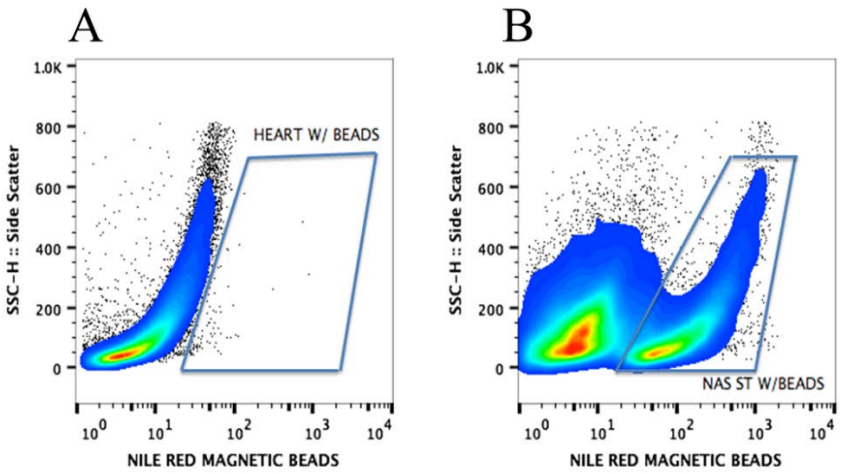

Figure 4.19. *Spectral characteristics of cardiac tissues compared with olfactory tissues.* Cardiac and olfactory tissues share common tissue types/layers, including epithelium, connective tissue and nerves. Cells dissociated from the *S. lewini* heart did not appear to have magnetic properties and did not bind to fluorescent magnetic beads. (A) Olfactory M+ population with beads. Gated (rhomboid) blue box shows live cells bound to beads. (B) Cardiac cells with beads. n.b. the minimal number of events in the gated area.

4.4.4 *Raman spectrometry*

A micro-Raman spectrometer was used to examine the elemental content of regions of interest identified in histology. Elemental analysis is achieved by examining spectral peaks in the wavelengths of light-energy read by the sensor in the spectrometer. Initially, r.o.i.'s were floated off glass slide slides and on to aluminum slides for analysis, as glass slides cannot be used for Raman spectroscopy. None of the characteristic Raman peaks (~ 665, 532 cm) were seen. Thus, M+ and M- cells were pipetted onto aluminum slides, allowed to dry, then analyzed. Multiple cell aliquots of M+ & M- cells produced similar Raman spectra, regardless of laser power, exposure time, magnification or number of accumulations (figure 4.20). Thus, Raman spectra produced

likely corresponded to the elemental composition of the cells/tissue. Signal to noise ratio (snr) was low, as is seen by the lack of clearly defined peaks (figure 4.20). While some small peaks can be observed in or near the magnetite wavelengths, the low snr and high fluorescence in the cells prevents any accurate elemental identification.

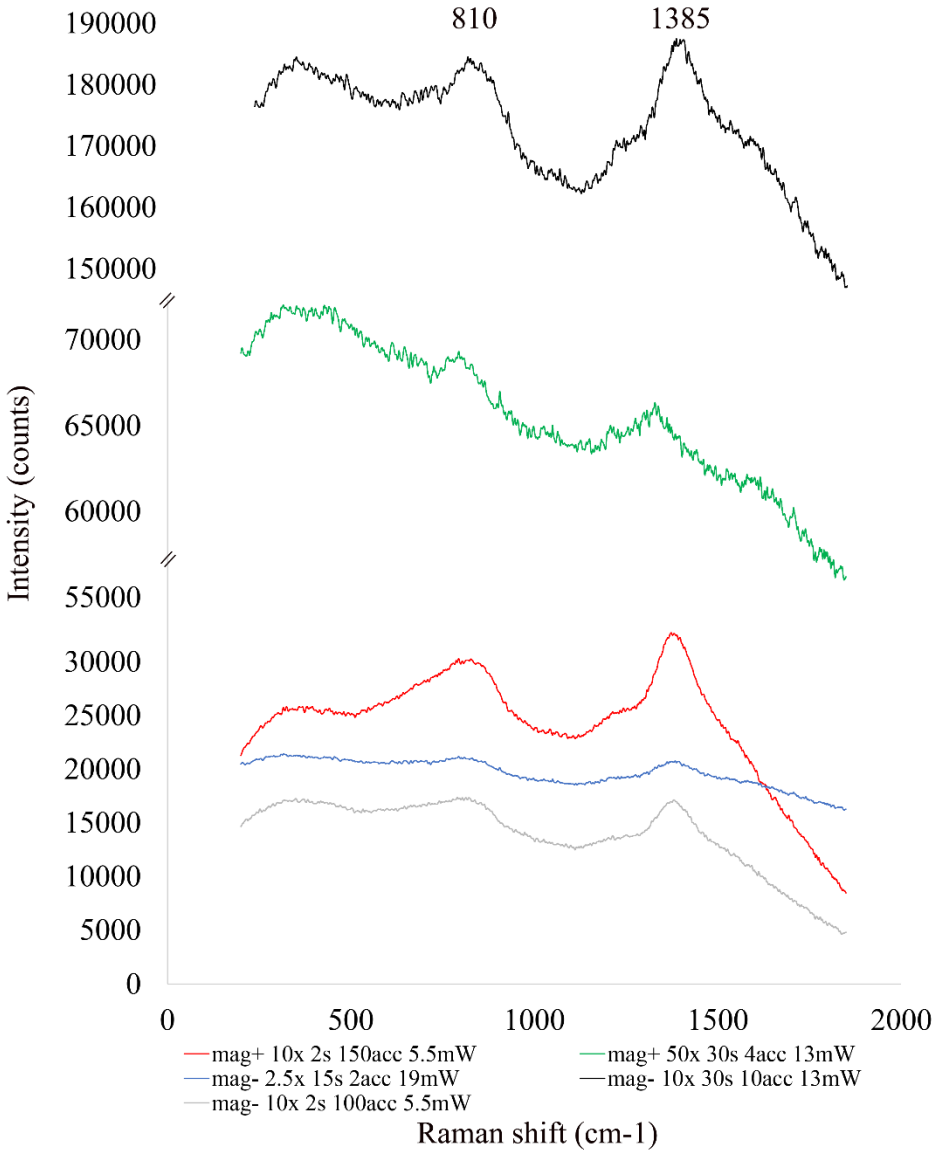

Figure 4.20. *Raman spectrum of M+ & M- cells (up to 2000cm λ).* No Raman peaks for magnetite (~665, 532) were observed in spectra. Intensity (# events recorded by ccd) reflects power, exposure time, magnification and accumulations. Angled parallel lines on Y-axis indicate a break in scale. M+ cells = red, blue, grey. M- cells = black, green. Legend shows: sample, magnification, exposure time (in seconds), accumulations, and laser power (mW).

To enrich the sample, the pellet of cells (within a 15 ml falcon tube) was allowed to desiccate. The desiccated pellet was mechanically agitated on a shaker-table before magnetic material was drawn out of the falcon tube (on to an aluminum slide) using a strong neodymium magnet. Magnetic material drawn out emerged as an amorphous but cohesive “clump”, approximately 400 x 530 µm at its largest dimensions (figure 4.21).

Figure 4.21. *Magnetic material extracted from desiccated M+ cell population*. Magnification at 10x.

Analysis of multiple locations on the clump produced Raman spectra with peaks emerging in the characteristic λ bands associated with iron-oxides (figure 4.22). In some cases, the same location was examined more than once, resulting in similar Raman spectra, but with shifted peaks in key locations (red trace and green trace – figure 4.22). As a reference, a piece of pure (geological) magnetite was also analyzed (black trace). Defined Raman peaks were seen at a number of locations, including the 665cm and 532cm wavenumbers. These specific peaks were, in the most part still small, and difficult to pick out from noise.

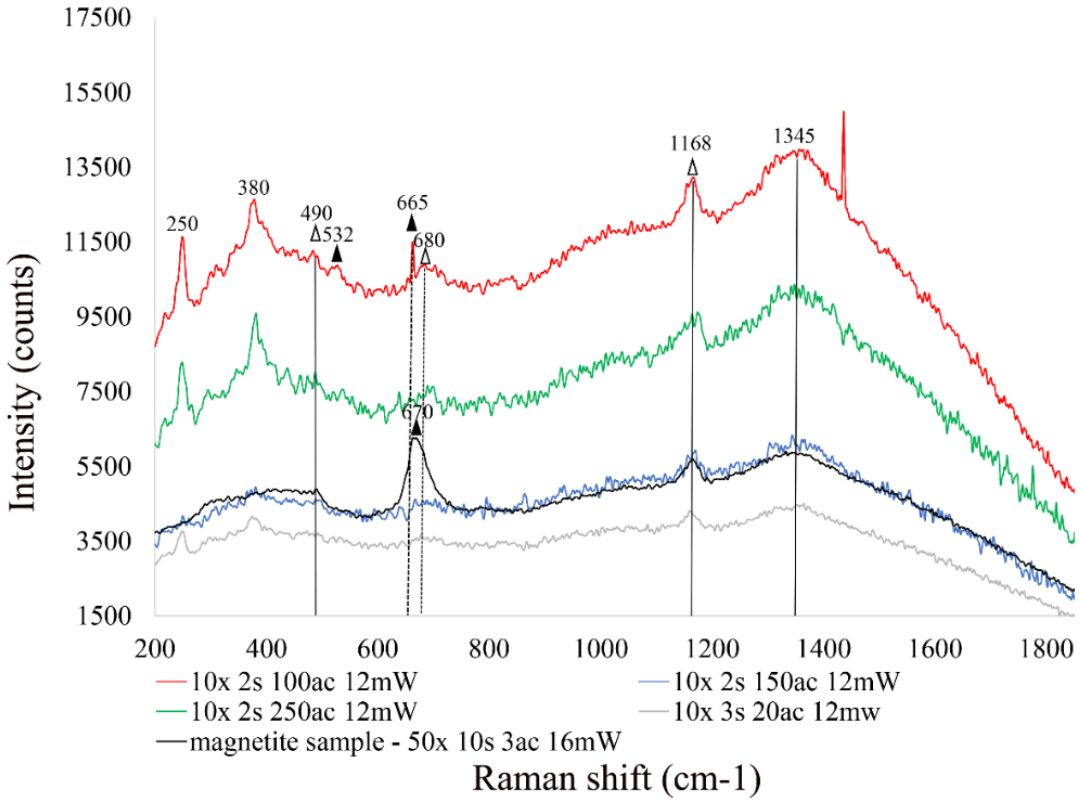

Figure 4.22. *Raman spectrum of extracted magnetic material.* A piece of pure magnetite was analyzed a reference for the specific Raman spectral characteristics under this laser (black trace). A clearly defined peak can be seen at 670cm, along with a (shoulder) peak at 490cm. Notably, no peak was seen at 532cm. A further defined peak was seen at 1168cm, along with a broad peak at 1345cm. Apparent peaks from the extracted magnetic material were seen at 380cm (green & blue trace), 490cm (red, green & blue trace), 532cm (red trace), 665cm (red trace). 670cm (green & blue trace – small), 680 (red & grey), 1168cm (all), and 1345cm (all).

The apparent shift in Raman peaks seen when the same location was analyzed more than once indicates a possible phase transition was occurring in the magnetic material. Analysis of a separate spot produced Raman spectra very similar to that of maghemite (Fe^2O^3). As a reference, a piece of geological maghemite was analyzed under the laser, producing clear peaks at λ 490cm, 613cm, 690cm, 1168cm, 1348cm. (figure 4.23A). By comparison, clearly defined Raman peaks from this locus of the magnetic extract were seen at almost the exact same λ (figure 4.23B), indicating maghemite in the sample.

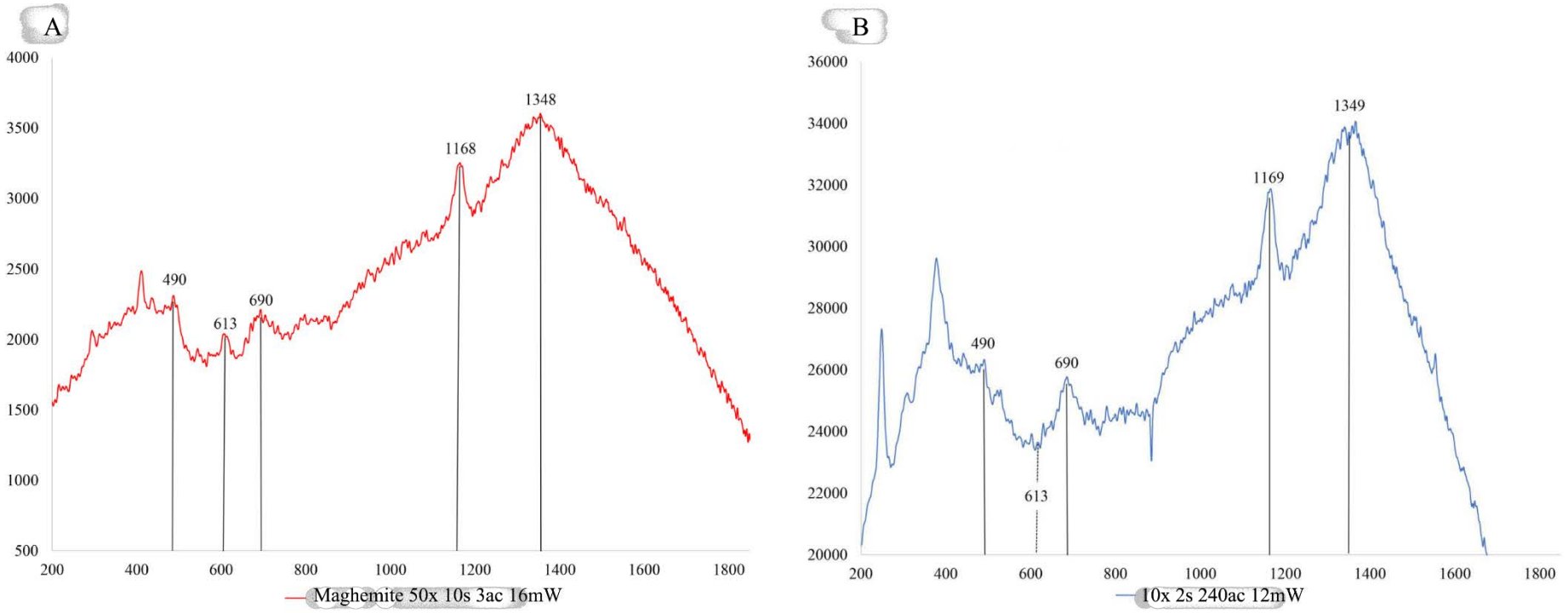

Figure 4.23. *Comparative Raman spectrum of geological maghemite with extracted magnetic material.* (A) Raman spectra of maghemite. (B) Raman spectra of magnetic material. The clearly defined Raman peaks in B, when compared to A indicate maghemite was the principal element under analysis at this locus.

The extracted magnetic material was not solely made up of iron oxides however. Raman spectra produced at two analyzed loci produced peaks that did not conform to magnetite or maghemite (figure 4.24). The elemental composition of these loci is unknown.

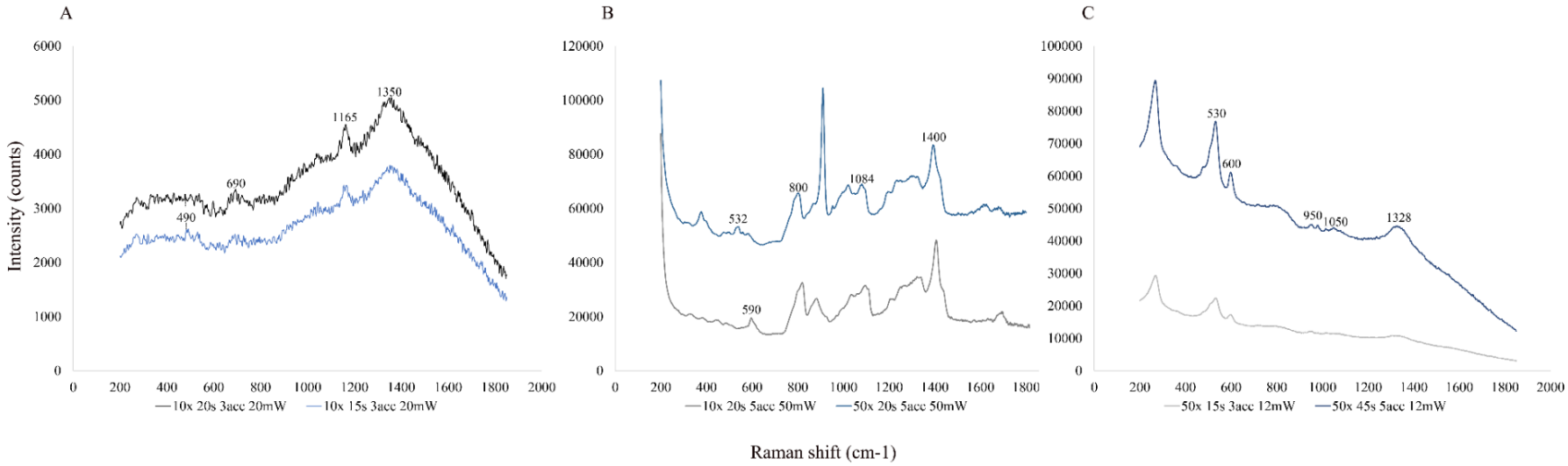

Figure 4.24. *Comparative Raman spectrum of different loci on extracted magnetic material.* (A) Raman spectra indicating iron oxide, seen at multiple loci. (B) & (C) Raman spectra of unknown elements possibly cellular material, indication the extracted material was not solely iron oxide.

4.4.5 *Electron microscopy*

A

Element	Weight %	Atomic %
O K	61.5	80.35
Mg K	0.63	0.54
S K	1.26	0.882
K K	4.58	2.45
Ca K	26.13	13.63
Fe K	5.9	2.21
Totals	100	100

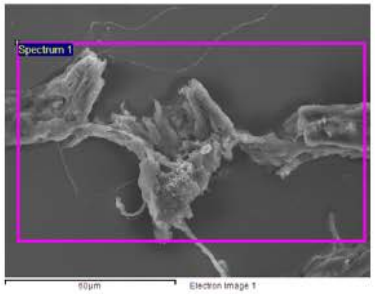

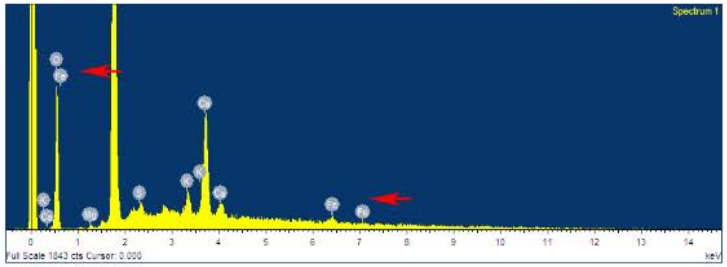

B

Element	Weight %	Atomic %
S K	55.49	68.47
Fe K	44.51	31.53
Totals	100	100

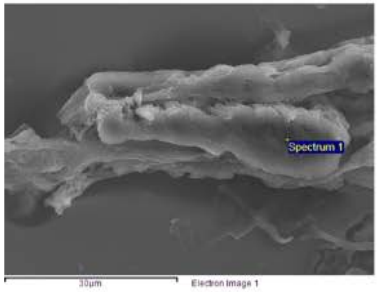

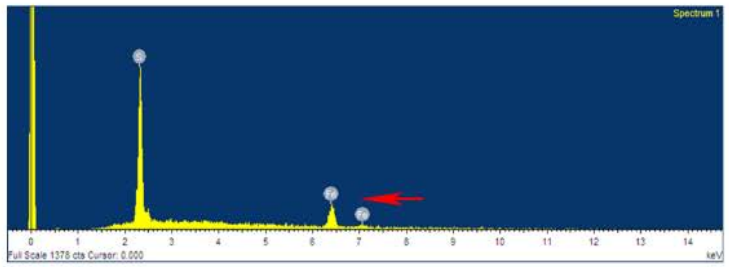

Figure 4.25. *SEM and EDS analysis of r.o.i's identified in Prussian Blue histology.* Figure shows two examples of structures examined using SEM. R.o.i's identified with Prussian Blue were contained within various structures. (A) Broad spectrum (low magnification) imaging and EDS analysis of an r.o.i. One strong peak, and two further peaks (red arrows) were seen. The strong Fe peak also overlapped with an O peak. Iron made up less than 2.5% of the elements present in the focal area. (B) High magnification (narrow focal area) imaging and EDS analysis of a separate r.o.i. Silicon and iron were the only elements identified in this instance.

SEM & TEM, with energy dispersive spectrometry were employed to try to visualize potential iron/magnetite containing structures identified in olfactory tissues via Prussian Blue histology. For SEM, r.o.i's were examined directly on the sectioned tissue. EDS analysis of r.o.i's identified the iron within tissues (figure 4.25). However, it was not possible to discern the exact structures in which the iron was contained.

TEM analysis of r.o.i's that were successfully embedded in resin could not identify specific iron containing cells, although crystalline structures were identified that were subsequently found to contain iron. Unfortunately, only the r.o.i from the filia olfactoria region was examined. For some r.o.i's, the process of transferring tissues from the slide to resin was ultimately unsuccessful. Thick and ultrathin sections were laid on to Formvar-coated 75 mesh and single slot grids. Unfortunately, some r.o.i's were so small that grid bar or the mesh obscured them. In one case, a thin section actually folded over the grid bar, preventing analysis of the r.o.i. A region of interest within the filia olfactoria was examined via TEM. At lower magnification (~27k x), bands of collagen fibers can be seen among other tissues (figure 4.26A & B). What appears to be a granular layer can also be seen, perhaps in association with these collagen bundles (figure 4.26B). Higher magnification imaging of this granular layer reveals these "granules" to be crystalline, with some appearing tessellate (figure 4.26C). It is notable too, that these crystals, which are ~ 50nm in cross-sectional length, also appear to be arranged in rows (figure 4.26D). These crystal structures were investigated using EDS (figure 4.27).

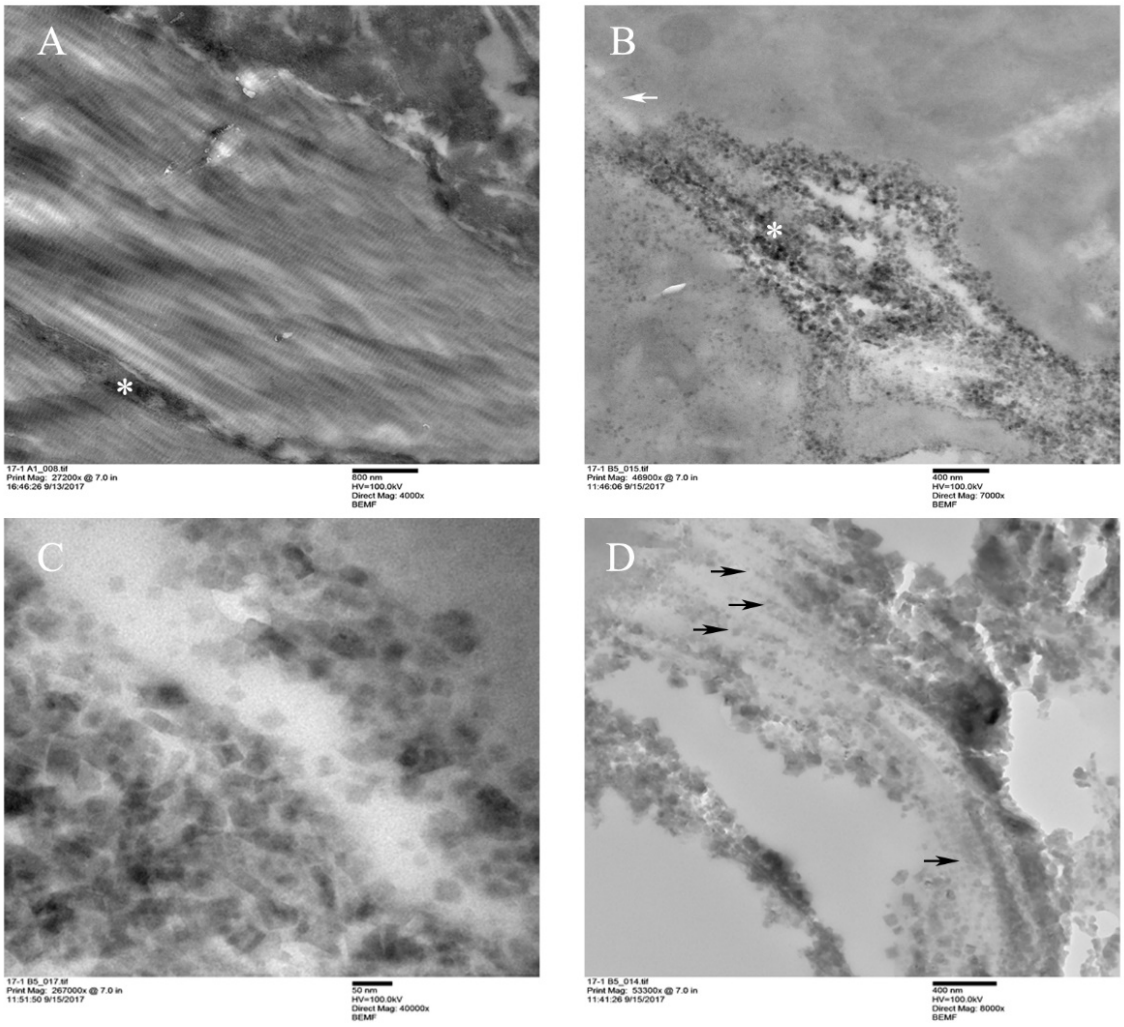

Figure 4.26. *TEM imaging of r.o.i. in filia olfactoria region*. Organized crystalline structures were seen interspersed with collagen fiber bundles. (A) TEM micrograph (27k x magnification) showing collagen fiber bundles, along with a darker "granular" region (starred). (B). Higher magnification micrograph (~47k x) showing apparent crystalline structures (starred) as well as collagen bundles (white arrow). (C) High magnification (267k x) micrograph of crystal structures. Crystals range in size from ~ 15nm to 50nm. (D) Micrograph (50k x) showing arrangement of crystals in rows/bands (black arrows).

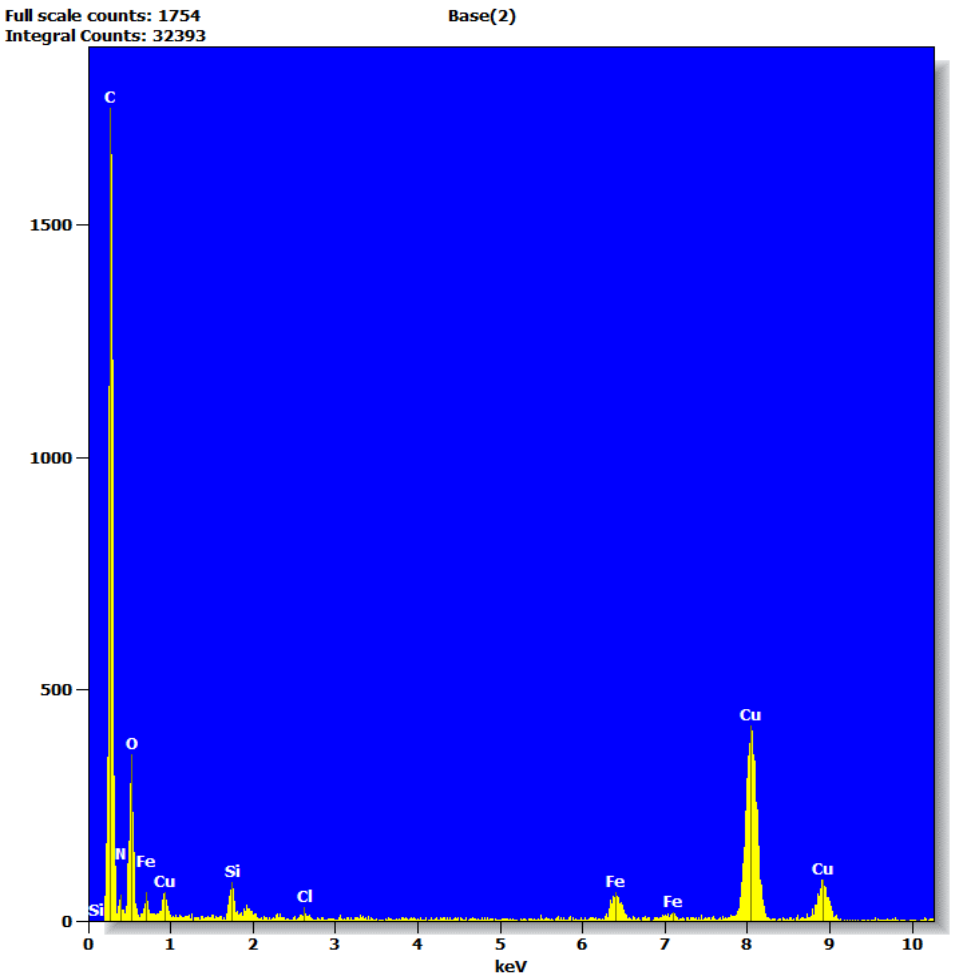

Figure 4.27. *EDS spectra for r.o.i. in olfactory connective tissue.* A clear peak for iron was seen (overlapping with oxygen), along with two further iron peaks. Peaks for copper likely come from the grid-bars on which the section was laid.

The spectra above come from a broader analysis of a point in the r.o.i. (pictured in figure 4.28). While carbon is the overwhelming contributor to the spectra (as might be expected) iron also presents a sizeable contribution. A sharper focused "point and shoot" analysis was carried out across 5 points within the r.o.i. Iron content across these 5 points was variable (figure 4.28), which is to be expected from biological structures. Iron content overall was not insignificant (~ 3%). Clearly, these crystal structures are not pure iron or magnetite but contain iron.

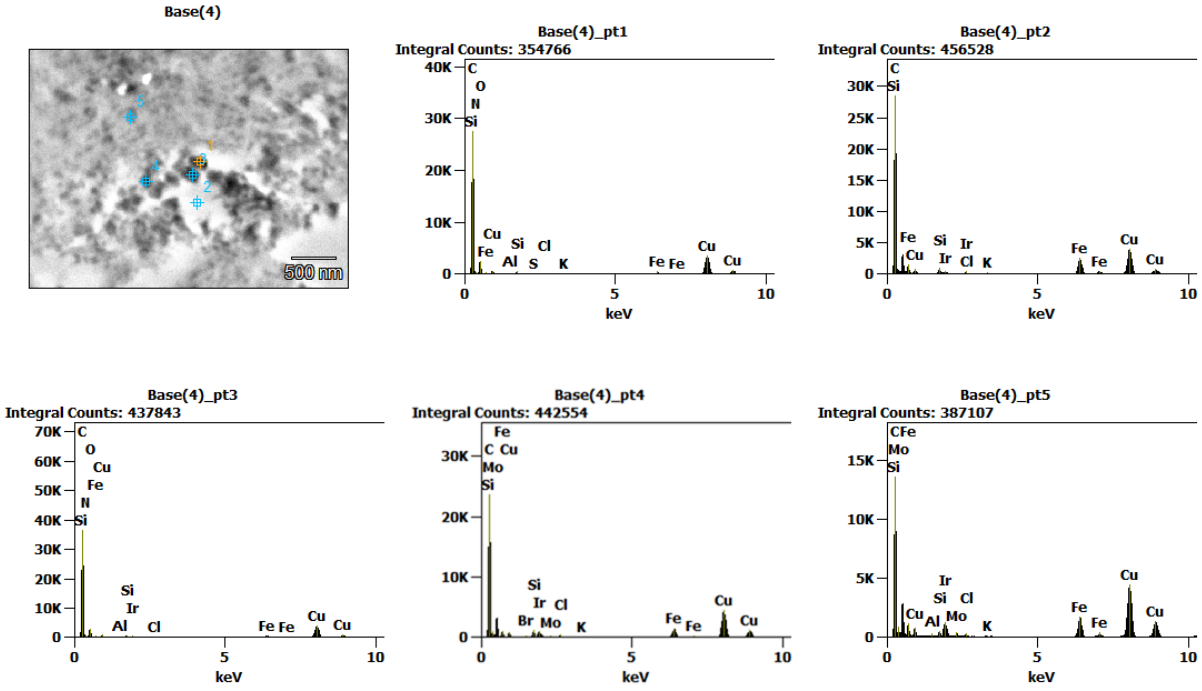

Figure 4.28. *"Point and shoot" EDS spectra for r.o.i. in olfactory connective tissue.* Blue (and 1 orange) cross hairs in the micrograph (top left) show locations of eds analysis. Iron contribution was variable across analysis points. Point 5 (top left point in micrograph) had the strongest iron signal of all locations.

4.5 *Discussion*

If the elasmobranch olfactory rosette does function as the structure in which an iron based magnetoreceptor is housed, a means of sensory transduction is required to convey magnetic field information back to the higher processing centers of the brain. Although an iron based magnetoreceptor is proposed to exist in the olfactory organ of some avian and teleost species, the olfactory nerve (cranial nerve 1) is not implicated in sensory transduction of magnetic information. This may seem unexpected, given the abundance of sensory axons from CN 1 that proliferate throughout the olfactory rosette. However, the fact that the trigeminal nerve (CN V) is implicated stands to reason. Sensory trigeminal fibers in fish are sensitive to pressure, stretch/contortion and vibration (Sneddon 2003). Electrophysiology experiments in *O.* mykiss, demonstrated a trigeminal nerve response to

presented changes to the local magnetic field (Hellinger & Hoffmann 2009). Thus, if CNV is widely distributed in olfactory tissues of sharks, as it is in teleost fishes, it may serve to detect movement/torque/vibration of iron/magnetite containing tissues.

In these investigations, rami of CNV were traced into and through the olfactory tissues of sandbar and scalloped hammerhead sharks using a combination of tract tracing techniques. The efficacy of labelling techniques was variable, with the use of Biotinylated Dextran Amine (BDA) resulting in the strongest and most widespread labelling. The olfactory epithelium in *S. lewini* does contain endogenous peroxidase, as is evidenced by the browning of the cells of the secondary folds (tips/buds of the lamellae) (figure 4.8). The quenching step (treating with Hydrogen Peroxide) prior to incubation with the ABC solution is designed to significantly reduce non-specific background staining. Thus, even if there was some non-specific staining of BDA labeled tissues, the extensive labeling seen is likely due to transport of BDA in trigeminal fibers, rather than being a false positive. In figure 4.8A, strong labelling can be seen in the central raphe, as well as in the primary lamellae. Notably, the labeling in the columns of the primary lamellae (in this image) is primarily seen at the lateral edges, where the connective tissue that supports the structure meets the epithelial layer. This is the lamina propria layer. The epithelium of the secondary folds of the lamellae also stem from a central supporting structure largely made up of connective tissue. Labeling can be seen extending into the secondary folds, perhaps to the basal lamina, but labeling extending into the epithelium is sparse.

Neurobiotin+ was also used to further investigate innervation of SOA CNV into the olfactory tissues of scalloped hammerhead sharks. While labelling was not as clear as with BDA, migration of the tracer was observed in the same tissue groups (raphe, lamina propria). Some signal was also seen in the epithelial layer (figure 4.10). While difficult to be precise, it appears that labeling within the epithelium was to the non-sensory ridges of the secondary folds of the lamellae, not the sensory 'trough' areas (Meredith 2011).

In *C. plumbeus,* a branch of CNV (possibly the deep ophthalmic branch) was cut and labelled with DiI. Gross dissection and tracing with Oil Red O revealed fine rami extending from the principle trunk of the deep ophthalmic branch, over the dorsal surface of the olfactory bulb, and into the tissues of the olfactory rosette. It was notable that this was only seen on the

medial branch of the bifurcated bulb. No other CNV supply to the olfactory organ was found in *C. plumbeus,* which is not to say that there is no other CNV supply.
Retrograde migration of DiI extended into the connective tissue sheath of the olfactory organ, and some lamellae (figure 4.4, 4.6). Observed labelling was not extensive and was only successful in one (of two total) applications. It is likely an alternative application method (for example pico-spritzing DiI solution directly into nerve tracts) would result in more extensive labelling. Cryo-sectioning of DiI labelled tissues is also not optimal, and has been documented to severely degrade the resolution of DiI labeling, (Teraski & Jaffe 1991). None the less, labelled tissues fluoresced strongly under red light (565 nm), but did not under green light (488 nm), indicating the signal seen was real, although auto-fluorescence was present in tissues of some sections (figure 4.5). Given the apparent limited supply of fibers from this deep ophthalmic branch, it follows that observed labelling was not widespread. However, more extensive labelling than was actually seen might be expected. These investigations in no way elucidate the functional role of CNV olfactory innervation. However, given that SOA CNV fibers are sensory in nature, are widespread in the olfactory rosette of *S. lewini* (the same cannot be said with confidence in *C. plumbeus* – although it is likely to be the case in all probability) and innervate the tissue layers invoked as the site of magnetite containing cells in *O. mykiss*, it can be argued that these findings do lend support to the olfactory magnetoreceptor hypothesis. Whether or not there is magnetite in elasmobranch olfactory tissues is another question.

Prussian Blue histology was used to screen for the presence of iron in olfactory tissues of both shark species. Positive staining was seen across tissue types, including the epithelium, the lamina propria, the connective tissue (filia olfactoria region) of primary lamellae, and in the olfactory bulb (figure 4.11). No structure or physical location was identified where iron might reliably occur. There appears, at least so far as the histology can demonstrate, no apparent order or organization to its' occurrence in these tissues.
The use of Prussian Blue stain to identify iron in the search for magnetite is not novel. Perhaps most famously, Fleissner et al. (2003), reported they had identified magnetite in the upper beak of homing pigeons using Prussian Blue. This claim was refuted by Treiber et

al. (2012), who demonstrated that the iron identified by Fleissner and colleagues was in-fact contained in iron-rich macrophages, not magnetosensitive neurons, as had been claimed. The particular methodology chosen for these investigations is a non-haem stain for iron, thus there should be no staining of hemoglobin in red blood cells. As an added control, all sharks used in histology were transcardially perfused. While this cannot be expected to remove every red blood cell, it can be expected to remove most. Of course, the removal of blood from the venous supply to tissues does not confer the removal of macrophages. Nonetheless, Prussian Blue histology is an effective way to screen for iron. Any identified regions of interest can be further analyzed to determine their nature and possible function.

Magnetic resonance imaging was employed to screen for iron in shark olfactory organs because it allows acquisition of non-invasive (destructive), high-resolution 3D data of soft tissue structures, and has been used to examine internal anatomy of teleost fishes (Sepulved et al. 2007; Rogers et al. 2008), as well as comparative brain anatomy in elasmobranch fishes (Yopak et al. 2007a; Yopak & Frank 2009). MRI has also been used to detect magnetite nano-particles in drug delivery efficacy studies in rats, and has been shown to be sufficiently sensitive to accurately detect particles as small as 200nm in size, even in low concentrations (Martinez Vera et al. 2014). Prussian blue histology is useful in screening for iron, however, the physical process is damaging to tissues, and iron containing regions may be lost during both sectioning and staining processes. MRI allowed visualization and mapping of sites of iron within each individual lamella, and proved a more efficient tool in terms of the number of sites of iron signal that were found across an individual olfactory organ. Rosettes were vacuum treated prior to imaging to remove any bubbles/air-pockets that induce magnetic susceptibility artefacts. It is for the same reason that only iron signal seen to be clearly with the tissues of the lamellae was included in these analyses. While the number of sites identified via MRI in rosettes from both species might not be considered large (mean of 34 in *S. lewini*, 36 in *C. plumbeus*), the approximate mean deposit size in each rosette (Table 4.1) can be considered to be large (63.9 μm in *S. lewini*, 78.8 μm in *C. plumbeus*). As all sharks used in the study were perfused prior to organ excision, it is improbable that these regions of signal are accumulations of red blood cells. It

is also unlikely (based on histological analyses) that these deposits are a single, large crystal, rather they are likely to be made up by an accumulation of iron or iron containing crystals and particles in the tissues. In magnetotactic bacteria, magnetosome size ranges between ~ 35 to 125 nm (Bazylinski & Frankel 2004), with 11 magnetosomes being required within a cell for it to freely align with the geomagnetic field (Faivre & Schüler 2008). While MRI can neither quantify the number of iron particles/crystals in a deposit or how they are arranged, nor confirm the species of iron, or magnetic nature of the iron (i.e. super-paramagnetic, single domain etc.), it can demonstrate that iron deposits within shark olfactory tissues are sufficiently large enough to serve in magnetic field detection, providing necessary criteria for crystal size, arrangement and magnetic domain are met.

To try to further quantify the occurrence of iron/magnetic material within the tissues. Dissociation techniques combined with flow cytometry were incorporated into the study. Eder et al (2012) dissociated olfactory rosettes in *O. mykiss* to quantify their occurrence and their magnetic dipole moment (a vector quantity used to measure the tendency of an object to interact with an external *magnetic* field). They found that across 50 animals used, a dissociated pair of rosettes would yield in the region of 10^4 single cells in suspension, of which between one and four cells would rotate freely under an applied rotating magnetic field. While the magnetic dipole moment they measured from these cells was sufficiently strong to passively align with the geomagnetic field (4–100 fAm2, corresponding to 0.05 milliTesla), it is highly unlikely 1-2 cells per rosette can be sufficient to serve as a magnetoreceptor. In this study, mean cell yield from a *S. lewini* olfactory rosette was 6.67 x 10^5 cells. Magnetic separation of cells with magnetic properties from those without produced a mean yield of 7.16 x 10^4 cells, approximately 10% of the parent population (Table 4.2). This would suggest the methods used by Eder and colleagues was not an efficient way to screen for magnetite. The findings of the Eder et al study were later refuted by Edelman et al. (2014), who used correlative light and electron microscopy (CLEM) coupled with electron energy loss spectroscopy (EELS) to examine intracellular structures of *O. mykiss* cells with magnetic properties. They concluded that the magnetic properties

likely derived from introduced extracellular structures containing iron, titanium and chromium, not biogenically derived magnetite.

Rather than trying to quantitatively examine the magnetic properties of cells, these investigations attempted to qualify the physical characteristics of cells showing magnetic properties (the magnetically filtered population) using flow cytometry. FCM analyses showed FSC and SSC from M- and M+ fractions were similar, indicating cells with magnetic properties likely come from the same population as non-magnetic cells, i.e. there would not appear to be a specialist, previously undescribed cell type that occurs in the olfactory rosette of sharks, and functions solely in magnetoreception. Without a refractive index reference for each cell type within olfactory tissues (which was not available), it is not possible to quantify the sizes of cells, or sort (count) cells based on size. Fluorescent magnetic beads are widely used in biotechnology, molecular biology and microbiology applications, such as to separate cells, detect pathogens, screen for specific cells associated with disease (Clarke & Davies 2001). In this study fluorescent carboxyl magnetic particles (0.35 μm) were used to characterize the magnetic properties of cells in the M+ fraction. Cells from the m+ fraction were found to bind strongly to the magnetic beads while the same cannot be said with the M- fraction. It is possible that strands of DNA in suspension and other cellular debris could bind with the carboxyl coating of the beads (figure 4.18). However, it would be expected that the same DNA and cellular debris (if not more) would be present in the suspension of the M- fraction. Thus, if cells, or cellular debris were binding to the carboxyl coating, as opposed to magnetic binding, no difference would be seen in the two fractions after the beads were added. The beads themselves have a paramagnetic coating, meaning that they will align in, or be attracted to an external magnetic field, but maintain no magnetic remanence of their own. Thus, the beads were attracted to and bound to the cells, rather than the cells being attracted to the beads. The magnetic material within the cells cannot therefore be paramagnetic, and so is likely single domain. Cells of the M+ fraction that bind to the beads thus likely contain ferromagnetic structures, but it cannot be concluded from this alone that these structures are comprised of $Fe^{3}0^{4}$.

The observation that a sizeable proportion of cells within shark olfactory tissues lends important support to their function as magnetoreceptors. Johnsen and Lohmann (2005) suggested that magnetoreception via iron-based structures might take place within a volume of tissue (rather than being localized to a specific area or structure). Taylor et al. al. (2017) summarized this concept, suggesting that organisms can encode information regarding the intensity and direction of the magnetic field by amalgamating changes in membrane potential across (iron-containing) cells distributed across three dimensions, allowing for comparison of heterogenous receptor activity.

In a recent theoretical review, (Krichen et al. 2017) proposed that biological cells that have a greater/higher magnetic permeability could function in transduction of magnetic field information, without the need for the classically accepted accessory structures (trigeminal innnervation, or electroreceptors). The arguments and calculations put forward suggest that cells with magnetic properties can encode information pertaining to geomagnetic intensity and polarity through acting as magnetoelectric materials – a change in the external magnetic field induces a change in the magnetic moment of the magnetic material within the cell (e.g. iron oxide), which subsequently confers a change in the electrical properties of the cell. The authors argued these changes in membrane potential should be differentially detectable by cell, thus providing information used in both the map step and the compass step of navigation. The former was argued to be encoded by changes to the polarity and magnitude of the resting potential of cell membrane. Effectively, changes to the magnetic moment of intracellular material (caused by changes to background magnetic field intensity) deform the shape of the cell and the thickness of it's membrane. Due to the constant resting voltage potential across the membrane, these conformational changes will induce changes to the residual electric field of the cell and to the polarization of the membrane, triggering an electrical current (transportation of ions) across the cell membrane. A compass reference was argued to be achievable through localized (rather than homogeneous) membrane deformation and subsequent changes in polarization and resting voltage potential. This assume heterogeneous distribution of magnetic particles within a cell. The force exerted by alignment of such particles with the polarity of the magnetic field would exert pressure on the membrane, inducing thinning (and

depolarization) at a particular pole. This, they argued, would allow an animal to detect polarity of the geomagnetic field, and distinguish north from south.
Thus, the sizeable population of M+ cells found in the olfactory rosettes of sharks could function in magnetoreception in a manner such as that described by Krichen et al. (2017), although the authors make no suggestion as to the neuronal passage of sensory transduction.

Raman spectroscopy is widely used in elemental analysis of geological and solid materials (including geologically formed magnetite), but has also been used to confirm the presence of biologically formed magnetite (Lee et al. 2003; Brooker et al. 2003; Watanabe et al. 2008). Magnetite has characteristic bands at Raman wavenumbers 668, 538, 490, 306 and 103 cm^{1} (Shebanova & Lazor 2003). Raman analyses of both sectioned tissues and dissociated cells in this study failed to identify any of these characteristic Raman bands (figure 4.20). Against a noisy background filled with fluorescence this can be considered unsurprising, particularly as magnetite is a poor Raman scatterer (Eder et al. 2014), and the size of individual (potential) iron oxide/magnetite deposits in tissues (especially in cells) is likely below the diffraction limited optical resolution of the CCD. To overcome this problem previous studies have harvested magnetosomes through dissociation and compressed magnetic filtrate into 3mm discs that were subsequently analyzed (e.g. Watanabe et al. 2008), or have used long-integration times (accumulations) to increase signal to noise ratio (e.g. Eder et al. 2014). Getting approval to collect sufficient magnetic filtrate from sharks to make compressed 3mm discs would be problematic. Thus, magnetic material from just one rosette was extracted (figure 4.21) and analyzed. Low exposure times with multiple accumulations were used to increase SNR, and reduce the chance of damage to the sample from the laser. Long exposure times, or too much power in the laser can heat the sample and induce a phase transition to another iron oxide species (Khan et al. 2015).
Various analyzed points on the magnetically extracted sample produced Raman spectra that included the characteristic spectra for magnetite (figure 4.22). Interestingly, Raman

bands corresponding to other iron oxides (maghemite - Fe^2O^3, lepidocrocite - FeOOH) were also seen (table 4.3).

Table 4.3. *Comparison of iron oxides examined, their associated Raman bands, and laser wavelength applied*. Table demonstrates that Raman bands are variable, not precise, and that observed bands may also be dependent upon wavelength.

Iron Oxides	Raman peak (cm)	Reference	Laser wavelength (nm)
Magnetosome	**662**,532, 403	Watanabe et al. 2008	532
	848, **665,** 432	Prozorov et al. 2014	785
	665, 535, 303	Eder et al. 2014	532
Fe^3O^4 Magnetite	**660**, 580, 300	Watanabe et al. 2008	532
	661, 535, 297	Lee et al. 2003	600
	667, 532	Oh et al. 1998	633
	668, 725	Gabrielli et al. 2006	633
	1322, **676**, 550, 418, 319, 298	Dünnwald & Otto 1989	514
	1345, **670**	Fe^3O^4 sample	785
	1345, **665**, 670, 532, *1168, 680*	This study	785
Fe^2O^3 Maghemite	**1168,** 1348, 690, 613, 490	Fe^2O^3 sample	785
	1169, 1349, 690, *613*, 490	This study	785
$5Fe^2O^39H_2O$ Ferrihydrite	716, **400**, 305	Legrand et al. 2001	458
	730, 692, 493, 347	Gabrielli et al. 2006	633
FeOOH Lepidocrocite	1054, 654, 528, 380, **255**	Watanabe et al. 2008	532
	1307, 1054, 654, 528, 380, **255**	Dünnwald & Otto 1989	514

It was also notable that repeated analysis of the same exact point produced slightly different spectra appearing to transition from bands characteristic of magnetite to bands characteristic of hematite (red trace & green trace, figure 4.22). The most likely reason for this is phase transition of iron oxide, most probably magnetite to maghemite, due to heating from the laser.

A reference spectrum, taken for comparison with apparent maghemite in the magnetically extracted sample, produced Raman peaks at almost identical wavenumbers, confirming the magnetic extract was iron-oxide based. It was interesting to note that distinct peaks were observed that were characteristic of Lepidocrocite (250 & 380 cm^{-1}, figure 4.22). Lepidocrocite is a pre-cursor to magnetite in the teeth of chitons (Brooker et al. 2003), and is also reduced by microbes in magnetite formation (Bazylinski et al. 2007).

Thus, it seems highly likely magnetically extracted material was primarily made up iron-oxides, most probably magnetite. Other elements present in biological structures and extracted with the accumulation of iron-oxide crystals, perhaps ionically bound to it, would account for other (non iron-oxide) Raman bands seen in the material (figure 4.24).

SEM and TEM can produce high resolution imaging to visualize microscopic structures of interest, and had the potential to be a valuable methodological tool in this study. However, electron microscopy, particularly TEM, is a poor method for screening for small iron deposit in exponentially larger structures. The methods adopted in this study attempted to improve the efficacy of using TEM, with a measurable level of success (figure 4.26). However, the methods were also prone to problems that would require repeated attempts to prepare identified regions of interest for TEM. Unfortunately, these methodologies are time consuming and costly. These two factors were principle constraints that limited the continued endeavor to characterize iron containing structures in identified regions of interest using SEM & TEM. However, the limited success that was seen warrants development and use of these methodologies in any future continuation of this study, or similar studies.

The crystals that were identified to contain iron with the connective tissue supporting structures of primary lamellae do not conform to the description of magnetite crystals in *O.*

mykiss rosettes, or in bacterial magnetosomes. The small amounts of iron contained within the crystals, as demonstrated by EDS analyses (figures 4.27 & 4.28) confirm that the crystals are not purely magnetite. They may still however, contain magnetite. This level of identification was not possible using this EDS system.

4.6 *Conclusions*

Shaw et al. (2015) commented that "studies aimed at understanding the mechanistic basis of magnetoreception by determining the anatomical location, structure and function of sensory cells have been inconclusive", and that no single technique has yet been able resolve this issue. Thus, correlative approaches are required to sequentially draw out the critical information needed to determine whether or not sharks possess the physical means and mechanisms necessary for an iron based magnetoreceptor.

The results of methodologies incorporated into these investigations present a reproducible, multi-faceted, correlative approach that can be used to screen for, identify and describe iron/magnetite containing structures that may function in magnetic field perception. Extensive trigeminal supply to the lamina propria layer and the non-sensory epithelium was found in scalloped hammerhead sharks, while similar but less extensive supply to the same tissue layers was seen in sandbar sharks. It is highly probable that higher resolution labelling with fluorescent tracers could be achieved by modifying and fine-tuning the physical processes of applying the label, as well as the histological procedures.

The combination of Prussian Blue histology, combined with MRI revealed widely dispersed iron in olfactory tissues of both species. While Prussian Blue has carries with it the caveat of being a non-specific stain that require caution when interpreting results (for fear of false positives), the case is not the same for MRI. Potential false positive signal is controlled for via perfusion and vacuum treatment, and while macrophages are traceable using MRI, this is only possible when the sample/tissue is enhanced with a contrast agent (e.g. gadolinium) or via cell labelling (e.g. with magnetic nanoparticles). Visualization of MRI optical sections showed that sites of iron signal potentially contained iron deposits more than sufficiently big enough to align with the magnetic field (assuming all other required conditions are

met). Given bigger sample sizes, and sufficient resources, future studies could incorporate MRI to further develop the comparative approach used here.

The tissue dissociation and flow cytometry techniques incorporated shed new light on the magnetic nature of a population of cells within the olfactory tissues, as well as elucidating the possible magnetic domain of these magnetic cells. This approach presents a relatively quick and easy means of acquiring this information. It is not limited to this however. Careful dissection and excision of individual cell layers in the olfactory tissues (e.g. sensory & non-sensory epithelium, o.r.n.'s, support cells, crypt cells, connective tissues etc.) followed by dissociation to single cell suspensions would allow for acquisition of refractive index references for all cells within the rosette. Thus, the type of cells, the size of cells and the number of cells that possess these magnetic attributes could be determined. Further, these cells could be sorted (collected), fixed appropriately, then analyzed using electron microscopy to study the ultrastructure of these cells and examine if and how iron structures are contained within cells, and act as magnetoreceptors.

Incorporating Raman spectrometry proved to be the key to determining the identity of the magnetic material in the olfactory tissues. It was concluded that the magnetic material extracted was primarily made up of iron-oxide, most likely magnetite. It is almost certain that using lower power laser excitation, in combination with short exposure times and multiple (100s) acquisitions would improve signal to noise ratio an produce more clearly defined Raman peaks. Given the poor scattering ability of magnetite, orienting the sample would also likely greatly improve diffraction. The amorphous "clump" of iron-oxide extracted from the cells simply cannot diffract light energy back to the CCD in the manner that a smooth, oriented piece of cut and polished magnetite can. Thus, future studies should utilize Raman, but combine iron-oxide from multiple samples, compressed into a smooth pellet, as has been done with magnetosomes. The size of the debris clump actually indicates that the number and physical size of iron deposits were underestimated. The volume of magnetite estimated in the tissue based on the calculations made from MRI analyses turns out to be considerably smaller than the iron oxide/magnetite actually extracted. This does not serve to reduce the value of MRI analysis however.

EM investigations were constrained by the technical difficulties of sample preparation, and the constraints of cost and time. However, the methods employed did bare fruit, and demonstrated a means to examine the ultrastructure of identified regions of interest. Continued that follow the recommendations set out above, particularly with regard to cell sorting via flow cytometry, should seek to investigate and describe the ultrastructure of cells harvested via the magnetic separation and enrichment methods presented and suggested.

Overall, these results present strong supporting evidence that sharks likely possess an olfactory based magnetoreceptor. However, the hypothesis cannot be accepted with any confidence at this time. Further study along the lines suggested here is required to bolster this support. Such studies should seek to gather the outstanding information on the critical physical structures required by an iron-based magnetoreceptor.
Even with an exquisite suite of data, the functional use of the proposed receptor structure remains unknown. Complementary studies, specifically electrophysiology of the candidate trigeminal branches, as well as the anterior lateral line (electrosensory) nerve will be vital in demonstrating functionality of the proposed magnetoreceptor.

References

Able, K.P., 2001. The concepts and terminology of bird navigation. *Journal of Avian Biology*, 32(2), pp.174–183.

Åkesson, S., Boström, J., Liedvogel, M., & Muheim, R. (2014). Animal navigation. In L Hansson & S Åkesson, eds. Animal Movement Across Scales. : Oxford University Press, pp 151-178

Akoev, G., Ilyinsky, O. & Zadan, P., 1976. Responses of electroreceptors (ampullae of Lorenzini) of skates to electric and magnetic fields. *Journal of Comparative Physiology A*, 106(2), pp.127–136.

Ambrosino, C.M., 2012. *Differential Behavior Of Ampullary Subunits In The Electrosensory System Of The Scalloped Hammerhead Shark (Sphyrna Lewini)*. University of Hawaii at Manoa. Available at: https://scholarspace.manoa.hawaii.edu/handle/10125/101238

Anderson, J.M. et al., 2017. Insight into shark magnetic field perception from empirical observations. *Scientific Reports*, 7(1).

Andreano, J.M. & Cahill, L., 2009. Sex influences on the neurobiology of learning and memory. *Learning & memory (Cold Spring Harbor, N.Y.)*, 16(4), pp.248–66.

Andrianov, G.N., Brown, H.R. & Ilyinsky, O.B., 1974. Responses of central neurons to electrical and magnetic stimuli of the ampullae of lorenzini in the Black Sea skate. *Journal of Comparative Physiology. A*, 93(4), pp.287–299.

Arniella, M.B., Fitak, R.R. & Johnsen, S., 2018. Unmapped sequencing reads identify additional candidate genes linked to magnetoreception in rainbow trout. *Environmental Biology of Fishes*, pp.1–11.

Aronson, L.R., Aronson, F.R. & Clark, E., 1967. Instrumental Conditioning And Light-Dark Discrimination In Young Nurse Sharks'. *Bulletin Of Marine Science* , 17(2), pp.249–256.

Bates, D., Maechler, M., Bolker, B., Walker, S. (2015). Fitting Linear Mixed-Effects Models Using lme4. Journal of Statistical Software, 67(1), 1-48.<doi:10.18637/jss.v067.i01>.

Baumgartner, J. et al., 2013. Magnetotactic bacteria form magnetite from a phosphate-rich ferric hydroxide via nanometric ferric (oxyhydr)oxide intermediates. *Proceedings of the National Academy of Sciences of the United States of America*, 110(37), pp.14883–8.

Bazylinski, D.A. & Frankel, R.B., 2004. Magnetosome formation in prokaryotes. *Nature Reviews Microbiology*, 2, pp.217–230.

Bazylinski, D.A., Frankel, R.B. & Konhause, K.O., 2007. Modes of Biomineralization of Magnetite by Microbes. *Geomicrobiology Journal*, 24(6), pp.465–475.

Beason, R. & Nichols, J., 1984. Magnetic orientation and magnetically sensitive material in a

transequatorial migratory bird. *Nature*, 309(5964), pp.151–153.

Beason, R. & Semm, P., 1996. Does the avian ophthalmic nerve carry magnetic navigational information? *The Journal of experimental biology*, 199, pp.1241–1244.

Bedore, C.N. & Kajiura, S.M., 2013. Bioelectric fields of marine organisms: voltage and frequency contributions to detectability by electroreceptive predators. *Physiological and biochemical zoology : PBZ*, 86(3), pp.298–311.

Belousova, T.A., Devitsina, G.V. & Malyukina, G.A., 1983. Functional peculiarities of fish trigeminal system. *Chemical Senses*, 8(2), pp.121–130.

Bennett, A.T.D., 1996. Do Animals Have Cognitive Maps? *Journal of Experimental Biology*, 199, pp.219–224.

Bett, N.N. et al., 2016. Evidence of Olfactory Imprinting at an Early Life Stage in Pink Salmon (Oncorhynchus gorbuscha). *Scientific Reports*, 6(36393).

Blakemore, R., 1975. Magnetotactic bacteria. *Science (New York, N.Y.)*, 190(4212), pp.377–379.

Boles, L. & Lohmann, K., 2003. True navigation and magnetic maps in spiny lobsters. *Nature*, 421, pp.60–63.

Bonfil, R. et al., 2005. Transoceanic migration, spatial dynamics, and population linkages of white sharks. *Science (New York, N.Y.)*, 310(5745), pp.100–3.

Bouvet, J.F., Delaleu, J.C. & Holley, A., 1987. Olfactory receptor cell function is affected by trigeminal nerve activity. *Neuroscience Letters*, 77, pp.181–186.

Bowler, D.E. & Benton, T.G., 2005. Causes and consequences of animal dispersal strategies: relating individual behaviour to spatial dynamics. *Biological Reviews*, 80(2), pp.205–225.

Brazeau, M. D., & Friedman, M. (2015). The origin and early phylogenetic history of jawed vertebrates. *Nature*, *520*(7548), 490–497. http://doi.org/10.1038/nature14438

Brill, R. et al., 2009. The repulsive and feeding-deterrent effects of electropositive metals on juvenile sandbar sharks (Carcharhinus plumbeus). *Fish. Bull*, 107, pp.298–307.

Brooker, L. et al., 2003. Multiple-front iron-mineralisation in chiton teeth (Acanthopleura echinata: Mollusca: Polyplacophora). *Marine Biology*, 142(3), pp.447–454.

Brower, L., 1996. Monarch butterfly orientation: missing pieces of a magnificent puzzle. *Journal of Experimental Biology*, 199(1).

Brown, F., Webb, H. & Barnwell, F., 1964. A compass directional phenomenon in mud-snails and its relation to magnetism. *The Biological Bulletin*, 127(2), pp.206–220.

Brown, H. & Ilyinsky, O., 1978. The ampullae of Lorenzini in the magnetic field. *Journal of comparative physiology*, 126(4), pp.333–341.

Bumbrah, G.S. & Sharma, R.M., 2016. Raman spectroscopy – Basic principle, instrumentation and selected applications for the characterization of drugs of abuse. *Egyptian Journal of Forensic Sciences*, 6(3), pp.209–215.

Butler, R.F. & Banerjee, S.K., 1975. Theoretical single-domain grain size range in magnetite and titanomagnetite. *Journal of Geophysical Research*, 80(29), pp.4049–4058.

Casper, B.M., Lobel, P.S. & Yan, H.Y., 2003. The Hearing Sensitivity of the Little Skate, Raja erinacea: A Comparison of Two Methods. *Environmental Biology of Fishes*, 68(4), pp.371–379.

Casper, B.M. & Mann, D.A., 2006. Evoked Potential Audiograms of the Nurse Shark (Ginglymostoma cirratum) and the Yellow Stingray (Urobatis jamaicensis). *Environmental Biology of Fishes*, 76(1), pp.101–108.

Casper, B.M. & Mann, D.A., 2009. Field hearing measurements of the Atlantic sharpnose shark Rhizoprionodon terraenovae. *Journal of Fish Biology*, 75(10), pp.2768–2776.

Chapman, B.B. et al., 2012. Partial migration in fishes: definitions, methodologies and taxonomic distribution. *Journal of Fish Biology*, 81(2), pp.479–499.

Chew, G.L. & Brown, G.E., 1989. Orientation of rainbow trout (Salmo gairdnen') in normal and null magnetic fields. *Can J Zool*, 67(3), pp.641–643.

Clark, E., 1959. Instrumental conditioning of lemon sharks. *Science*, 130(3369), pp.217–8.

Clarke, C. & Davies, S., 2001. Immunomagnetic cell separation. In S. A. Brooks & U. Schumacher, eds. *Metastasis Reseach Protocols Volume II Analysis of Cell Behavior In Vitro and In Vitro*. Totowa, NJ: Humana Press Inc.

Cooper, J.C. et al., 1976. Electroencephalographic evidence for retention of olfactory cues in homing coho salmon. *Science* , 192(4245), pp.1247–1249.

Corwin, J.T., 1978. The relation of the inner ear structure to the feeding behavior in sharks and rays. *Scanning Electron Microscopy*, 2, pp.1105–1112.

Corwin, J.T. 1981a. Audition in elasmobranchs. pp. 81–102. *In:*W.N. Tavolga, A.N. Popper & R.R. Fay (ed.) Hearing and Sound Communication in Fishes, Springer-Verlag, New York.

Corwin, J.T. 1981b. Peripheral auditory physiology in the lemon shark: evidence of parallel otolithic and non-otolithic sound detection. J. Comp. Physiol. 142A: 379–390.

Cotton CF, Grubbs RD. Biology of deep-water chondrichthyans: Introduction. Deep Sea Res Part II Top Stud Oceanogr. 2015;115:1–10. doi: 10.1016/j.dsr2.2015.02.030

Cresci, A. et al., 2016. Earth-strength magnetic field affects the rheotactic threshold of zebrafish swimming in shoals. *Comparative Biochemistry and Physiology, Part A*, 204(2017), pp.169–176.

Cullity, B.D. (Bernard D. & Graham, C.D. (Chad D.., 2009. *Introduction to magnetic materials*

2nd ed., Hoboken: IEEE/Wiley.

Deutschlander, M., Borland, S. & Phillips, J., 1999. Extraocular magnetic compass in newts. *Nature*, 400, pp.324–325.

Deutschlander, M.E., Phillips, J.B. & Borland, S.C., 2000. Magnetic Compass Orientation in the Eastern Red-Spotted Newt, Notophthalamus viridescens: Rapid Acquisition of the Shoreward Axis. *Copeia*, 2000(2), pp.413–419.

Diebel, C.E. et al., 2000. Magnetite defines a vertebrate magnetoreceptor. *Nature*, 406(6793), pp.299–302.

Dingle, H., 1996. *Migration : the biology of life on the move*, Oxford University Press.

Dixson, A., 2012. *Zebrafish magnetite and long-lived Rohon-Beard neurons : Expanding Our View Of Two Zebrafish Sensory Systems In Development And Adulthood*, ProQuest Dissertations Publishing. Available at: https://thesis.library.caltech.edu/6835/.

Drioli, M. & Chiaramonte, G., 2005. *Potamotrygon motoro*, IUCN Global Species Programme Red List Unit. Available at: http://www.iucnredlist.org/details/39404/0 [Accessed February 15, 2018].

Dünnwald, J. & Otto, A., 1989. An investigation of phase transitions in rust layers using raman spectroscopy. *Corrosion Science*, 29(9), pp.1167–1176.

Durif, C.M.F. et al., 2013. Magnetic Compass Orientation in the European Eel. *PLoS ONE*, 8(3), pp.1–7.

Edelman, N.B. et al., 2014. No evidence for intracellular magnetite in putative vertebrate magnetoreceptors identified by magnetic screening. *Proceedings of the National Academy of Sciences of the United States of America*, 112(1).

Eder, S., Gigler, A.M., et al., 2014. Sub-Micrometer-Scale Mapping of Magnetite Crystals and Sulfur Globules in Magnetotactic Bacteria Using Confocal Raman Micro-Spectrometry A. Al-Ahmad, ed. *PLoS ONE*, 9(9), p.e107356.

Eder, S.H.K. et al., 2012. Magnetic characterization of isolated candidate vertebrate magnetoreceptor cells. *Proceedings of the National Academy of Sciences of the United States of America*, 109(30), pp.12022–7.

Edrén, S. & Gruber, S., 2005. Homing ability of young lemon sharks, Negaprion brevirostris. *Environmental Biology of Fishes*, pp.267–281.

Ellen, P. & Anschel, S., 1981. Problem solving in the rat: cognitive/physiological mechanisms. *Behavioral and Neural Biology*, 33(4), pp.402–418.

Eschmeyer, W.N. & Fong, J.D., 2018. California Academy of Sciences - Catalog of Fishes - Species by Family.

Faivre, D. & Schüler, D., 2008. Magnetotactic Bacteria and Magnetosomes. *Chemical Reviews*, 108(11), pp.4875–4898.

Filimon, F., 2015. Are All Spatial Reference Frames Egocentric? Reinterpreting Evidence for Allocentric, Object-Centered, or World-Centered Reference Frames. *Frontiers in human neuroscience*, 9, p.648.

Fischer, J.H. et al., 2001. Evidence for the use of magnetic map information by an amphibian. *Animal Behaviour*, 62, pp.1–10.

Fitak, R.R. et al., 2017. Candidate genes mediating magnetoreception in rainbow trout (Oncorhynchus mykiss). *Biology letters*, 13(4), p.20170142.

Fleissner, G. et al., 2007. Iron-mineral-based magnetoreception in birds: the stimulus conducting system. *Journal of Ornithology*, 148(S2), pp.643–648.

Fleissner, G. et al., 2003. Ultrastructural analysis of a putative magnetoreceptor in the beak of homing pigeons. *Journal of Comparative Neurology*, 458(4), pp.350–360.

Fowler, S., 2014. *The Conservation Status of Migratory Sharks*, Bonn: UNEP/CMS Secretariat.

Fraden, J., 2010. *Handbook of Modern Sensors: Physics, Designs, and Applications - Jacob Fraden - Google Books* 4th ed., New York: Springer.

Frankel, R.B., Blakemore, R.P. & Wolfe, R.S., 1979. Magnetite in Freshwater Magnetotactic Bacteria. *Science*, 203, pp.1355–1356.

Freake, M. & Phillips, J., 2005. Light ?Dependent Shift in Bullfrog Tadpole Magnetic Compass Orientation: Evidence for a Common Magnetoreception Mechanism in Anuran and Urodele Amphibians. *Ethology*, 254, pp.241–254.

Fuss, T., Bleckmann, H. & Schluessel, V., 2014a. Place learning prior to and after telencephalon ablation in bamboo and coral cat sharks (Chiloscyllium griseum and Atelomycterus marmoratus). *Journal of Comparative Physiology A*, 200(1), pp.37–52.

Fuss, T., Bleckmann, H. & Schluessel, V., 2014b. The shark Chiloscyllium griseum can orient using turn responses before and after partial telencephalon ablation. *Journal of Comparative Physiology A: Neuroethology, Sensory, Neural, and Behavioral Physiology*, 200(1), pp.19–35.

Fuss, T., Bleckmann, H. & Schluessel, V., 2014c. Visual discrimination abilities in the gray bamboo shark (Chiloscyllium griseum). *Zoology*, 117(2), pp.104–111.

Fuss, T. & Schluessel, V., 2015. Something worth remembering: visual discrimination in sharks. *Animal Cognition*, 18(2), pp.463–471.

Gabrielli, C. et al., 2006. Development of a Coupled SECM-EQCM Technique for the Study of Pitting Corrosion on Iron. *Journal of The Electrochemical Society*, 153(3), p.B68.

Gallagher, A.J. et al., 2014. Evolved for Extinction: The Cost and Conservation Implications of Specialization in Hammerhead Sharks. *BioScience*, 64(64), pp.619–624.

Gallistel, C.R., 1990. *The organization of learning*, Cambridge, MA: MIT Press.

Gardiner, J.M. et al., 2012. Sensory Physiology And Behavior of Elasmobranchs. In J. C. Carrier, J. A. Musick, & M. R. Heithaus, eds. *Biology of Sharks and Their Relatives*. Boca Raton: CRC Press, pp. 349–401.

Gardiner, J.M. & Atema, J., 2007. Sharks need the lateral line to locate odor sources: rheotaxis and eddy chemotaxis. *The Journal of experimental biology*, 210, pp.1925–1934.

Gardiner, J.M., Whitney, N.M. & Hueter, R.E., 2015. Smells Like Home: The Role of Olfactory Cues in the Homing Behavior of Blacktip Sharks, Carcharhinus limbatus. *Integrative and Comparative Biology*, 55(3), pp.495–506.

Gilbert, P.W., Hodgson, E.S. & Mathewson, R.F., 1964. Electroencephalograms of Sharks. *Science*, 145(3635), pp.949–951.

Giles S, Friedman M, Brazeau MD. Osteichthyan-like cranial conditions in an Early Devonian stem gnathostome. Nature. 2015;520:82–85. doi: 10.1038/nature14065

Gould, J.L., 2015. Animal Navigation: Birds Have Magnetic Maps. *Current biology : CB*, 25(19), pp.R836-8.

Gould, J.L., 2008a. Animal Navigation: The Evolution of Magnetic Orientation. *Current Biology*, 18(11), pp.R482–R484.

Gould, J.L., 1984. Magnetic Field Sensitivity In Animals. *Ann. Rev. Physiol*, 46, pp.585–98.

Gould, J.L., 2008b. Magnetoreception. *Current biology : CB*, 18(11), pp.R482–R484.

Griffin, D.R., 1952. Bird Navigation. *Biol Rev Camb Philos Soc*, 27, pp.359–353.

Grogan, E.., Lund, R. & Greenfest-Allen, E., 2012. The Origin and Relationships of Early Chondrichthyans. In J . Carrier, J . Musick, & M. Heithaus, eds. *Biology of Sharks and Their Relatives*. Boca Raton: CRC Press, pp. 3–30.

Gruber, S., Hamasaki, D. & Davis, B., 1975. Window to the epiphysis in sharks. *Copeia*, 1975(2), pp.378–380.

Gruber, S.H., 1977. The Visual System of Sharks : Adaptations and Capability. *American Zoologist*. 17 (2), pp.453–469.

Gruber, S.H., Nelson, D.R. & Morrissey, J.F., 1988. Patterns Of Activity And Space Utilization Of Lemon Sharks, Negaprion Brevirostris, In A Shallow Bahamian Lagoon. *Bulletin Of Marine Science*, 43(1), pp.61–76.

Guttridge, T.L. et al., 2013. Social learning in juvenile lemon sharks, Negaprion brevirostris. *Animal Cognition*, 16(1), pp.55–64.

Guttridge, T.L. et al., 2009. The role of learning in shark behaviour. *Fish and Fisheries*, 10(4), pp.450–469.

Guttridge, T.L. & Brown, C., 2014. Learning and memory in the Port Jackson shark, Heterodontus portusjacksoni. *Animal Cognition*, 17(2), pp.415–425.

Hanson, M., Westerberg, H. & Oblad, A.M., 1990. The Role Of Magnetic Statoconia In Dogfish {Squalus Acanthias). *iJ. exp. Biol*, 151(5), pp.205–218.

Hara, T.J., 1975. Olfaction in fish. *Progress in Neurobiology*, 5, pp.271–335.

Hasler, A.D., Scholz, A.T. & Horrall, R.M., 1978. Olfactory Imprinting and Homing in Salmon. *American Scientist*, 66(3), pp.347–355.

Heinicke MP, Naylor GJP, Hedges SB. Cartilaginous fishes (Chondrichthyes) In: Hedges SB, Kumar S, editors. The Timetree of Life. Volume IX. Oxford: University Press; 2009. pp. 320–327.

Hellinger, J. & Hoffmann, K.-P., 2009. Magnetic field perception in the rainbow trout, Oncorhynchus mykiss. *Journal of comparative physiology. A, Neuroethology, sensory, neural, and behavioral physiology*, 195(9), pp.873–9.

Heupel, M.R. & Simpfendorfer, C.A., 2005. Quantitative analysis of aggregation behavior in juvenile blacktip sharks. *Marine Biology*, 147(5), pp.1239–1249.

Hodson, R., 2000. Magnetoreception in the short-tailed stingray, Dasyatis brevicaudata. University of Aukland. Available at: http://researchspace.auckland.ac.nz/handle/2292/5421

Hofmann, M.H., 1999. Nervous System. In W. C. Hamlet, ed. *Sharks, Skates, and Rays: The Biology of Elasmobranch Fishes*. Baltimore: The Johns Hopkins University Press, pp. 273–299.

Hsu, C.-Y. et al., 2007. Magnetoreception system in honeybees (Apis mellifera). *PloS one*, 2(4), p.e395.

Hutchinson, M. et al., 2012. The effects of a lanthanide metal alloy on shark catch rates. *Fisheries Research*, 131, pp.45–51.

Immelmann, K. & Suomi, S.J., 1981. Sensitive phases in development. In K. Immelmann et al., eds. *Behavioural Development: the Bielefeld Interdisciplinary Project*. Cambridge: Cambridge University Press, pp. 395–431.

Johnsen, S. & Lohmann, K.J., 2008. Magnetoreception in animals. *Physics Today*, 61(3), pp.29–35.

Johnsen, S. & Lohmann, K.J., 2005. The physics and neurobiology of magnetoreception. *Nature reviews. Neuroscience*, 6(9), pp.703–12.

Jones, J.C.R., 2016. Pre-and Post-embedding Immunogold Labeling of Tissue Sections. *Methods Mol Biol*, 1474, pp.291–307.

Kajiura, S.M. & Holland, K.N., 2002. Electroreception in juvenile scalloped hammerhead and

sandbar sharks. *The Journal of experimental biology*, 205(Pt 23), pp.3609–21.

Kalmijn, A.., 1966. Electro-perception in sharks and rays. *Nature*, 212, pp.1232–1233.

Kalmijn, A., 1981. Biophysics of geomagnetic field detection. *IEEE Transactions on Magnetics*, 17(1), pp.1113–1124.

Kalmijn, A., 1982. Electric and magnetic field detection in elasmobranch fishes. *Science (New York, N.Y.)*, 218(4575), pp.916–918.

Kalmijn, A.J. 1988a. Hydrodynamic and acoustic field detection. pp. 83–130. *In:* J. Atema, R.R. Fay, A.N. Popper & W.N. Tavolga (eds.) Sensory Biology of Aquatic Animals, Springer-Verlag, New York.

Kalmijn, A., 2000. Detection and processing of electromagnetic and near-field acoustic signals in elasmobranch fishes. *Philosophical transactions of the Royal Society of London. Series B, Biological sciences*, 355(1401), pp.1135–41.

Kelly, J.C. & Nelson, D.R., 1975. Hearing thresholds of the horn shark, Heterodontus francisci. *The Journal of the Acoustical Society of America*, 58(64).

Khan, U.S. et al., 2015. Transformation mechanism of magnetite nanoparticles. *Materials Science-Poland*, 33(2), pp.278–285.

Kirschvink, J.L., Dizon, A.E. & Westphal, J.A., 1986. Evidence from Strandings for Geomagnetic Sensitivity in Cetaceans. *Journal of Experimental Biology*, 120, pp.1–24.

Kirschvink, J.L. & Gould, J.L., 1981. Biogenic magnetite as a basis for magnetic field detection in animals. *Biosystems*, 13, pp.181–201.

Kirschvink, J.L., Walker, M.M. & Diebel, C.E., 2001. Magnetite-based magnetoreception. *Current opinion in neurobiology*, 11(4), pp.462–7.

Klimley, A.P., 1993. Highly directional swimming by scalloped hammerhead sharks, Sphryna lewini, and subsurface irradiance, temperature, bathymetry and geomagnetic field. *Marine Biology*, 22, pp.1–22.

Klimley, a. P., Kihslinger, R.L. & Kelly, J.T., 2005. Directional and Non-directional Movements of Bat Rays, Myliobatis californica, in Tomales Bay, California. *Environmental Biology of Fishes*, 74(1), pp.79–88.

Komeili, A. et al., 2006. Magnetosomes are cell membrane invaginations organized by the actin-like protein MamK. *Science* , 311(5758), pp.242–5.

Kramer, G (1953). Does information about the height of the sun play a role in navigation/homing behaviour? J. Ornithol., 94:201-219.

Kritzler, H. & Wood, L., 1961. Provisional Audiogram for the Shark, Carcharhinus leucas. *Science*, 133(3463), pp.1480–1482.

Van Der Laan, R., Eschmeyer, W.N. & Fricke, R., 2014. Family-group names of Recent fishes. *Zootaxa*, 3882(1), pp.1–230.

Lea, J.S.E. et al., 2018. Ontogenetic partial migration is associated with environmental drivers and influences fisheries interactions in a marine predator. *ICES Journal of Marine Science*.

Lee, A.P. et al., 2003. Contribution of Raman spectroscopy to identification of biominerals present in teeth of Acanthopleura rehderi, Acanthopleura curtisiana, and Onithochiton quercinus. *Biopolymers*, 72(4), pp.299–301.

Legrand, L. et al., 2001. A Raman and infrared study of a new carbonate green rust obtained by electrochemical way. *Corrosion Science*, 43, pp.1739–1749.

Li, Q. et al., 2017. Correlation between particle size/domain structure and magnetic properties of highly crystalline Fe3O4 nanoparticles. *Scientific Reports*, 7(1).

Liedvogel, M. et al., 2007. Chemical magnetoreception: bird cryptochrome 1a is excited by blue light and forms long-lived radical-pairs. *PloS one*, 2(10), p.e1106.

Light, P., Salmon, M. & Lohmann, K., 1993. Geomagnetic orientation of loggerhead sea turtles: evidence for an inclination compass. *Journal of Experimental Biology*, 182, pp.1–10.

Lisney, T.J. & Cavanagh, R.D., 2003. *Chiloscyllium griseum*, IUCN Global Species Programme Red List Unit. Available at: http://www.iucnredlist.org/details/41792/0 [Accessed February 15, 2018].

Lohmann, K. et al., 1995. Magnetic orientation of spiny lobsters in the ocean: experiments with undersea coil systems. *The Journal of experimental biology*, 198, pp.2041–8.

Lohmann, K. & Lohmann, C., 1994. Detection of Magnetic Inclination Angle By Sea Turtles: a Possible Mechanism for Determining Latitude. *The Journal of experimental biology*, 194(1), pp.23–32.

Lohmann, K., 2004. Geomagnetic map used in sea-turtle navigation. *Nature*, 428, pp.909–910.

Lohmann, K.J., Lohmann, C.M.F. & Endres, C.S., 2008. The sensory ecology of ocean navigation. *The Journal of experimental biology*, 211, pp.1719–1728.

Lohmann, K.J., Lohmann, C.M.F. & Putman, N.F., 2007. Magnetic maps in animals: nature's GPS. *The Journal of experimental biology*, 210, pp.3697–705.

Lohmann, K.J., Putman, N.F. & Lohmann, C.M.F., 2008. Geomagnetic imprinting: A unifying hypothesis of long-distance natal homing in salmon and sea turtles. *Proceedings of the National Academy of Sciences of the United States of America*, 105(49), pp.19096–101.

Maeda, K. et al., 2008. Chemical compass model of avian magnetoreception. *Nature*, 453(7193), pp.387–390.

Mann, S. et al., 1988. Ultrastructure, morphology and organization of biogenic magnetite from sockeye salmon, Oncorhynchus nerka: implications for magnetoreception. *Journal of Experimental Biology*, 140(1).

Mann, S., Sparks, N. & Board, R., 1990. Magnetotactic bacteria: microbiology, biomineralization, palaeomagnetism and biotechnology. *Advances in microbial physiology*, 31, pp.125–181.

Marcotte, M.M., 2014. Homing in the New Zealand eagle ray, Myliobatis tenuicaudatus. *Marine and Freshwater Research*, 65(4), p.306.

Marhold, S., Wiltschko, W. & Burda, H., 1997. A magnetic polarity compass for direction finding in a subterranean mammal. *Naturwissenschaften*, 423, pp.421–423.

Martinez Vera, N.P. et al., 2014. Tracking of Magnetite Labeled Nanoparticles in the Rat Brain Using MRI. *PLoS ONE*, 9(3).

Maus, S. (Cooperative I. for R. in E.S., 2010. Geomagnetism. *Historical main field change and declination*. Available at: http://geomag.org/info/declination.html [Accessed August 2, 2016].

McCleave, J.D. & Power, J.H., 1978. Influence of weak electric and magnetic fields on turning behavior in elvers of the American eel Anguilla rostrata. *Marine Biology*, 46(1), pp.29–34.

McComb, D.M. et al., 2010. Temporal Resolution and Spectral Sensitivity of the Visual System of Three Coastal Shark Species from Different Light Environments. *Physiological and Biochemical Zoology*, 83(2), pp.299–307.

McCutcheon, S.M. & Kajiura, S.M., 2013. Electrochemical properties of lanthanide metals in relation to their application as shark repellents. *Fisheries Research*, 147, pp.47–54.

Meredith, T.L., 2011. *Anatomy And Physiology Of The Elasmobrach Olfactory System*. Florida Atlantic University. Available at: https://fau.digital.flvc.org/islandora/object/fau%3A3801/datastream/OBJ/view/Anatomy_and_physiology_of_the_elasmobranch_olfactory_system.pdf

Meyer, C.G., Holland, K.N. & Papastamatiou, Y.P., 2005. Sharks can detect changes in the geomagnetic field. *Journal of the Royal Society, Interface / the Royal Society*, 2(2), pp.129–30.

Meyer, C.G., Papastamatiou, Y.P. & Holland, K.N., 2010. A multiple instrument approach to quantifying the movement patterns and habitat use of tiger (Galeocerdo cuvier) and Galapagos sharks (Carcharhinus galapagensis) at French Frigate Shoals, Hawaii. *Marine Biology*, 157(8), pp.1857–1868.

Molteno, T.C.A. & Kennedy, W.L., 2009. Navigation by induction-based magnetoreception in elasmobranch fishes. *Journal of biophysics (Hindawi Publishing Corporation : Online)*, 2009, p.380976.

Montgomery, J. & Bodznick, D., 1993. Hindbrain circuitry mediating common mode suppression of ventilatory reafference in the electrosensory system of the little skate Raja erinacea. *Journal of experimental biology*, 215, pp.203–215.

Montgomery, J. & Bodznick, D., 1999. Signals and noise in the elasmobranch electrosensory system. *The Journal of experimental biology*, 202(# (Pt 10)), pp.1349–55.

Montgomery, J. & Skipworth, E., 1997. Detection of Weak Water Jets by the Short-Tailed Stingray Dasyatis brevicaudata (Pisces. *Copeia*, 9(4), pp.881–883.

Montgomery, J. & Walker, M., 2001. Orientation and navigation in elasmobranchs: which way forward? *Environmental Biology of Fishes*, pp.109–116.

Montgomery, J.C., 1980. Dogfish horizontal canal system: responses of primary afferent, vestibular and cerebellar neurons to rotational stimulation. *Neuroscience*, 5(10), pp.1761–9.

Moore, A. & Riley, W.D., 2009. Magnetic particles associated with the lateral line of the European eel Anguilla anguilla. *Journal of fish biology*, 74(7), pp.1629–34.

Van Moorter, B. et al., 2009. Memory keeps you at home: a mechanistic model for home range emergence. *Oikos*, 118(5), pp.641–652.

Mora, C. V et al., 2004. Magnetoreception and its trigeminal mediation in the homing pigeon. *Nature*, 432(November), pp.508–511.

Mora, C. V. et al., 2014. Behavioral modification of visually deprived lemon sharks (Negaprion brevirostris) towards magnetic fields. *Journal of Navigation*, 115(4), pp.346–353.

Mora, C. V., Davison, M. & Walker, M.M., 2009. Conditioning as a Technique for Studying the Sensory Systems Involved in Animal Orientation, Homing and Navigation – a Review. *Journal of Navigation*, 62(4), p.571.

Mouritsen, H. & Ritz, T., 2005. Magnetoreception and its use in bird navigation. *Current opinion in neurobiology*, 15(4), pp.406–14.

Mouritsen, H. et al., 2013. Sun Compass Orientation Helps Coral Reef Fish Larvae Return to Their Natal Reef. *PLoS ONE*, 8(6).

Musick, J.A. & Cotton, C., 2015. Bathymetric limits of chondrichthyans in the deep sea: A re-evaluation. *Deep Sea Research Part II: Topical Studies in Oceanography*, 115, pp.73–80.

Myklatun, A. et al., 2018. Zebrafish and medaka offer insights into the neurobehavioral correlates of vertebrate magnetoreception. *Nature Communications*, 9(1), p.802.

Myrberg, A.A., 2000. The acoustical biology of elasmobranchs. *Environmental Biology of Fishes*, 60, pp.31–45.

Nagaoka, H., 1909. The Inductance Coefficients of Solenoids. *Journal of the College of Science, Imperial University*, 27(6), pp.1–33.

Naisbett-Jones, L.C. et al., 2017. A Magnetic Map Leads Juvenile European Eels to the Gulf Stream. *Current Biology*, 27.

Nams, V.O., 2006. Detecting oriented movement of animals. *Animal Behaviour*, 72(5), pp.1197–1203.

Naylor, G. et al., 2005. Reproductive Biology and Phylogeny of Chondrichthyes: Sharkes, Rays, and Chimaeras. In T. I. Walker & W. C. Hamlett, eds. *Reproductive Biology and Phylogeny of Chondrichthyes*. Enfield (New Hampshire): Science Publishers, pp 1-25.

Nelson, D.R., 1967. Hearing Thresholds, Frequency Discrimination, and Acoustic Orientation in the Lemon Shark, Negaprion Brevirostris (Poey). *Bulletin of Marine Science*, 17(3), pp.741–768.

Newton, K.C. & Kajiura, S.M., 2017. Magnetic field discrimination, learning, and memory in the yellow stingray (Urobatis jamaicensis). *Animal Cognition*, 20(4), pp.603–614.

Nishi, T., Archdale, M.V. & Kawamura, @bullet Gunzo, 2018. Behavioural evidence for the use of geomagnetic cue in Japanese glass eel Anguilla japonica orientation. *Ichyology Research*, 65, pp.161–164.

NOAA/NCEI, 2015. The World Magnetic Model. *World Magnetic Model 2015*. Available at: https://www.ngdc.noaa.gov/geomag/WMM/DoDWMM.shtml [Accessed August 2, 2018].

Nosal, A.P. et al., 2016. Olfaction Contributes to Pelagic Navigation in a Coastal Shark A. P. Klimley, ed. *PLOS ONE*, 11.

Novales Flamarique, I. & Hawryshyn, C.W., 1997. Is the use of underwater polarized light by fish restricted to crepuscular time periods? *Vision research*, 37(8), pp.975–89.

O'Connell, C. et al., 2011. Analysis of permanent magnets as elasmobranch bycatch reduction devices in hook-and-line and longline trials. *Fishery Bulletin*, pp.394–402.

O'Connell, C.P. et al., 2011. Response of juvenile lemon sharks, Negaprion brevirostris, to a magnetic barrier simulating a beach net. *Ocean & Coastal Management*, 54(3), pp.225–230.

Ogden J.C., Quinn T.P., 1984. Migration in Coral Reef Fishes: Ecological Significance and Orientation Mechanisms. In: McCleave J.D., Arnold G.P., Dodson J.J., Neill W.H. (eds) Mechanisms of Migration in Fishes. NATO Conference Series (IV Marine Sciences), vol 14. Springer, Boston, MA

O'Keefe, J. & Nadel, L., 1978. *The hippocampus as a cognitive map*, Oxford: Clarendon Press.

O'Leary, D.P. et al., 1981. Magnets in guitarfish vestibular receptors. *Experientia*, 37(1), pp.86–88.

Odling-Smee, L. & Braithwaite, V.A., 2003. The role of learning in fish orientation. *Fish and Fisheries*, 4(3), pp.235–246.

Oh, S.J., Cook, D.C. & Townsend, H.E., 1998. Characterization of Iron Oxides Commonly Formed as Corrosion Products on Steel. *Hyperfine Interactions*, 112(1/4), pp.59–66.

Osipova, E.A. et al., 2016. Influence of magnetic field on zebrafish activity and orientation in a plus maze. *Behavioural Processes*, 122, pp.80–86.

Papastamatiou, Y.P. et al., 2011. Scales of orientation, directed walks and movement path structure in sharks. *The Journal of animal ecology*, 80(4), pp.864–74.

Papastamatiou, Y.P. et al., 2013. Telemetry and random-walk models reveal complex patterns of partial migration in a large marine predator. *Ecology*, 94(11), pp.2595–2606.

Paulin, M., 1995. Electroreception and the compass sense of sharks. *Journal of Theoretical Biology*, 174, pp.325–339.

Payne, N.L. et al., 2018. Combining abundance and performance data reveals how temperature regulates coastal occurrences and activity of a roaming apex predator. *Global Change Biology*, 24, pp.1884–1893.

Peach, M.B., 2001. The dorso-lateral pit organs of the Port Jackson shark contribute sensory information for rheotaxis. *Journal of Fish Biology*, 59(3), pp.696–704.

Phillips, J., 1986. Two magnetoreception pathways in a migratory salamander. *Science (New York, N.Y.)*, 233(4765), pp.765–767.

Phillips, J. B. (1996). Magnetic navigation. *Journal of Theoretical Biology*, **180**, 309–19.

Phillips, J.B., Schmidt-Koenig, K., & Muheim, R. (2006). True navigation: Sensory bases of gradient maps. In M.F. Brown and R.G. Cook (Eds.), *Animal Spatial Cognition: Comparative, Neural, and Computational Approaches.* [On-line]. Available: pigeon.psy.tufts.edu/asc/phillips/

Phillips, J., Jorge, P. & Muheim, R., 2010. Light-dependent magnetic compass orientation in amphibians and insects: candidate receptors and candidate molecular mechanisms. *Journal of the Royal Society, Interface*, 7(2), pp.241–256.

Phillips, J.B. et al., 2001. The role of extraocular photoreceptors in newt magnetic compass orientation: parallels between light-dependent magnetoreception and polarized light detection in vertebrates. *The Journal of experimental biology*, 204(Pt 14), pp.2543–52.

Portavella, M. et al., 2002. The effects of telencephalic pallial lesions on spatial, temporal, and emotional learning in goldfish. *Brain Research Bulletin*, 57(3–4), pp.397–399.

Poucet, B., 1993. Spatial Cognitive Maps in Animals: New Hypotheses on Their Structure and Neural Mechanisms. *Psychological Review*, 100(2), pp.163–182.

Prato, F.S. & Kavaliers, M., 1996. Behavioural responses to magnetic fields by land snails are dependent on both magnetic field direction and light. *Proceedings: Biological Sciences*, 263(1376), pp.1437–1442.

Priede, I.G. et al., 2006. The absence of sharks from abyssal regions of the world's oceans. *Proceedings. Biological sciences*, 273(1592), pp.1435–41.

Prozorov, T. et al., 2014. Manganese incorporation into the magnetosome magnetite: magnetic signature of doping. *European Journal of Mineralogy*, 26(4), pp.457–471.

Putman, N.F. & Lohmann, K.J., 2008. Compatibility of magnetic imprinting and secular variation. *Current Biology*, 18(14), pp.R596–R597.

Putman, N.F. et al., 2014. An Inherited Magnetic Map Guides Ocean Navigation in Juvenile Pacific Salmon. *Current Biology*, 24(4), pp.446–450.

Putman, N.F. et al., 2018. Geomagnetic field influences upward movement of young Chinook salmon emerging from nests. *Biology letters*, 14(2).

Puzdrowski, R., 1988. Afferent projections of the trigeminal nerve in the goldfish, Carassius auratus. *Journal of morphology*, 198, pp.131–147.

Quinn, T.P., 1980. Evidence for celestial and magnetic compass orientation in lake migrating sockeye salmon fry. *Journal of Comparative Physiology. A*, 137(3), pp.243–248.

Quinn, T.P. & Brannon, E.L., 1982. The use of celestial and magnetic cues by orienting sockeye salmon smolts. *Journal of Comparative Physiology. A*, 147(4), pp.547–552.

Ritz, T., Adem, S. & Schulten, K., 2000. A model for photoreceptor-based magnetoreception in birds. *Biophysical journal*, 78(2), pp.707–18.

Rivera-Vicente, A.C., Sewell, J. & Tricas, T.C., 2011. Electrosensitive spatial vectors in elasmobranch fishes: Implications for source localization. *PLoS ONE*, 6(1).

Robbins, W.D., Peddemors, V.M. & Kennelly, S.J., 2011. Assessment of permanent magnets and electropositive metals to reduce the line-based capture of Galapagos sharks, Carcharhinus galapagensis. *Fisheries Research*, 109(1), pp.100–106.

Rodriguez, F. et al., 1994. Performance of goldfish trained in allocentric and egocentric maze procedures suggests the presence of a cognitive mapping system in fishes. *Animal Learning & Behavior*, 22(4), pp.409–420.

Rodríguez, F. et al., 2002. Spatial memory and hippocampal pallium through vertebrate evolution: insights from reptiles and teleost fish. *Brain Research Bulletin*, 57(3–4), pp.499–503.

Rogers, B.L. et al., 2008. Utilizing magnetic resonance imaging (MRI) to assess the effects of angling-induced barotrauma on rockfish (Sebastes). *Canadian Journal of Fisheries and Aquatic Sciences*, 65(7), pp.1245–1249.

Rommel Jr., S.A. & McCleave, J.D., 1973. Sensitivity of American Eels (Anguilla rostrata) and Atlantic Salmon (Salmo salar) to Weak Electric and Magnetic Fields. *Journal of the Fisheries Research Board of Canada*, 30(5), pp.657–663.

Sand, O. & Karlsen, H.E., 2000. Detection of infrasound and linear acceleration in shes. *Phil. Trans. R. Soc. Lond. B*, 355, pp.1295–1298.

Sandberg, R., & Holmquist, B. (1998). Orientation and Long-Distance Migration Routes: An Attempt to Evaluate Compass Cue Limitations and Required Precision. *Journal of Avian Biology, 29*(4), 626-636.

Schaeffer, B. and Williams M. E. 1977. Relationships of fossil and living elasmobranchs. American Zoologist 17: 293-302.

Schluessel, V. & Bleckmann, H., 2012. Spatial learning and memory retention in the grey bamboo shark (Chiloscyllium griseum). *Zoology*, 115(6), pp.346–353.

Schluessel, V. & Bleckmann, H., 2005. Spatial memory and orientation strategies in the elasmobranch Potamotrygon motoro. *Journal of Comparative Physiology A: Neuroethology, Sensory, Neural, and Behavioral Physiology*, 191(8), pp.695–706.

Schluessel, V., Herzog, H. & Scherpenstein, M., 2015. Seeing the forest before the trees-spatial orientation in freshwater stingrays (Potamotrygon motoro) in a hole-board task. *Behavioural Processes*, 119, pp.105–115.

Schuijf, A. 1974. Field studies of directional hearing in marine teleosts. Ph.D. Dissertation, University of Utrecht, Utrecht.119 pp.

Schuijf, A. 1975. Directional hearing of cod (*Gadus morhua*) under approximate free field conditions. J. Comp. Physiol. 98: 307–332

Schüler, D., 2008. Genetics and cell biology of magnetosome formation in magnetotactic bacteria. *FEMS Microbiology Reviews*, 32(4), pp.654–672.

Schulten, K. & Swenberg, C.E., 1978. A biomagnetic sensory mechanism based on magnetic field modulated coherent electron spin motion. *… für Physikalische Chemie*, 111, pp.1–5.

Schulten, K., Swenberg, C.E. & Weller, A., 1978. A Biomagnetic Sensory Mechanism Based on Magnetic Field Modulated Coherent Electron Spin Motion. *Zeitschrift für Physikalische Chemie*, 111(1), pp.1–5.

Semm, P. & Demaine, C., 1986. Neurophysiological Properties Of Magnetic Cells In The Pigeons Visual-System. *Journal of Comparative Physiology. A*, 159, pp.619–625.

Sepulved, C.A. et al., 2007. Cranial endothermy and a putative brain heater in the most basal tuna species, Allothunnus fallai. *Journal of Fish Biology*, 70(6), pp.1720–1733.

Shaw, J. et al., 2015. Magnetic particle-mediated magnetoreception. *Journal of the Royal Society, Interface*, 12(110), p.499.

Shcherbakov, V.P. & Winklhofer, M., 1999. The osmotic magnetometer: a new model for magnetite-based magnetoreceptors in animals. *European Biophysics Journal*, 28(5), pp.380–392.

Shebanova, O.N. & Lazor, P., 2003. Raman spectroscopic study of magnetite (FeFe2O4): a new assignment for the vibrational spectrum. *Journal of Solid State Chemistry*, 174, pp.424–430.

Siegenthaler, A. et al., 2016. Aversive responses of captive sandbar sharks Carcharhinus plumbeus to strong magnetic fields. *Journal of Fish Biology*, 89(3), pp.1603–1611.

Silver, W.L., 1979. Olfactory responses from a marine elasmobranch, the atlantic stingray, Dasyatis sabina. *Marine Behaviour and Physiology*, 6(4), pp.297–305.

Sneddon, L.U., 2002. Anatomical and electrophysiological analysis of the trigeminal nerve in a teleost fish, Oncorhynchus mykiss. *Neuroscience letters*, 319(3), pp.167–71.

Sneddon, L.U., 2003. Trigeminal somatosensory innervation of the head of a teleost fish with particular reference to nociception. *Brain research*, 972(1–2), pp.44–52.

Snow, P.J., Plenderleith, M.B. & Wright, L.L., 1993. Quantitative Study of Primary Neurone Populations of Three of Elasmobranch Fish Sensory Species. *The Journal Of Comparative Neurology*, 334, pp.97–103.

Sung Lee, J. et al., 2015. Magnetic multi-granule nanoclusters: A model system that exhibits universal size effect of magnetic coercivity. *Scientific Reports*, 5(1), p.12135.

Teraski, M. & Jaffe, L.A., 1991. Organization of the sea urchin egg endoplasmic reticulum and its reorganization at fertilization. *Journal of Cell Biology*, 114(5), pp.929–940.

Thalau, P. et al., 2006. The magnetic compass mechanisms of birds and rodents are based on different physical principles. *Journal of the Royal Society, Interface / the Royal Society*, 3(9), pp.583–7.

Theisen, B., Zeiske, E. & Breucker, H., 1986. Functional Morphology of the Olfactory Organs in the Spiny Dogfish (Squalus acanthias L.) and the Smallâ€spotted Catshark (Scyliorhinus canicula (L.)). *Acta Zoologica*, 67(2), pp.73–86.

Tolman, E.C., 1948. Cognitive Maps In Rats And Men. *The Psychological Review*, 55(4), pp.189–208.

Torres, F.F., Botanica, D. & Paulo, S., 1986. Magnetite magnetotaxis algae. *Biophysical Journal*, 50(August 1986), pp.375–378.

Treiber, C.D. et al., 2012. Clusters of iron-rich cells in the upper beak of pigeons are macrophages not magnetosensitive neurons. *Nature*, 484(7394), pp.367–70.

Tricas, T.C., 2001. The neuroecology of the elasmobranch electrosensory world: why

peripheral morphology shapes behavior. *Environmental Biology of Fishes*, 60, pp.77–92.

Tricas, T.C., Kajiura, S.M. & Summers, A.P., 2009. Response of the hammerhead shark olfactory epithelium to amino acid stimuli. *Journal of comparative physiology. A, Neuroethology, sensory, neural, and behavioral physiology*, 195(10), pp.947–54.

Tricas, T.C. & New, J.G., 1998. Sensitivity and response dynamics of elasmobranch electrosensory primary afferent neurons to near threshold fields. *Journal of comparative physiology. A, Sensory, neural, and behavioral physiology*, 182(1), pp.89–101. Available at: http://www.ncbi.nlm.nih.gov/pubmed/9447716.

Varanelli, C.C. & McCleave, J.D., 1974. Locomotor activity of atlantic salmon parr (Salmo salar L.) in various light conditions and in weak magnetic fields. *Animal Behaviour*, 22(1), pp.178–186.

Vilches-Troya, J., Dunn, R.F. & O 'leary, D.P., 1984. Relationship of the Vestibular Hair Cells to Magnetic Particles in the Otolith of the Guitaflish Sacculus. *The Journal Of Comparative Neurology*, 226, pp.489–494.

Walker, M., 1984. Learned magnetic field discrimination in yellowfin tuna,Thunnus albacares. *Journal of Comparative Physiology. A*, 155(5), pp.673–679.

Walker, M.., Diebel, C.E. & Kirschvink, J.L., 2006. Magnetoreception. In T. J. Hara & B. Zielinski, eds. *Fish Physiology: Sensory Systems Neuroscience*. London: Academic Press, pp. 335–374.

Walker, M.M., 1998. On a Wing and a Vector: a Model for Magnetic Navigation by Homing Pidgeons. *J. theor. Biol*, 192, pp.341–349.

Walker, M.M. et al., 1988. Production of single-domain magnetite throughout life by sockeye salmon, Oncorhynchus nerka. *The Journal of experimental biology*, 140, pp.51–63.

Walker, M.M. et al., 1997. Structure and function of the vertebrate magnetic sense. *Nature*, 390(6658), pp.371–6.

Walker, M.M., Diebel, C.E. & Kirschvink, J.L., 2004. Detection an Use of the Earth's Magnetic Field by Aquatic Vertebrates. In *Sensory Processing in Aquatic Environments*. New York: Springer-Verlag, pp. 53–74.

Walker, M.M., Kirschvink, J.L. & Chang, S.-B.R., 1984. A Candidate Magnetic Sense Organ in the Yellowfin Tuna, Thunnus albacares. *Science*, 224, pp.751–753.

Wallraff, H. G. (1974). *Das Navigationssystem der Vögel*. R.Oldenbourg Verlag, Munich.

Watanabe, S. et al., 2008. Laser Raman Spectroscopic Study on Magnetite Formation in Magnetotactic Bacteria. *Materials Transactions*, 49(4), pp.874–878.

Weng, K. et al., 2008. Migration of an upper trophic level predator, the salmon shark Lamna ditropis, between distant ecoregions. *Marine Ecology Progress Series*, 372(Longhurst

1998), pp.253–264.

Weng, K.C. et al., 2007. Migration and habitat of white sharks (Carcharodon carcharias) in the eastern Pacific Ocean. *Marine Biology*, 152(4), pp.877–894.

Werry, J.M. et al., 2014. Reef-fidelity and migration of tiger sharks, Galeocerdo cuvier, across the coral sea. *PLoS ONE*, 9(1).

Wheeler, H., 1982. Inductance Formulas for Circular and Square Coils. *Proceedings of the IEEE*, 70(12), pp.1449–1450.

Wiltschko, R. & Wiltschko, W., 2006. Magnetoreception. *BioEssays : news and reviews in molecular, cellular and developmental biology*, 28.2(2), pp.157–168.

Wiltschko, W. et al., 2010. Magnetoreception in birds: no intensity window in "fixed direction" responses. *Die Naturwissenschaften*, 97(1), pp.37–42.

Wiltschko, W. & Wiltschko, R., 1972. Magnetic compass of European robins. *Science (New York, N.Y.)*, 176(4030), pp.62–64.

Wiltschko, W. & Wiltschko, R., 2005. Magnetic orientation and magnetoreception in birds and other animals. *Journal of Comparative Physiology. A.*, 191(8), pp.675–93.

Winklhofer, M. et al., 2001. Clusters of superparamagnetic magnetite particles in the upper-beak skin of homing pigeons: evidence of a magnetoreceptor? *European Journal of Mineralogy*, 13(4), pp.659–669.

Winklhofer, M. & Kirschvink, J.L., 2010. A quantitative assessment of torque-transducer models for magnetoreception. *J. R. Soc. Interface*, 7, pp.273–289.

Winn, H.E., Salmon, M., Roberts, N., 1964. Sun-compass oritentation by parrot fishes. *Ethology*. 21 (7), pp. 798-812.

Yopak, K.E., 2012. Neuroecology of cartilaginous fishes: the functional implications of brain scaling. *Journal of Fish Biology*, 80(5), pp.1968–2023.

Yopak, K.E. et al., 2007a. Variation in brain organization and cerebellar foliation in chondrichthyans: sharks and holocephalans. *Brain, behavior and evolution*, 69(4), pp.280–300.

Yopak, K.E. et al., 2007b. Variation in cerebellar foliation in cartilaginous fishes: Ecological and behavioral considerations. *Brain, behavior and evolution*, 69, pp.280–300.

Yopak, K.E. & Frank, L.R., 2009. Brain size and brain organization of the whale shark, Rhincodon typus, using magnetic resonance imaging. *Brain, behavior and evolution*, 74(2), pp.121–42.

Yopak, K.E., Lisney, T.J. & Collin, S.P., 2015. Not all sharks are swimming noses'': variation in olfactory bulb size in cartilaginous fishes. *Brain Struct Funct*, 220, pp.1127–1143.

Zhou, Z. et al., 2016. SCIENCE CHINA Identification of zebrafish magnetoreceptor and cryptochrome homologs. *South China Life Sciences*, 59(12), pp.1324–1331.

Zoeger, J. et al., 1981. Magnetic material in the head of the common Pacific dolphin. *Science*, 213(4510), pp.892–894.